AGU ADVANCING EARTH AND SPACE SCIENCE

Reviews of Geophysics®

A Review on Bank Retreat: Mechanisms, Observations, and Modeling

Kun Zhao[1,2] , Giovanni Coco[2] , Zheng Gong[1,3] , Stephen E. Darby[4] , Stefano Lanzoni[5] , Fan Xu[6] , Kaili Zhang[1,2] , and Ian Townend[7]

[1]State Key Laboratory of Hydrology-Water Resources and Hydraulic Engineering, Hohai University, Nanjing, China, [2]School of Environment, University of Auckland, Auckland, New Zealand, [3]Jiangsu Key Laboratory of Coast Ocean Resources Development and Environment Security, Hohai University, Nanjing, China, [4]School of Geography and Environmental Sciences, University of Southampton, Southampton, UK, [5]Department of Civil, Environmental and Architectural Engineering, University of Padua, Padua, Italy, [6]State Key Laboratory of Estuarine and Coastal Research, East China Normal University, Shanghai, China, [7]Ocean and Earth Sciences, University of Southampton, Southampton, UK

Abstract Bank retreat plays a fundamental role in fluvial and estuarine dynamics. It affects the cross-sectional evolution of channels, provides a source of sediment, and modulates the diversity of habitats. Understanding and predicting the geomorphological response of fluvial/tidal channels to external driving forces underpins the robust management of water courses and the protection of wetlands. Here, we review bank retreat with respect to mechanisms, observations, and modeling, covering both rivers and (previously neglected) tidal channels. Our review encompasses both experimental and in situ observations of failure mechanisms and bank retreat rates, modeling approaches and numerical methods to simulate bank erosion. We identify that external forces, despite their distinct characteristics, may have similar effects on bank stability in both river and tidal channels, leading to the same failure mode. We review existing data and empirical functions for bank retreat rate across a range of spatial and temporal scales, and highlight the necessity to account for both hydraulic and geotechnical controls. Based on time scale considerations, we propose a new hierarchy of modeling styles that accounts for bank retreat, leading to clear recommendations for enhancing existing modeling approaches. Finally, we discuss systematically the feedbacks between bank retreat and morphodynamics, and suggest that to move this agenda forward will require a better understanding of multifactor-driven bank retreat across a range of temporal scales, with particular attention to the differences (and similarities) between riverine and estuarine environments, and the role of feedbacks exerted by the collapsed bank soil.

Plain Language Summary As one of the most persistent and dominant processes that shape rivers, estuaries, and coastal regions, bank retreat is of great relevance to the management of water courses and the protection of wetlands. Here, we review bank retreat processes with respect to both rivers and tidal channels, including observations of erosion/failure processes and bank retreat rate, as well as methods proposed for numerical modeling. We highlight that different hydrodynamic forces associated with fluvial and estuarine settings may nevertheless have similar effects on bank stability. Using data from the literature we show that observed bank retreat rates are not only controlled by flow strength and soil composition (e.g., discharge, vegetation cover, and critical shear stress for erosion), but are also related to other factors, such as channel width and bank geometry. We summarize recent developments in bank retreat modeling, discuss their advantages and challenges, and propose some recommendations for their future use. Overall, this review deepens our understanding of bank erosion/collapse processes, and how they shape both fluvial and estuarine landscapes.

1. Introduction

Bank retreat results from the complex of processes causing the detachment of bank soil under the actions of hydraulic and gravitational forces, subaerial processes, bioturbation, as well as resisting actions that depend on soil properties, and which are possibly mediated by vegetation cover. In general, the processes which cause bank retreat can be divided in two main classes: flow-driven bank erosion and gravity-driven bank collapse (Simon et al., 2000; Thorne & Tovey, 1981). Bank retreat is of fundamental importance to fluvial, estuarine, and coastal dynamics, and encompass a wide range of spatial and temporal scales, with important physical, ecological, and socio-economic repercussions (Figure 1). Bank retreat drives the cross-sectional evolution of channels (Gong et al., 2018; Thorne et al., 1998a; van der Wegen et al., 2008), facilitates the initiation and development of channel
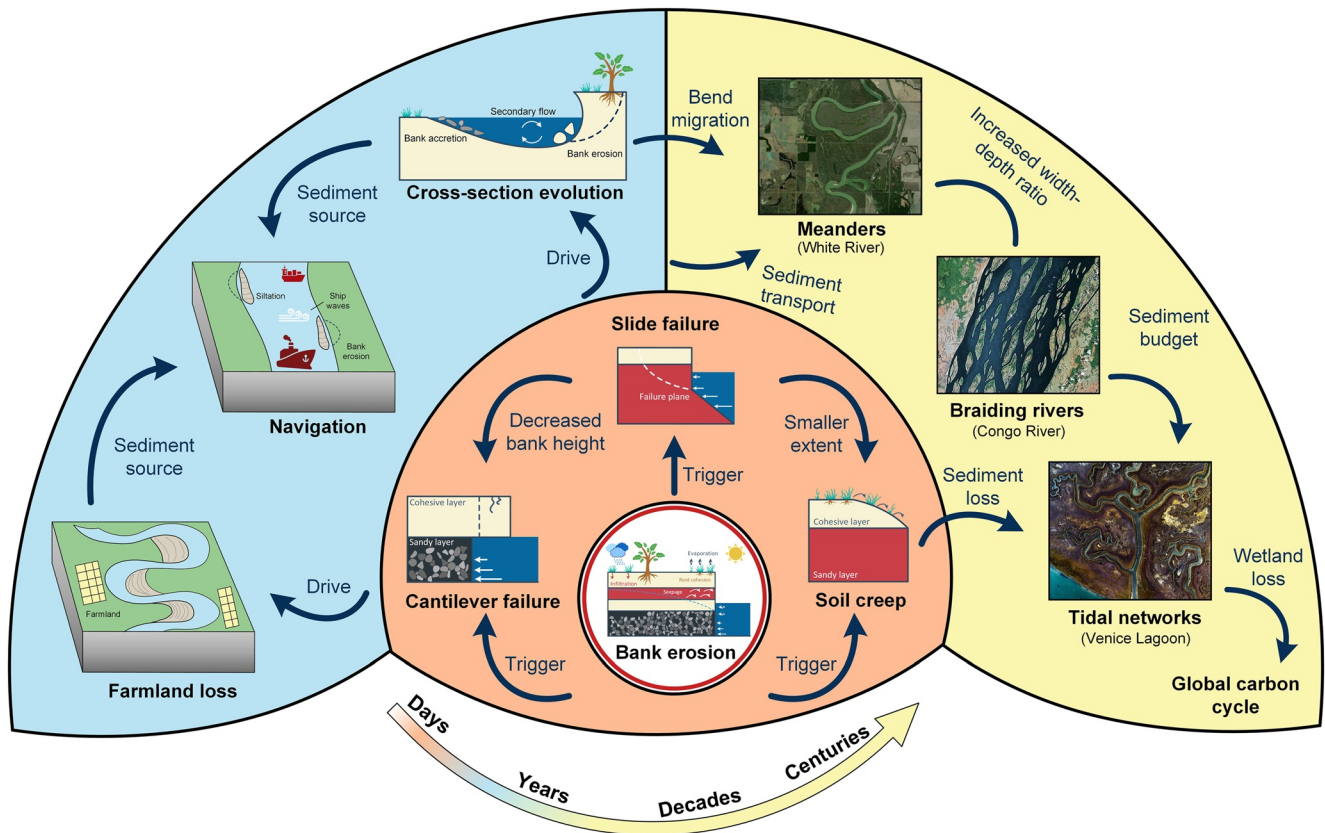
Figure 1. Bank retreat events and their impacts across a range of temporal and spatial scales. Aerial photos are with permission from Google Earth, and the image of Venice Lagoon is taken by Milan Radisics on 4 August 2018.

meandering (Ikeda et al., 1981; Marani et al., 2002; Seminara, 2006), alters floodplain morphology (Beechie et al., 2006; Han & Brierley, 2020), and affects the dynamics of free and forced bars forming within the channel bed (Blondeaux & Seminara, 1985; Solari et al., 2002; van Dijk et al., 2012). Bank retreat has also been suggested as a major source of sediment load, thereby significantly altering sediment transfer dynamics. This latter phenomenon occurs at a global scale as shown by studies conducted in New Zealand (Griffiths, 1979; Watson & Basher, 2006), Europe (Duró et al., 2020; J. W. Poesen et al., 1996), the Midwestern (Simon et al., 2000) and southern United States (Simon & Darby, 2002), Canada (Nanson & Hickin, 1986), Russia (Dong, Nittrouer, et al., 2019), China (Xia et al., 2016; Yao et al., 2011), Egypt (Abate et al., 2015), and many other countries.

From an ecological perspective, bank retreat modulates the diversity of species and vegetation units (Piégay et al., 1997), provides sediment supply to create habitats on a floodplain and over channel bars (Florsheim

et al., 2008), affects nutrient and contaminant dynamics (Marron, 1992; Reneau et al., 2004), induces salt-marsh loss (Deegan et al., 2012) and so modulates the global carbon cycle (Kirwan & Mudd, 2012). With respect to socio-economic effects, bank retreat is responsible for farmland and wetland loss (Qin et al., 2018; Turner, 1990), population displacement (Best, 2019), reservoir siltation (Ben Slimane et al., 2016), damage to riparian infrastructure and hydraulic structures (C. R. Hackney et al., 2020; Hooke, 1979), and creates pathways for pollutant transport (Castillo & Gómez, 2016).

As pointed out above, bank retreat is in general caused by flow-driven particle-by-particle erosion (flow-driven bank erosion) and gravity-driven mass failure (bank collapse). Flow-driven bank erosion consists of the removal of bank materials under the direct action of water flow (near-bank channel flow, over-bank flow, and seepage flow), and can be enhanced by subaerial processes. Bank collapse, in contrast, occurs when the forces that tend to move soil downslope (soil weight, seepage forces, and excess pore water pressure) exceed the resisting forces of the bank (cohesion imparted by the soil and root matrix, matric suction, and hydrostatic pressure head) (Fox & Wilson, 2010; Langendoen & Simon, 2008; Rinaldi & Darby, 2007; Simon et al., 2000; Thorne, 1982). Unlike the continuous, progressive, nature of flow-driven bank erosion, bank collapse is episodic and is associated with various modes of failure, including shear, tensile, and toppling, that depend on bank soil properties, bank height, near-bank water depth and the presence or absence of vegetation (Cancienne & Fox, 2008; Nardi et al., 2012; Patsinghasanee et al., 2018; Thorne et al., 1998a; Zhao et al., 2020).

A large body of literature has been produced on bank dynamics in fluvial environments. Considerably less attention has been devoted to tidal environments, where research has to date focused mainly on the retreat of salt marsh borders rather than tidal channel banks. Existing reviews on the subject tend to focus on specific aspects, rather than delineating a general framework which addresses comprehensively the mechanisms that cause bank retreat and synthesizes observations, as well as modeling frameworks describing the commonly observed bank failure mechanisms. It is thus timely to provide a thorough review that highlights recent developments about the understanding and the prediction of bank retreat and point out future research needs that deserve attention to improve our fundamental knowledge of bank retreat processes.

On the basis of field and laboratory observations, we specifically focus on a unifying description of failure mechanisms leading to bank retreat, and refer the reader to Piégay et al. (2005) and Florsheim et al. (2008) for prior comprehensive reviews of the geomorphic and ecological functions of bank retreat. The reader is also referred to Couper (2004), who reviewed how temporal and spatial scales are treated in bank retreat research, and discussed the linkages between these scales. We do not consider in situ measurement instrumentation, and refer readers interested in this aspect to Lawler (1993a). Since our focus is bank retreat, we only review the effect of subsurface flow on bank erosion/collapse and refer the reader to Fox and Wilson (2010) and Bernatek-Jakiel and Poesen (2018) for the specific aspects of seepage flows. Existing review articles of bank retreat mainly focus on fluvial environments (Castro-Bolinaga & Fox, 2018; Chassiot et al., 2020; Thorne et al., 1998a), while tidal systems are not discussed by any of these works. The present contribution is intended to fill this gap. We note that a large body of literature concerning numerical models have also been reviewed, for instance by Thorne et al. (1998b) and Rinaldi and Darby (2007). Still, numerical methods advance rapidly and an assessment of recent developments is now timely.

The present contribution aims at setting the various processes causing bank retreat in both fluvial and tidal environments within a rational and comprehensive framework which integrates experimental observations and numerical modeling. Given the similarity with failure mechanisms observed in many other physical systems, indicating linkages in a broader context, we have considered also the literature concerning cliff retreat in salt-marsh and marine-ice landscapes, slope stability, gully and tidal channel headcuts, and the stability of reservoir banks. Overall, we pursue a holistic view, covering observations of failure mechanisms, empirical predictive functions, as well as mathematical and numerical modeling.

This review is structured as follows. Section 2 defines a general classification of bank retreat and provides a detailed description of the various types of failure mechanisms. Section 3 reviews the mechanisms of bank collapse, as observed mainly from laboratory experiments. We distinguish bank collapse with respect to different driving forces: subaerial processes, bank surface flow (including near-bank channel flow and overbank flow), seepage flow, fluctuations in soil pore-water pressure, and waves. We discuss also the role of vegetation, biological disturbances, and hydrostatic pressure head. Section 4 reviews the empirical relations developed to predict

bank retreat rate in terms of hydraulic and geometric factors such as discharge, precipitation, and bank height. The comparison of the existing relations highlights the necessity to account for both hydraulic and geotechnical factors. Section 5 reviews the approaches adopted to model bank erosion/collapse and proposes a hierarchical classification of models. The advantages and limitations of each method are pointed out, and some modeling recommendations are provided. Section 6 reviews the feedbacks between bank retreat and morphodynamics, showing how bank retreat affects morphodynamic evolution and analyzing the importance of its integration into morphodynamic models. Finally, Section 7 discusses the open questions, and provides recommendations for future research.

2. Classification of Bank Retreat

We consider in detail the main aspects characterizing the two classes of processes which cause bank retreat: flow-driven bank erosion and bank collapse. The latter can be further classified using additional criteria. In terms of failure mode, Thorne and Tovey (1981) identified three types of cantilever failure: shear, beam, and tensile. Based on the shape of the failure surface, Simon et al. (2000) distinguished between planar and rotational failure types. Nardi et al. (2012) and Zhao et al. (2020) extended the above classification on the basis of experimental observations of non-cohesive riverbanks. However, many misinterpretations still exist partly because of the different terminologies often used to describe the same processes. For instance, the term *beam failure* and *toppling failure* are applied to describe the same failure mode (Bendoni et al., 2014; Nardi et al., 2012; Samadi et al., 2013), and *pop-out failure* is also called *tensile failure* (Fox & Felice, 2014). When investigating bank failure mechanisms along Arno River, Dapporto et al. (2003) used the term *slab-type failure* to include both mechanisms of toppling and planar failures, and some new terms are also introduced to distinguish different bank collapse processes such as *soil fall*, *alcove-type failure*, and *shallow slide failure*. Therefore, it is necessary to start by defining the classification of bank erosion that we will adopt in this review (Figure 2). In this contribution, we use the failure mode to distinguish each type of bank collapse.

2.1. Flow-Driven Bank Erosion

2.1.1. Surface Flow Erosion

This type of erosion is quite common in sand- and silt-composed banks, and is also termed as *fluvial erosion* (Darby et al., 2007; Thorne & Tovey, 1981). Here, we use the general term *surface flow erosion* to include both fluvial and estuarine settings (Fagherazzi et al., 2004; Gong et al., 2018). Surface flow erosion can be defined as the removal of bank material by the water flowing near to the bank of a channel (near-bank channel flow), or over the bank surface itself (overbank flow). This type of erosion is commonly enhanced by subaerial processes (Rinaldi & Darby, 2007). The rate of erosion depends on near-bank and/or overbank hydrodynamics and bank soil erodibility. It is usually evaluated using an excess shear stress formula of the type (Partheniades, 1965):

$$E_l = K_l \left(\tau_b - \tau_c \right) \tag{1}$$

where E_l is the unit length erosion rate (m/s), K_l is the volumetric erosion coefficient for surface flow erosion (m³/N/s), τ_b is the boundary shear stress exerted by the flowing water (Pa), and τ_c is the critical shear stress for sediment erosion (Pa). Previous studies show a high degree of variability in τ_c, with values ranging from 0.001 to 2 Pa. Typically, the value of τ_c depends on the type and texture of sediment composing the bank, the presence of vegetation, etc. In particular, the two extreme values indicated for τ_c roughly correspond to very-erodible and slightly-erodible material, respectively (Hanson & Simon, 2001; Midgley et al., 2012; Simon & Thomas, 2002). The coefficient K_l can be assumed to depend on τ_c and estimated through the relation:

$$K_l = a \cdot \tau_c^{-0.5} \tag{2}$$

where *a* is a regression coefficient, taking the value of 0.2 according to Hanson and Simon (2001) and 0.1 according to Simon and Collison (2002). Nevertheless, a large variability is expected for *a* since, to our knowledge, Equation 2 has been calibrated on the basis of two relatively limited databases.
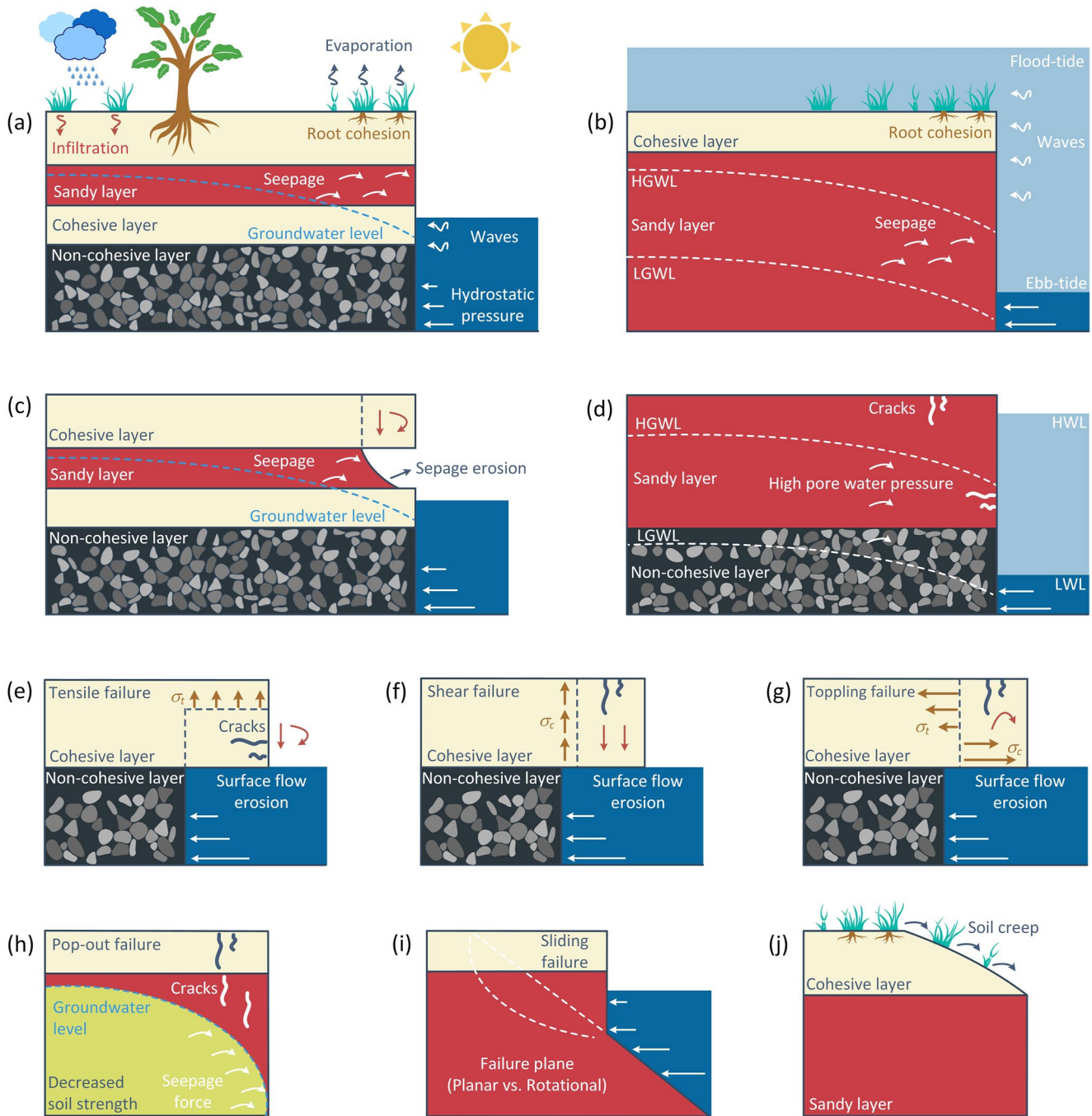
Figure 2. Sketch of typical bank configurations showing controlling factors in (a) fluvial and (b) tidal environments. Classification of bank retreat mechanisms and of the associated controlling factors: bank collapse induced by (c) seepage erosion and (d) water level changes; (e–g) cantilever failure resulting from (e) tensile, (f) shear, and (g) toppling mechanisms; (h) pop-out failure; (i) sliding failure with planar or rotational failure plane; and (j) soil creep. Here, σ_c and σ_t are the compressive stress and tensile strength, respectively, along the failure plane.

2.1.2. Seepage Erosion

Seepage erosion results from the entrainment of soil particles by subsurface flow (T. Dunne, 1990). An exit point/region on the bank surface is necessary for the soil particles to be dislodged from the bank interior (Wilson et al., 2007). Seepage erosion is commonly observed in layered streambanks (Figure 2c) where high infiltration rates cause the development of perched water tables between layers of varying hydraulic conductivity (Fox et al., 2007). Note that seepage erosion is often termed as *subsurface flow erosion*, *sapping*, *piping*, and *internal*

Table 1
Empirical Relations for Estimating Bank Retreat Rate Obtained From Laboratory Experiments

| | Coefficient | | | Units | | |
Type	K_s (or b)	a	R^2	Left	Right	References
Induced by seepage						
Dimensional form						
$E_m = bQ_s^a$	0.79	1.25	0.92	kg/s	cm³/s	Fox et al. (2006)[a]
	0.29	2.2	0.91	kg/s	cm³/s	Akay et al. (2018)[b]
	0.08	2.3	0.91			With fibrous protection
$E_m = K_s(i - i_c)^a$	0.04	1.2	0.54	kg/s	(−)	Chu-Agor et al. (2009)
$t_b = b \cdot i^a$	81.87	−1.43	0.91	min	(−)	Karmaker and Dutta (2013)
	150.57	−1.36	0.95			
	249.28	−1.42	0.93			
	2.08	−2.46		min	(−)	Masoodi et al. (2018)
Dimensionless form						
$q_s^* = K_s(\tau_s^*)^a$	584	1.04	0.86	(−)	(−)	Fox et al. (2006)
	90	4		(−)	(−)	Akay et al. (2018)
	25	5.4				With fibrous protection
$q_s^* = K_s(\tau_s^* - \tau_{cs}^*)^a$	584	1.04		(−)	(−)	Fox et al. (2007)
Induced by lateral flow						
$E_l = be^{at}$	Related to initial width, flow rate, and slope		0.88	cm/min	min	Qin et al. (2018)
				m/s	s	Wells et al. (2013)

[a]An average of the coefficients in Fox et al. (2006) is provided. [b]The coefficient in Akay et al. (2018) has been recalculated to ensure unit consistency. Variables are summarized in the list of Symbols.

erosion (Fox & Wilson, 2010; Wilson et al., 2013). Based on laboratory experiments, the rate of seepage erosion is typically quantified by an excess shear stress equation of the form (Fox et al., 2007):

$$q_s^* = K_s(\tau_s^* - \tau_{cs}^*)^a \tag{3}$$

where q_s^* is the dimensionless sediment flux ($= q_s/\sqrt{(\Delta - 1)gD^3}$, with Δ the ratio of bank soil density to water density, g the acceleration due to gravity (m/s²), and D the grain size of the bank material (mm)), τ_s^* is the dimensionless shear stress induced by the seepage flow ($= \frac{C_2'' U_d}{(s-1)K_{\text{sat}}\lambda_b}$, with C_2'' an empirical parameter depending on sediment packing, U_d Darcy's velocity (m/s), K_{sat} saturated hydraulic conductivity (m/s), and λ_b porosity of the bank material), τ_{cs}^* is the corresponding critical value for seepage erosion, K_s is the seepage erodibility coefficient, and a is an exponent. Table 1 reports the values suggested in literature for the empirical parameters K_s and a.

2.2. Bank Collapse

2.2.1. Tensile Failure

This type of failure occurs when the tensile stress induced by the weight of the lower part of a cantilever block exceeds the critical tensile strength of the bank soil (Thorne & Tovey, 1981). It is characterized by the presence of tension cracks on the portion of bank that is going to fail (Figure 2e). The detachment may also occur along a horizontal or arched surface under the action of a slight rotational component (Nardi et al., 2012). The collapse of bank material leads to the formation of an alcove-shaped surface, and therefore tensile failure is sometimes termed as *alcove-type failure* (Dapporto et al., 2003). Tensile failure is commonly observed when the upper bank is composed of cohesive layers or covered by vegetation (J. E. Pizzuto, 1984), the roots of which impart

considerable resistance to tensile stresses. In many studies, tensile failure has also been defined using the terms *undercutting* (Wilson et al., 2007), *soil fail*, and *shallow slide failure* (Dapporto et al., 2003).

2.2.2. Shear Failure

Shear failure occurs when the driving shear force, F_D, acting on a potential failure surface overcomes the resisting shear force, F_R. The analysis of this kind of failure is typically performed on the basis of a safety factor, F_S, defined as (Osman & Thorne, 1988):

$$F_S = F_R/F_D \tag{4}$$

Shear failure occurs when F_S is less than 1. The resisting forces are calculated by the sum of shear stress, τ (kPa), acting along the potential failure surface. This overall stress can be expressed by the relation (Fredlund & Rahardjo, 1993):

$$\tau = \left[c' + (\sigma - u_a)\tan\phi'\right] + \left[(u_a - u_w)\tan\phi^b\right] \tag{5}$$

where c' is the effective soil cohesion (kPa), σ is the total normal stress (kPa), u_a is the pore-air pressure (kPa), the difference $\sigma - u_a$ is the net (effective) normal stress, and ϕ' is the effective internal friction angle (°). The first term in square brackets on the right-hand side of Equation 5 represents the shear stress for saturated soils. The second term accounts for the additional effects which arise when the soil is partially saturated. Here, u_w is the pore-water pressure (kPa), $(u_a - u_w)$ is the matric suction in unsaturated soil (kPa), and ϕ^b is the angle expressing the rate of increase in strength relative to the matric suction (°). The value of ϕ^b is generally between 10° and 20°, and approaches ϕ' at saturation (Fredlund & Rahardjo, 1993).

Shear failure can be categorized into cantilever shear failures (Figure 2f) and sliding failure (Figure 2i). For a cantilever profile, shear failure is determined by shear acting along a vertical, or inclined, surface, thereby detaching the cantilever block as the crack propagates down from the bank top. This kind of failure is restricted to sandy soils of low cohesion or silty soils of high water-content (e.g., at bank-full stage or when the tidal plain is inundated, see Figure 1 in Zhao et al. (2020)) and to areas where the vegetation cover is sparse (Thorne & Tovey, 1981). For high banks, sliding failures are more common than other types of failure because shear stress increases with bank height faster than soil strength (Terzaghi, 1951). Sliding failures can be further subdivided into planar and rotational failures (Figure 2i), depending on the shape of the failure surface (Simon et al., 2000).

2.2.3. Toppling Failure

Toppling failure is characterized by a rotational component of movement (Figure 2g). It is also called *beam* or *slab failure* and is a very common mechanism in both fluvial and tidal environments (Allen, 1989; Francalanci et al., 2013; Nardi et al., 2012; Samadi et al., 2013). Toppling failure is accompanied by one or several deep tension cracks on the bank top, and eventually occurs when the moment along the failure plane overcomes the resistance provided by soil cohesion and/or vegetation roots (Van Eerdt, 1985). Contrary to cantilever shear failure, toppling failure is driven by excess moment rather than excess shear stress (see Figures 2f and 2g).

2.2.4. Pop-Out Failure

Pop-out failure (also called *tension failure*, see e.g., Fox and Felice (2014)) occurs when seepage forces are greater than soil resistance, or shear/tension strength decreases owing to an increased soil pore-water pressure (Figure 2h). Unlike seepage erosion characterized by particle entrainment and mobilization, pop-out failure consists of a block failure with the formation of tension cracks (Chu-Agor et al., 2008).

2.2.5. Erosion and Failure Resulting From Loss of Matric Suction

This type of processes occurs due to a loosening of the weak links between particles (especially sand) when the pores are saturated by water and the weight of bank soil increases (Nardi et al., 2012). This kind of failure differs from tensile failure because the bank soil is close to saturation. It can be regarded as the consequence of tensile failures and occurs at the endpoint of the commonly observed arched shape close to the water surface.

2.2.6. Soil Creep

Soil creep is a gravity-induced viscous-like slow deformation which produces a net downslope transport of bank soils (Figure 2j) and is commonly observed in salt-marsh banks (Mariotti et al., 2016, 2019). Although the

behavior is similar to shear failure, soil creep occurs at a much slower rate of deformation (around 20–50 mm/year, see Mariotti et al. (2019)).

3. Mechanisms Leading to Bank Retreat

Bank collapse can be triggered by subaerial process, surface flows which establish in fluvial and tidal environments, seepage flow, wind and ship waves, as well as by variations in soil strength (i.e., soil cohesion) resulting from water level changes, rainfall impacts and infiltration, and evaporation. Other factors such as vegetation root reinforcement and hydrostatic pressure head, in contrast, favor bank stability and so might affect the bank collapse mode. Based on experimental and in situ observations, here, we review mechanisms leading to bank collapse with respect to subaerial process, surface flow, seepage flow, fluctuations in soil pore-water pressure head, and waves, paying specific attention to the role of vegetation, biological disturbances, and hydrostatic pressure head.

3.1. Subaerial Process

Subaerial processes are commonly associated with the slow-motions driven by local climate variations that directly deliver bank soil to the channel, or which act as preparatory processes which weaken the face of the bank prior to surface flow erosion (Couper & Maddock, 2001). Their contribution to bank retreat has been analyzed by introducing the concept of "process zonation", that is, identifying the dominant factor among near-bank hydrodynamics, bank soil properties, vegetation cover, and local climate change (e.g., temperature and rainfall) (Abernethy & Rutherfurd, 1998; Henshaw et al., 2013; Lawler, 1992; Lawler et al., 1999).

In the middle and lower reaches of a river (horizontal zonation), fluvial erosion and bank collapse events dominate bank retreat, while subaerial erosion serves as a preparatory process reducing the resistance of bank soils by up to 80% of their original strength (Kimiaghalam et al., 2015; Wynn et al., 2008). In contrast, bank retreat is controlled by subaerial processes in headwater streams or where hydrodynamic power is insufficient to cause soil erosion without prior weakening of bank materials (Prosser et al., 2000; Veihe et al., 2011). For example, it has been demonstrated that 85% of the annual retreat of coastal cliffs in a cold temperate climate may occur due to subaerial erosion (Bernatchez & Dubois, 2008). Similarly, direct measurements carried out in bedrock rivers show that the lateral bank retreat can be substantially enhanced by the higher erodibility of rock exposed to continuous wetting-drying cycles (Montgomery, 2004). Subaerial erosion typically affects the upper part of the bank while the lower part is subject to fluvial erosion. This gives rise to a vertical zonation of the controls of bank erosion which eventually determine the bank morphology depending on the soil characteristics (e.g., the silt-clay content (Couper, 2003; J. Pizzuto, 2009; Veihe et al., 2011)).

Overall, subaerial processes may play a fundamental role in bank retreat. Repeated wetting-drying cycles (leading to associated desiccation) and freeze-thaw sequences are widely recognized as major subaerial processes in both fluvial and estuarine systems (Bernatchez & Dubois, 2008; Couper & Maddock, 2001). Wetting of bank soils is generally the result of prolonged high flows, exchanges between surface water and groundwater (due to water level variations), and infiltration of precipitation (Simon et al., 2000; Xin et al., 2022). This process affects bank retreat by increasing soil pore-water pressure with a consequent weakening of the linkage between soil particles (e.g., matric suction mentioned by Nardi et al. (2012)) which eventually makes the bank soils more susceptible to surface flow erosion (Zhao et al., 2020). We refer the reader to Section 3.4 for more details about this mechanism. On the other hand, the reduction in soil-moisture content associated with drying may lead to soil desiccation with consequent fissuring and exfoliation of the bank surface (Figure 3a). The strength of the bank is therefore weakened, especially for cohesive banks where soil aggregates are separated by desiccation cracks (Couper, 2003; Thorne & Tovey, 1981). For example, in the St. Lawrence River, desiccation followed by a rapid rewetting was found to increase bank retreat rate by several orders of magnitude (Gaskin et al., 2003).

Freezing periods cause an expansion of water within soil voids which weakens the linkage between soil particles, while the subsequent thawing action directly induces subaerial erosion (Yumoto et al., 2006). Short-duration of freeze-thaw successions facilities the growth of needle-ice on the bank face (Figure 3b), while annual freeze-thaw cycles may lead to the development of deep cracking and, consequently, soil mass failure (Kimiaghalam et al., 2015; Lawler, 1993b). In general, freeze-thaw cycles play an important role in subaerial erosion in regions where the bank is subject to deep seasonal frost (Chassiot et al., 2020). Although the number of freeze-thaw cycles is likely the major factor for subaerial erosion (Kimiaghalam et al., 2015; Wynn et al., 2008), several
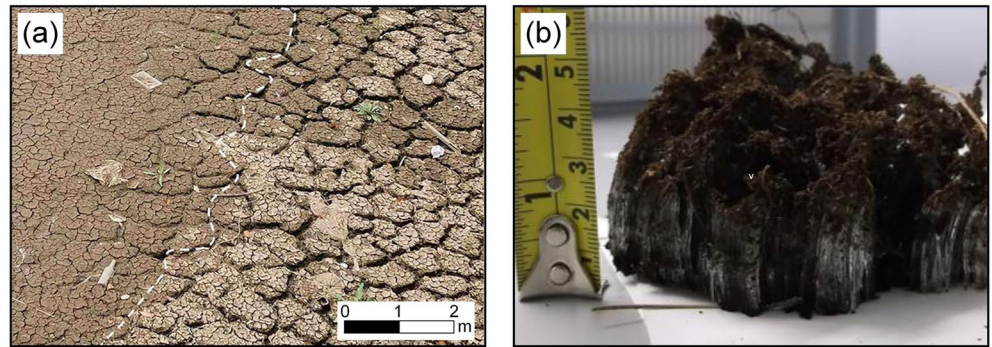
Figure 3. (a) Soil desiccation on a muddy bank. The wet (left) and dried (right) mud areas are distinguished by the white dashed line (adapted from Zeng et al. (2022)). (b) Typical needle ice formation under freeze-thaw cycles (adapted from C. Li et al. (2018)).

studies have also highlighted that silt-clay content (Couper, 2003), soil water content (Ferrick & Gatto, 2005), and vegetation cover (Prosser et al., 2000; Wynn & Mostaghimi, 2006) matter as well. Banks with a higher soil moisture and silt-clay content are more affected by freeze-thaw cycles, while vegetation cover dramatically reduces the frequency of these cycles.

3.2. Surface Flow

3.2.1. Near-Bank Channel Flow

Near-bank channel flow is generally responsible for the removal of soil particles from the bank. For high enough flow velocities, this removal may undermine the bank toe, eventually leading to the formation of a bank profile with cantilever-shape (Thorne & Tovey, 1981). Samadi et al. (2011) carried out several flume experiments using soil blocks of silt and silt-clay, respectively, to mimic the actual bank configuration caused by artificially reproduced undermining. The observed failure process included: (a) tensile failure in the lower part of the bank; (b) tension cracks on the bank top; and (c) toppling failure forming a vertical cracked interface (Figure 4a). The flume experiments also suggested that the pattern of cantilever failure is dominated by toppling failure rather than the simple shear-type mechanism considered by Darby et al. (2007) and Rinaldi et al. (2008).

To overcome the drawbacks induced by an artificially reproduced undermining, several downscaled physical experiments have been conducted in recent years under conditions of uniform and steady flow. Patsinghasanee et al. (2018) used two types of cohesive materials with different silt-clay contents to investigate the process of bank collapse under similar hydraulic conditions. The observed failure sequence was similar to that reported by Samadi et al. (2011). The tension cracks on the bank top seemed to develop only when the cantilever was close to failure. A slight increase in silt-clay content was found to have negligible effect on bank failure patterns, but could significantly shorten the time taken to collapse. A number of studies have been also carried out to investigate the role of impulsive flow due to dam-breaks (Cantelli et al., 2004; Zech et al., 2008), near-bank bed evolution (Yu et al., 2015), bank height (Patsinghasanee et al., 2017), channel bed slope (Qin et al., 2018), and near-bank turbulence (Das et al., 2019; Roy et al., 2019). Even though the focus of Qin et al. (2018) was gully erosion, this type of process can be regarded as a downscaled case of bank erosion relevant also for tidal environments (e.g., for channel head migration). It is however worthwhile to note that downscaled physical models are useful to obtain general information on bank failure patterns (D. M. Wood, 2014), but entail uncertainties about the interpretation of the collected data which restrict their use in formal quantitative analysis. For example, tension cracks on the surface of the bank (Figure 4a), and the consequent tensile failures documented by Samadi et al. (2011) are not observed in many downscaled experiments. Besides, only a few of the existing downscaled physical experiments attempted to capture variations in bank soil parameters (e.g., soil stress and pore-water pressure) occurring during bank collapse.

Recently, Zhao et al. (2020) set up a laboratory experiment with limited scaling effects to investigate the role of bank height, H_b, and near-bank water depth, H_w, on bank collapse. Results showed that the failure patterns correlate to the ratio H_w/H_b (i.e., the relative water depth). For relatively small values of H_w/H_b (less than 0.5,
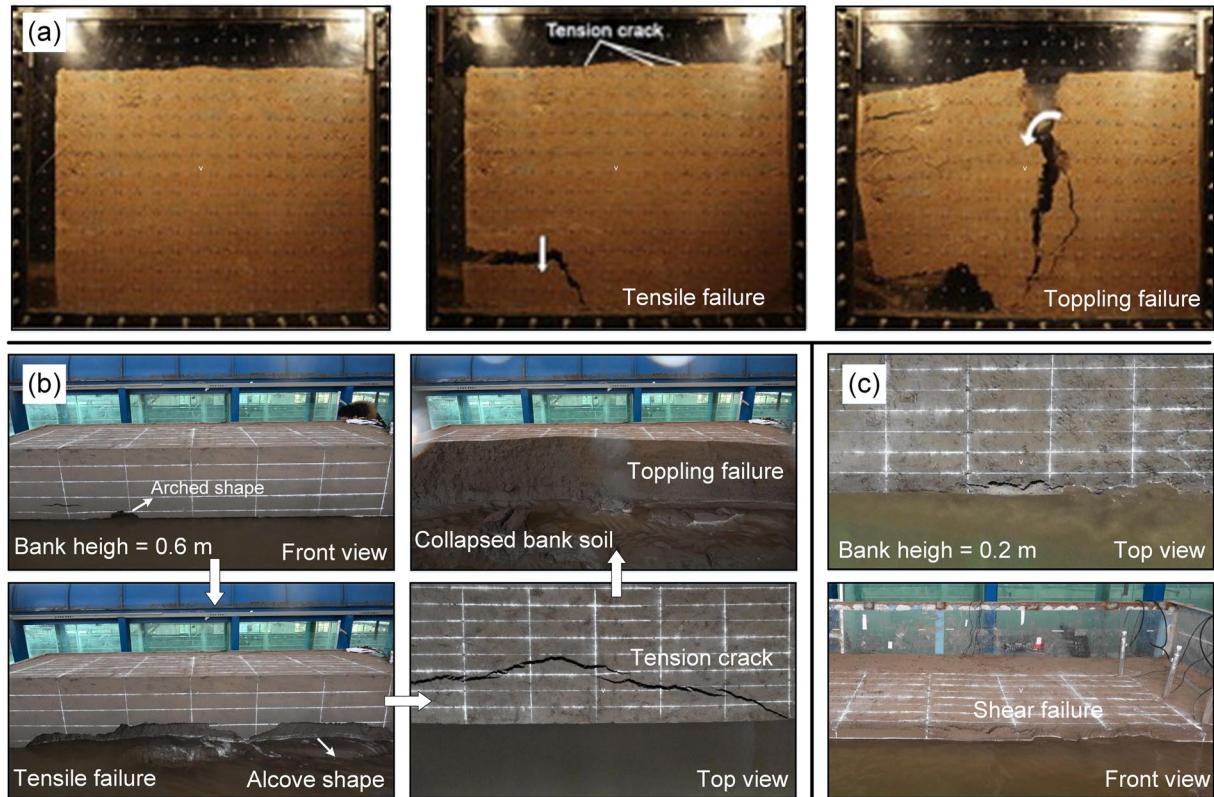
Figure 4. (a) Typical overhanging failures in response to artificial undermining (adapted from Samadi et al. (2013)). Bank height in subplot (a) was 0.8 m. (b and c) Typical erosion and failure processes experienced by vertical banks in response to near-bank channel flow, for a water depth of 0.15 m, and bank height of (b) 0.6 m and (c) 0.2 m (adapted from Zhao et al. (2020)).

Figure 4b), the decrease in matric suction led to the occurrence of cracks and consequent tensile failures. Several deep tension cracks were observed on the bank top, followed immediately by toppling failure. For values of H_w/H_b close to 1 (Figure 4c), tension cracks were first observed on the bank top. A large (compared to the stress exerted by soil weight) hydrostatic pressure head prevented the occurrence of toppling failure. Shear failures thus occurred along a vertical (or inclined) surface separating the cantilever block from the bank top. Extending the experimental analysis to a broader range of values of the ratio H_w/H_b, K. Zhang et al. (2021) further pointed out the need to include water content variation when predicting shear or toppling failure. Their experimental framework provides a new way to predict failure patterns by combining hydraulic and geotechnical control factors.

Natural rivers usually convey bedload and/or suspended load downstream. The transported grains, in turn, stresses the channel bed/bank, possibly affecting bank retreat. Bedload saltation produces an abrasion of the exposed bank surface. The development of an alluvial cover due to bed aggradation alters the cross-sectional distribution of shear stresses affecting indirectly bank retreat. Field and laboratory evidence of abrasion-induced bank retreat is plentiful in bedrock rivers (see e.g., the shallow depressions in Figure 5a), where the channel bed and banks often consist of rocks covered by a thin layer of alluvium (Carter & Anderson, 2006; Fuller et al., 2016; Hartshorn et al., 2002). The direct bumping and abrasion by saltating grains can increase channel width by up to an order of magnitude as compared to channels with negligible bedload (Baynes et al., 2020; Fuller et al., 2016). On the other hand, bank retreat of bedrock channels can be indirectly affected by the increased bed roughness which characterizes the formation of an alluvial cover. Experimental observations have shown that this increase in roughness enhances the deflection of saltating bedload particles toward the bank surface (Figure 5b and 5c), causing rates of lateral erosion to grow by as much as a factor of 7 (Fuller et al., 2016).

The effects of alluvial cover on bank retreat depend also on the channel planform (e.g., meandering, braiding, and pinch-swell undulation), which strongly reflects on flow and sediment routing (Carter & Anderson, 2006; Mishra et al., 2018). In braided gravel-bed channels, lateral incision is weakly sensitive to the rate of sediment
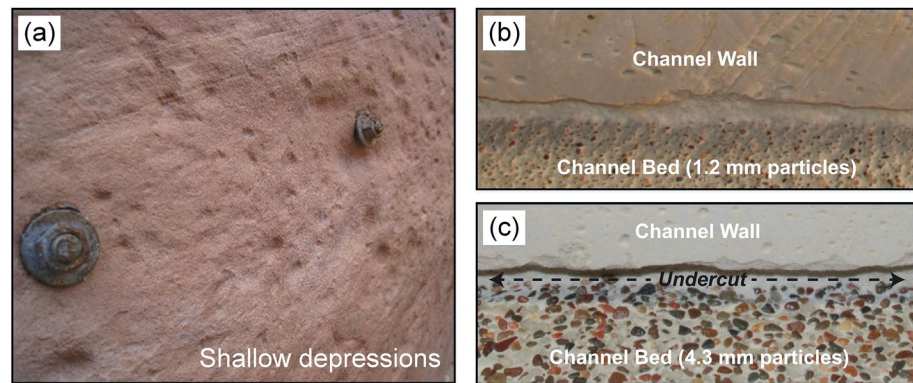
Figure 5. (a) Field evidence of bedrock wall erosion by sediment impacts. (b and c) Laboratory evidence showing the role of bed roughness on bedrock wall erosion (adapted from Fuller et al. (2016)).

transport (Bufe et al., 2016, 2019). Conversely, in sharp bedrock bends an increased sediment supply accelerates bank retreat and shifts its location upstream (Mishra et al., 2018). In bedrock channels, the development of an alluvial cover alters the cross-sectional distribution of shear stress, ultimately leading to a transition from vertical incision of the rocky bed to lateral expansion due to bank retreat (Turowski et al., 2008). As a result, a substantial sediment supply not only leads to the formation of a significant alluvial cover but is commonly accompanied by a fast lateral bedrock erosion (Finnegan et al., 2007; T. Li et al., 2020).

In alluvial meandering rivers, high sediment loads favor a rapid accretion of the point bar at the inner bank, which forces erosion at the outer bank (bar push effects) and consequently enhances the annual migration rate (Constantine et al., 2014; Donovan et al., 2021; E. Eke et al., 2014). On the other hand, nearly clear water conditions associated with a scarce sediment supply facilitate a progressive incision of the channel bed, which causes outer bank instability and ultimately speeds up meander migration. For example, the sharp reduction in sediment supply (around 80%) caused by upstream damming was responsible for the increased bank retreat rate observed in the Jingjing Reach of the Changjiang River over the last 20 years (Xia, Zong, Zhang, et al., 2014; Xia et al., 2017).

Overall, sediment load plays a vital role in the bank retreat process, and more research is needed to quantify its contribution to bank retreat rate.

In cold environments, the failure by near-bank channel flow may be also affected by soil deterioration (i.e., freeze-thaw cycles) and the formation of ice blocks, which has been proven to be important especially in coastal and estuarine settings (Bernatchez & Dubois, 2008). The collapsed ice blocks may be swept away at high tide, thus further enhancing bank erosion by attacking the bank surface and by undercutting bank materials, while during ebb tides they add friction to the system (Black et al., 2018). We refer the reader interested in erosion processes in cold environments to Chassiot et al. (2020), who systematically evaluated and summarized the effects of ice on bank retreat. Another mechanism resulting in the formation of a cantilever is found in marine ice cliffs, where the cantilever is caused by the action of warmer deep water (DeConto & Pollard, 2016). Regardless of the peculiarities of cold environments, bank collapse processes are still detected whereby the cliff evolution is related to cliff height and water depth (Bassis et al., 2021).

3.2.2. Overbank Flow

Overbank flow occurs over the bank surface, as commonly observed in gullies and tidal channels, and controls headcut retreat in these environments. Gully headcuts, characterized by near-vertical steps, form often in dry-hot valleys as concentrated overland flow initiates erosion on a gully bed composed of a hard-upper layer and a soft-lower layer (A. Chen et al., 2013; Rengers & Tucker, 2014). When passing over the overhanging block (Figure 6a), the
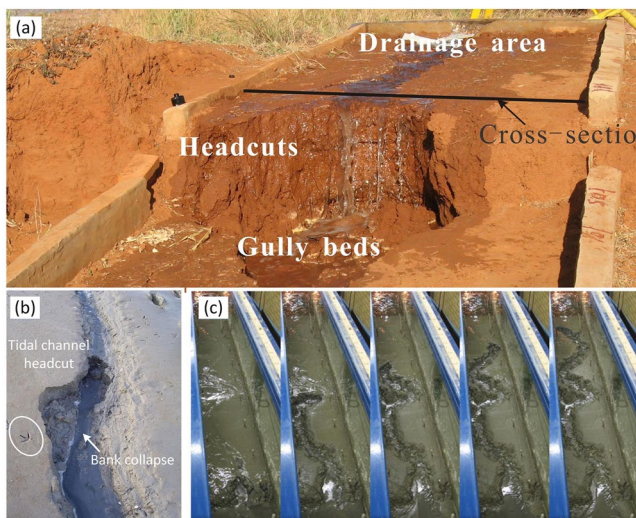
Figure 6. Headcut retreat for: (a) gully and (b and c) tidal channel head. In panel (a), the length and width of the drainage area are 5 and 2 m, respectively, and the initial headcut height is 0.5 m. In panel (b), the circled bird footprint is about 0.04 m. In panel (c), the width and length of the flume are 0.4 and 2 m, respectively, and the time between each snapshot is 6 hr (adapted from Dong, Xiong, et al. (2019) and Kleinhans et al. (2009)).

overbank flow either moves along the sidewall scouring the overhanging profile (on-wall runoff) or directly falls into the channel forming a plunge pool (off-wall runoff). With the development of scouring erosion in the lower headcut layer, the overhanging block gradually becomes larger, ultimately triggering different types of mass failure such as tensile, sliding, and toppling (A. Chen et al., 2015). In the presence of a vegetation cover, tensile failure occurs in the middle face of the headcut below the root zone, leaving behind an overhanging block. Failure takes place when block weight exceeds vegetation root strength (Rengers & Tucker, 2014).

Experimental studies have addressed the development and migration of gully headcuts with emphasis on different factors such as bed slope (Bennett, 1999), flow discharge (Bennett et al., 2000), and soil texture (Wells et al., 2009). Several studies focus on mass failure rather than plunge pool erosion. For example, Stein and LaTray (2002) set up a specific gully bed where a relatively erosive base soil is overlaid by a relatively hard soil layer. For this geometry, mass failures were observed as a result of undercutting in the plunge pool immediately downstream. Experimental and in situ studies have also been conducted to investigate the failure process of headcuts in response to on-wall runoff. A. Chen et al. (2013) performed flow scouring experiments with a set-up involving a lower sandy layer and an upper clay layer. Results showed that the collapse of overhanging layers was dominated by the development of the lower scour holes. The occurrence of upper cracks significantly accelerated the collapse process. Compared to off-wall runoff, on-wall runoff played a more important role in the development of scour holes, and headcut collapse was found to depend on runoff duration rather than runoff intensity. This implies that variations in soil strength, rather than cantilever development, are responsible for mass failure, since soil cohesion decreases dramatically with the increase in soil moisture (Rajaram & Erbach, 1999). Similar findings emerged from the in situ observations of Rengers and Tucker (2015), who pointed out that high water content rather than hydraulic scour was the main cause for mass failure. Other factors such as summer flash floods, winter snowmelt, prolonged summer dry periods, and drying-rewetting cycles can also be correlated with headcut collapse (Dong, Xiong, et al., 2019; Rengers & Tucker, 2014). For instance, Dong, Xiong, et al. (2019) conducted 11 *in situ* flow scouring experiments with different discharges. Results showed that the variation in discharge had little effect on mass failure frequency, whereas drying-rewetting cycles accounted for 64% of the observed mass failure. We refer the reader to J. Poesen et al. (2003), Valentin et al. (2005), and Castillo and Gómez (2016) for more information on gully headcut erosion.

Similar to gully headcuts, but with a much smaller spatial scale, a fast retreat of tidal channel heads is commonly observed on tidal flats. Symonds and Collins (2007) reported an annual headcut retreat rate of up to 400 m/year in response to a managed coastal realignment. Through laboratory experiments and in situ observations, Kleinhans et al. (2009) found that the retreat of tidal channel heads was induced not only by gradual erosion of the channel bed, but also by repeated cantilever or sliding failures at the headcut border typical of cohesive sediments (Figures 6b and 6c). They also concluded that the failure was mainly related to soil weakness induced by waves, rain, or excess pore-water pressure. Other studies have been carried out to investigate the role of tidal channel headcuts on, for example, the evolution of tidal flats (Ni et al., 2014), tidal channels (Xu et al., 2019), and tidal networks (Geng et al., 2019; Kleinhans et al., 2012; Xu et al., 2017).

3.3. Seepage Flow

Bank collapse related to seepage flow can be attributed directly to seepage erosion and resultant tensile failure (direct influence), or indirectly to the effects of seepage flow on soil properties (indirect influence) (Fox & Wilson, 2010). Since the indirect influence is mainly related to soil pore-water pressure, we refer the reader to Section 3.4 for more details. To mimic bank collapse in response to seepage erosion, Fox et al. (2006) and Wilson et al. (2007) performed lysimeter experiments using reconstructed banks packed with three different soil layers (Figure 7). They suggested that increasing bank height, or hydraulic head, leads to more bank retreat (i.e., a decrease in bank stability), and alters the associated pattern of bank collapse. For large bank heights and high hydraulic heads, they observed a sequence of seepage erosion at the bank toe, tensile failure in the middle of the bank, and toppling failure. For small bank heights and low hydraulic heads, tensile failure was absent and bank erosion was sometimes characterized by seepage erosion (i.e., no toppling failure occurred).

A series of studies were also carried out to investigate how seepage flow erosion is affected by bank slope (Fox et al., 2007), soil density (soil texture) (Chu-Agor et al., 2008; Fox & Felice, 2014), bank stratification (Lindow et al., 2009), root reinforcement (Akay et al., 2018; Cancienne & Fox, 2008), and soil chemical properties (Masoodi et al., 2017, 2019). Cancienne and Fox (2008) found that, under the same hydraulic conditions,
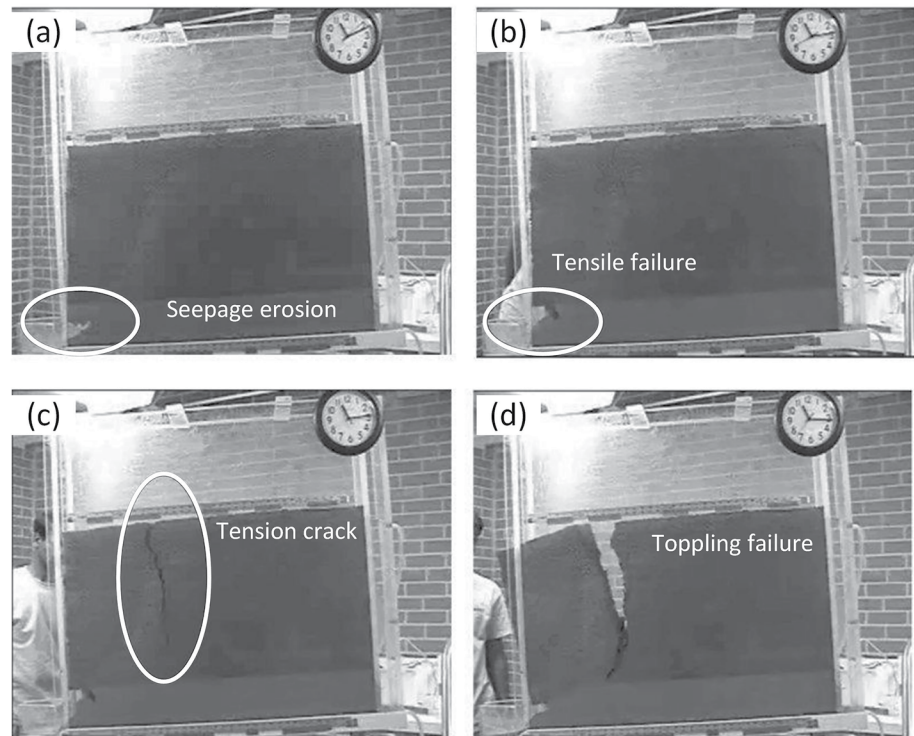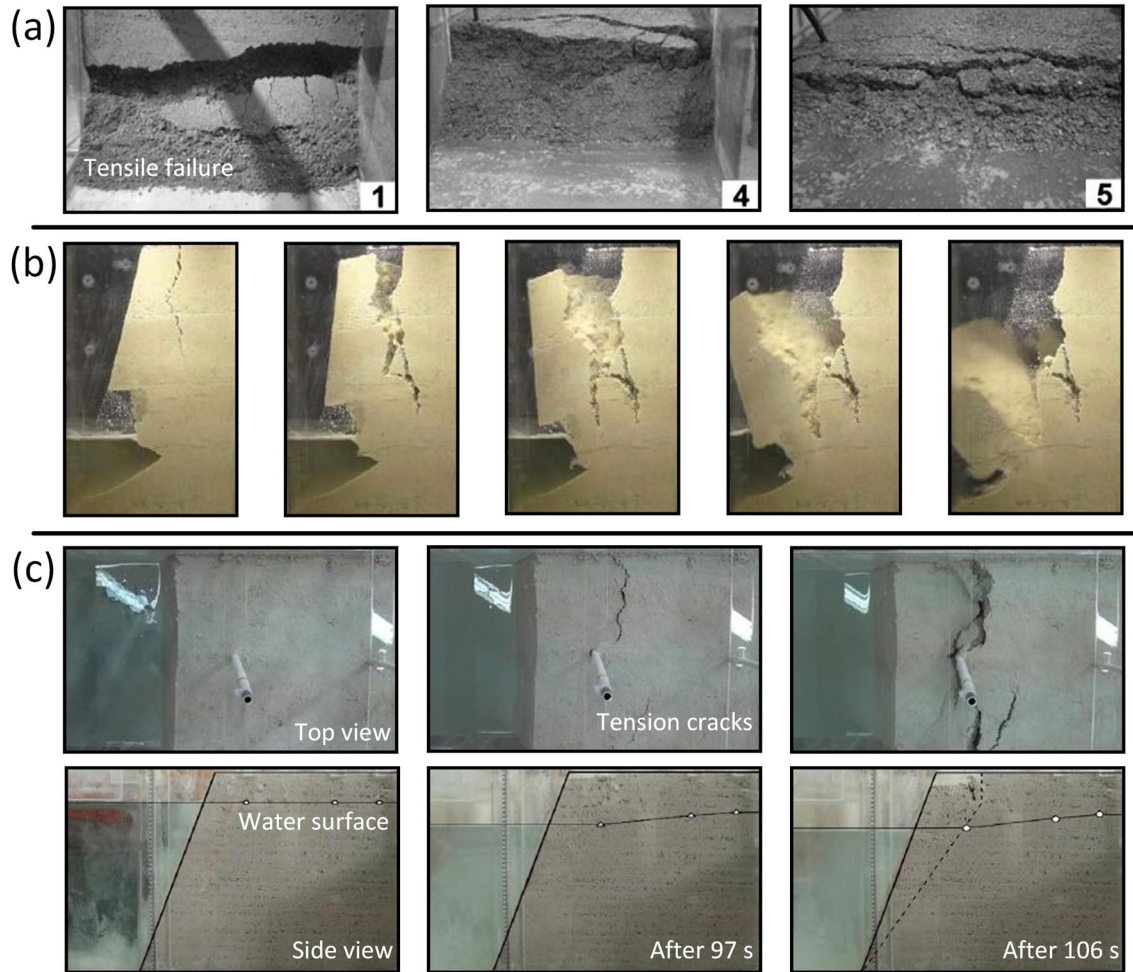
Figure 7. Erosion and failure processes of river banks in response to seepage: (a) seepage erosion; (b) tensile failure in the middle of the bank; (c) tension cracks on the bank top; and (d) toppling failure. Bank height is 0.8 m, and seepage flow within the bank body is from right to left (adapted from Fox et al. (2006)).

seepage erosion and undercutting patterns exhibit remarkable differences in vegetated and unvegetated contexts. Unlike their unvegetated counterparts, vegetated bank blocks were characterized by the absence of unimodal undercutting (see Figure 2 in Chu-Agor et al. (2008)) and the formation of shallow multimodal cuts along the entire width of the bank face. To evaluate and predict the development of seepage erosion followed by toppling failure or the triggering of pop-out failure, Fox and Felice (2014) proposed a dimensionless seepage mechanism number based on the ratio between resistive cohesion forces and destabilizing forces. This number reasonably predicted the type of observed seepage failures, and is suitable for streambanks or hillslopes experiencing steady seepage forces. On the basis of in situ observations, Masoodi et al. (2019) found a high correlation coefficient ($R^2 = 0.81$) between soil dispersion (see Glossary) and the volume of the undercutting cavity caused by seepage. At the same time, many studies aimed at developing empirical sediment transport functions relating seepage erosion rates to controlling factors (Chu-Agor et al., 2008, 2009; Fox & Felice, 2014; Fox et al., 2006, 2007; Karmaker & Dutta, 2013; Wilson et al., 2007). For example, on the basis of 71 lysimeter experiments, Karmaker and Dutta (2013) suggested that the seepage flow gradient and the vertical stratigraphy have a dominant effect on bank stability. We refer the reader to Section 4.1 for more details about these empirical relations.

3.4. Fluctuations in Soil Pore-Water Pressure

The bank soil tends to be unsaturated above the water surface and saturated below the water surface. In tidal settings, due to the periodical rising and falling of the water level, this difference is less evident (e.g., when the water level in tidal channels is just below the elevation of the bank top during the early stage of the ebb tide, see Figure 1 in Zhao et al. (2020)). For unsaturated soils, increasing soil pore-water pressure implies a smaller matric suction and hence reduced soil strength. For saturated soils, the matric suction is zero and the soil shear strength ultimately depends on the effective normal stress. The transition from saturated to unsaturated soil (and vice versa), clearly indicated by soil pore-water pressure, is mainly driven by variations in water level, and often leads to bank collapse. For example, Nardi et al. (2012) investigated the basic processes and possible factors influencing the instability of relatively coarse (sandy-gravel) river banks in response to water

Figure 8. Erosion and failure processes of river banks in response to water level (a and b) rising and (c) falling. (a) Coarse sandy-gravel bank of height 0.7 m; (b) fine sand bank of height 0.5 m; and (c) compacted sand bank of height 0.47 m (adapted from Nardi et al. (2012), Arai et al. (2018), and Chen, Hsieh, and Yang (2017)).

level changes (Figure 8a). Contrary to cohesive banks, for which bank failure is commonly observed during the falling water stage (saturated-unsaturated transition), they suggested that the reduction of apparent cohesion (e.g., matric suction) during the rising water stage (unsaturated-saturated transition) caused the instability of the banks. This finding indicates an inherent difference in bank failure mechanisms between sandy-gravel and sand-clay banks, arising from the distinct response of soil strength to very high water-content. In contrast to clay soils, silt is prone to losing almost all strength (i.e., static liquefaction) when approaching a saturated state (Yamamuro & Lade, 1998). Using finer cohesionless uniform sand, Arai et al. (2018) observed more cantilevers and, consequently, toppling failures as a result of the stronger apparent cohesion and tensile strength (Figure 8b). They also stated that dry granular flow, as reported by Nardi et al. (2012), was absent, emphasizing the role of soil grain size on bank collapse patterns.

For cohesive banks and decreasing water levels, Francalanci et al. (2013) observed that excess pore-water pressure and decreasing hydrostatic pressure head could trigger tensile failures in the middle part of banks mimicking marsh cliffs. In tidal environments, these two pressures tend however to counterbalance at high tides. C. Chen, Hsieh, and Yang (2017) and Khatun et al. (2019) both stated that a rapid drawdown was a major cause for sand-compacted bank instability (Figure 8c). However, the main cause of bank failure with respect to water level drawdown is still unclear. Two destabilizing effects are in fact triggered during a falling water stage (Simon et al., 2000). On one hand, the drawdown of water level implies a progressive reduction of the stabilizing action exerted by the hydrostatic pressure head. On the other hand, positive pore-water pressure leads to a reduction in soil shear strength. Applying stress-strain analysis and taking into account varying hydrostatic pressure head,

Gong et al. (2018) concluded that bank retreat rate is partly related to the rate of water level change. In particular, the maximum bank retreat was found to occur in conjunction with the maximum rate of decrease in hydrostatic pressure head. Deng et al. (2018) demonstrated that pore-water pressure, resulting from the delay between groundwater level and river stage, was mainly responsible for shear-type bank collapse. For banks with relatively low soil permeability, the initial groundwater level may also play an important role in controlling bank stability. Anyhow, bank instability caused by a falling water stage might in general be related to bank geometry, stratigraphy, and soil properties such as soil density and permeability (Pollen-Bankhead & Simon, 2010). Further research is needed to fully unravel the failure mechanism with respect to water level drawdown.

Other factors such as evapotranspiration and infiltration (induced by vegetation, seepage and rainfall) can cause fluctuations in soil pore-water pressure and thus are also likely to affect bank stability. Vegetation affects soil pore-water pressure either by extracting soil moisture via evaporation, or by intercepting rainfall that would otherwise infiltrate into the bank. Both processes potentially reduce positive pore-water pressure and instead facilitate the development of matric suction. For instance, Simon and Collison (2002) and Pollen-Bankhead and Simon (2010) pointed out that the variation in matric suction due to evapotranspiration might provide more benefits to riverbank stability than the mechanical effects associated with vegetative root reinforcement. Given the timescale, evapotranspiration may be relevant in fluvial environments, while it likely plays only a minor role in tidal settings. Indeed, the period during which the salt marsh surface is inundated could be too short for evapotranspiration to result in clear reductions in matric suction. Nevertheless, Dacey and Howes (1984) observed that marsh plants might lower the water table and reduce pore pressure very quickly. Their findings identified a new mechanism for salt-marsh bank stability whereby the generation of excess pore-water pressure and removal of hydrostatic pressure during the ebb tide are counteracted by a quick increase in matric suction. Wynn and Mostaghimi (2006) suggested that vegetation covers facilitate stream bank stability not only by intercepting rainfall, but also by reducing subaerial processes such as soil desiccation and freeze-thaw cycles, which make the banks more vulnerable to surface flow erosion (Chassiot et al., 2020). However, as pointed out by Durocher (1990), canopy interception and stemflow can concentrate rainfall locally around the plant roots, determining local highs of pore-water pressure which weaken bank stability.

Seepage flow has also been suggested to affect soil pore-water pressure and, consequently, bank stability. Fox et al. (2006) observed a sharp increase in soil pore-water pressure owing to the transition from unsaturated to saturated conditions caused by seepage, followed immediately by several bank failures. Lindow et al. (2009) found that variations in soil pore-water pressure consequent to seepage depend on the initial bank slope. For banks with a gentle slope, a relatively small increase in soil pore-water pressure is sufficient to trigger bank collapse (Fox & Wilson, 2010). In tidal settings, seepage flow due to diurnal changes of water level is responsible for periodic transitions from unsaturated to saturated conditions and vice versa. In the presence of high water levels (e.g., inundating tides and large river flow), water overtops and enters through the creek bank, making at least part of the bank soil fully saturated. This process is possibly enhanced by a higher permeability of the upper soil layer, as a result of macropores created by plant root and organism burrowing (Harvey et al., 2019; Xin et al., 2022). In contrast, groundwater gradually seeps out from the bank during falling tides and, together with high evapotranspiration (due to some combination of sun, wind and temperature), can lead to complete drying or, even desiccation of bank material (Derksen Hooijberg et al., 2019; McKew et al., 2011). The drying-wetting of tidal channel banks and marsh edges during tidal cycles thus plays a key role on retreat processes in tidal environments.

Finally, infiltration of rainfall may lead to a loss of matric suction and, therefore, may reduce bank soil strength and bank stability (Simon et al., 2000). Using a prototype model, Okura et al. (2002) showed that the generation of excess pore-water pressure as a result of continuous rainfall infiltration resulted in bank instability and landslide fluidization. For tidal environments, Mariotti et al. (2019) observed that creep movement of a salt-marsh bank was more accentuated during rainfall events. Therefore, they suggested that this behavior is likely governed by effective stresses and their dependence on pore water pressure. L. Z. Wu et al. (2017) investigated the role of rainfall intensity on the development of pore-water pressure. Results showed that increasing rainfall intensity facilitated the development of high soil pore-water pressure, possibly producing gravity-driven landslides. A review of slope stability analysis under rainfall-driven infiltration, with a focus on conceptual models, analytical analysis, and numerical modeling, has also been undertaken by L. L. Zhang et al. (2011).

3.5. Waves

Bank instability is also caused by the attack by wind waves and ship wakes in rivers, salt marsh channels, and navigable waterways. The associated mechanisms of bank collapse can be attributed to (a) terrace erosion adjacent to the bank toe, (b) removal of soil particles from the bank (wave erosion), (c) mechanical fatigue of the bank soil, and (d) changes in soil pore-water pressure. On the basis of in situ experiments, Nanson et al. (1994) found that for small rivers, boat-generated waves may dominate bank erosion as compared to surface flow erosion and seepage erosion. Duró et al. (2019) reported that, for a relatively constant water level, boat-induced waves caused the formation of a mildly-sloping terrace adjacent to the bank toe, which progressively dominated the bank erosion process. Emergent vegetation however plays a significant role in reducing wave erosion by attenuating the wave impact (Coops et al., 1996) and reinforcing the soil through the root system (Gabel et al., 2017).

Sunamura (1982) designed a laboratory experiment to investigate wave erosion mechanisms at the base of a beach cliff. He found that turbulence due to wave runup destabilized the sand and generated a shear stress on the cliff face, leading to cliff erosion/collapse. To quantify the relative importance of vessel-generated versus wind waves to salt marsh cliff retreat, Houser (2010) carried out a field study in the Savannah River. He found that locally generated wind waves were largely responsible for the observed cliff retreat. In the case of soil-geotextile filtration, Faure et al. (2010) observed that erosion of the middle part of revetments was induced by the up-and-down drag force exerted by waves along the bank. More recently, studies have been carried out by Ji et al. (2017, 2019) to investigate the role of bank profile morphology on the stability of reservoir banks. Under the action of wave erosion, a concave cavity was found to occur near the water surface, leading to tension cracks on the bank top and consequent toppling or sliding failures. Using the width of the collapsed portion of the bank as a metric, they concluded that a convex shape was the most unfavorable condition for bank stability, followed by a concave shape, straight shape, and a multi-stepped shape. Contrary to surface flow erosion, wave erosion occurs only around the water surface and so results in a large underwater shoal, which in turn provides resistance to bank collapse. As a result, this kind of failure mechanism is episodic and essentially inactive until the submerged bank toe is removed by other processes such as surface flow erosion or artificial dredging.

Apart from direct erosion under wave attack, bank soil may also be rendered unstable as a result of mechanical fatigue in response to wave loading (Coops et al., 1996; Hooke, 1979). Ginsberg and Perillo (1990) reported that the continuous impinging due to locally-generated waves may lead to mechanical fatigue, significantly reducing channel bank stability. To gain more insight into the effect of dynamic wave loads, Bendoni et al. (2014) developed a theoretical model to account for the instantaneous action of waves rather than averaging the waves over long time intervals. Contrary to a simple static model, the dynamic response can account for the elastic potential energy and inertial effects, resulting in higher stress and consequently predicting more rapid bank failure. Using laboratory experiments, they also concluded that water inside the tension cracks and low water levels in front of the bank were the two most favorable conditions to trigger bank collapse.

High excess pore-water pressures inside the bank, triggered by cyclic wave loadings, can also be an important cause for upper bank collapse (Faure et al., 2010). Francalanci et al. (2013) carried out a prototype laboratory experiment to reproduce salt marsh cliff retreat under the combined action of tides and wind waves. The successive development of tension cracks and upper bank deformation, tensile failure in the middle of the front surface, and toppling failure was the typical succession of the observed failure processes (Figure 9a). This kind of failure sequence is similar to that experienced by banks in response to surface flow (Patsinghasanee et al., 2018; Samadi et al., 2011), seepage flow (Fox et al., 2006; Wilson et al., 2007), or water level changes (Arai et al., 2018; Nardi et al., 2012). Overall, this shows that external forces operating in different environmental contexts may have similar effects on bank stability, leading to similar failure mode(s). Although in the experiments of Francalanci et al. (2013) tidal cycles were the main reason for crack formation and upper bank deformation, the authors suggested that wind waves are likely to provide an additional mechanism accelerating the occurrence of bank collapse. Any overtopping waves are in fact likely to induce water infiltration within the tension cracks on the bank top and promote the occurrence of extra pore-water pressures inside the bank. They also pointed out that the presence of vegetation roots made some notable differences (Figure 9). For instance, tension cracks on vegetated banks were generally smaller and narrower, and measured pore-water pressures at low tides were generally lower (10% decrease) than when vegetation was absent, both factors contributing to delay the occurrence of bank collapse.
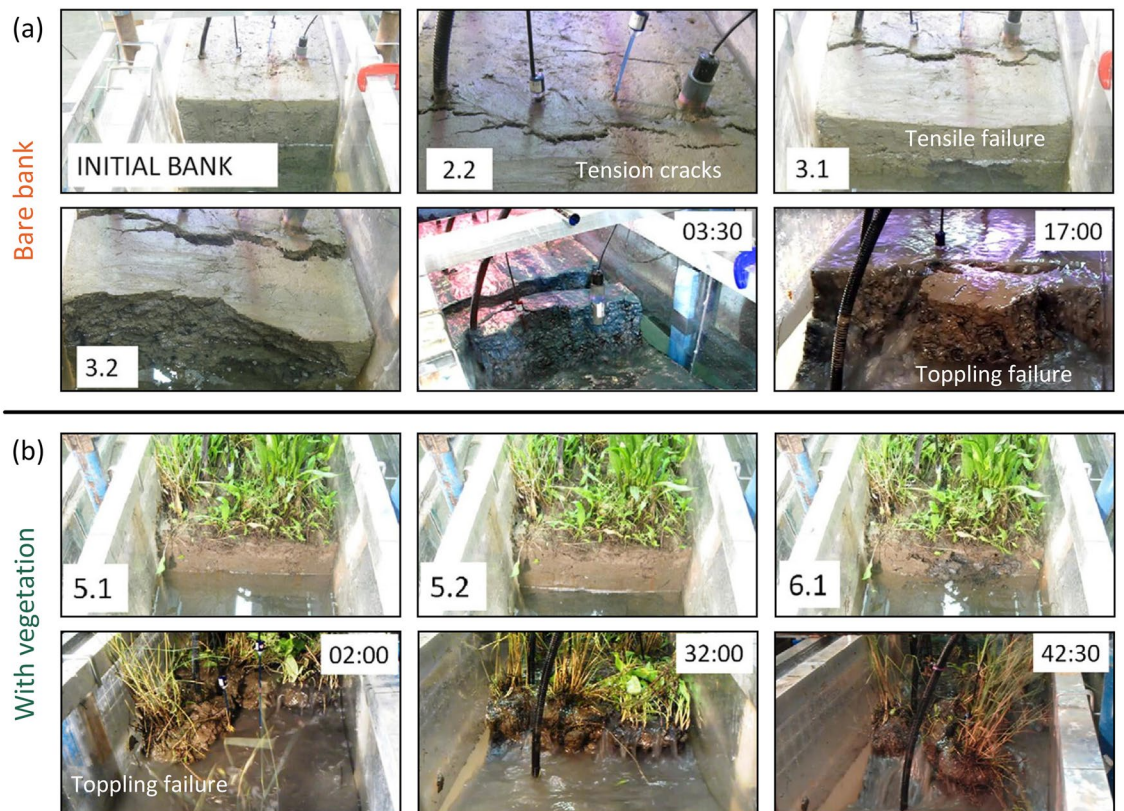
Figure 9. Erosion and failure processes of marsh cliffs in response to tidal currents and wind waves, (a) without and (b) with vegetation. The onward time from the beginning of Experiments 4.1 and 8.1 are reported on each photo, showing the occurrence of mass failure, while other photos display the final geometry of bank surface during each experiment. Bank height was 0.6 m (adapted from Francalanci et al. (2013)).

The combined influences of waves and vegetation roots on bank stability has been highlighted by many other studies (Mariotti et al., 2019; Y. Chen & Collins, 2007; Y. Chen et al., 2011). Contrary to coarse roots with high resistance to soil creep, Y. Chen et al. (2019) found that fine roots with high resistance were more effective in stabilizing marsh banks in response to flow- and wave-induced erosion. However, Feagin et al. (2009) argued that soil type, rather than salt marsh plants, is the primary variable affecting the erosion rate of the salt marsh edge, thus challenging the common perspective that salt marsh plants prevent wave-induced erosion. This conclusion is also consistent with the work of Bendoni et al. (2016), who stated that vegetation roots prevent particle-by-particle erosion on the upper layers of the bank and, hence, facilitate the formation of cantilever profiles, which in turn, may lead to more frequent mass failure events.

Biological disturbances matter as well. Biofilms provide a positive or negative effect on sediment stability depending on the driving forces (e.g., steady flow vs. waves (X. Chen et al., 2021; X. D. Chen, Zhang, et al., 2017)), while a negative effect is provided by shells and crabs (Bortolus & Iribarne, 1999; Quaresma et al., 2007; Thompson & Amos, 2002). A comprehensive review is provided by Harvey et al. (2019), who summarized the mechanisms of bank instability induced by burrows as: (a) altering bank geometry, (b) inducing subsurface flow (seepage), and (c) facilitating erosion at bank surface and burrow entrances. Overall, more research is needed to establish general parameterizations that can describe and quantitatively predict the influence of vegetation and biological disturbances on salt-marsh stability.

4. Bank Retreat Rate

On the basis of laboratory experiments and in situ observations, many empirical relations have been developed to relate bank retreat rate to controlling factors such as flow discharge, near-bank flow velocity and bank geometry. A summary of typical empirical functions to predict bank retreat rate, and their regression coefficients, is shown

Table 2
Empirical Correlations for Estimating Bank Retreat Rate Obtained From Field Observations

Type	Coefficient				R^2	Units		Time scale[a]	References
	K (or b)	a	$Q_c/c/P_c$	d		Left	Right		
(1) Induced by seepage									
$C_s = bQ_s^a$	3.7	2.12			0.69	g/L	L/day	Event	Wilson et al. (2007)
$E_m = K_s(Q_s - Q_c)^a$	1,700	1	0.2		0.89	g/min	L/min	Event	Midgley et al. (2013)
$V_s = b * CEI + d$	99.156	1		−39627	0.77	cm³	(−)	(−)	Masoodi et al. (2017)
(2) Induced by near-bank channel flow									
$E_l = b * A_d^a$	2.45	0.45			0.4	m/year	km²	Short	Hooke (1980)
	0.05	0.44			0.67	m/year	km²	(−)	Van De Wiel (2003)
	0.012	0.4			0.64	m/year	km²	Long	De Rose and Basher (2011)
$E_l = b * U_c^a$	6.66E−9	0.86			0.75	m/s	m/s	Short	J. E. Pizzuto and Meckelnburg (1989)
$E_l = b * D_f^a + c$	6.07	1	4.53		0.94	mm/year	(−)	Short	Lawler (1986)
$E_l = b * Q_l^a$	0.0016	0.6				m/year	m³/s	(−)	Rutherfurd (2000)
$E_a = b * e^{(Q_l/a)} + c$	0.6	472.299	0.636		0.98	km²/year	m³/s	Long	Yao et al. (2011)
$E_v = b * H_{ub}^a + c$	22.88	1	−3.93		0.73	m³/year	m	Seasonal	Z. Zhang et al. (2019)
(3) Induced by overbank flow									
$E_l = b * A_d^a$	5.1	0.5			0.62	m/year	km²	Medium	Seginer (1966) (Bror-Hayil)
	6	0.5			0.84				Ruhama
	2.1	0.5			0.85				Tkuma
	0.01	0.23			0.39	m/year	m²	Short	Vandekerckhove, Poesen, et al. (2001)
$E_a = b * A_d^a$	0.4	0.59			0.77	m²/year	m²	Long	Burkard and Kostaschuk (1997)
$V_g = b * A_d^a$	1.71	0.6			0.65	m³	m²	Medium	Vandekerckhove et al. (2000)
$E_v = b * A_d^a$	0.02	0.57			0.93	m³/year	m²	Medium	Vandekerckhove, Muys, et al. (2001)
	0.04	0.38			0.39	m³/year	m²	Short	Vandekerckhove, Poesen, et al. (2001)
	0.069	0.38			0.51	m³/year	m²	Medium	Vandekerckhove et al. (2003)
$E_v = b * P_s^a$	5.56E−3	2.31			0.67	m³/year	mm	Medium	Capra et al. (2009)
$E_l = b * S^a + c$	4.85	1	30.64		0.8	m/s	(−)	Medium	Samani et al. (2010)
$E_l = b * (A_d * P_s)^a$	6.466E−9	1.424			0.89	(−)	(−)	Long	Rieke-Zapp and Nichols (2011)
$E_a = b * [(\Phi_{60}A_i)^{0.24}S]^a$	0.154	3.2588			0.62	m²/year	m²	Medium	Z. Li et al. (2015)
$E_l = b * P_s^2 + c * P_s + d$	7E−4	2	−0.06	1.11	0.94	m	mm	Short	Dong, Wu, et al. (2019)
(4) Induced by waves									
$E_l = K_w(P_w - P_c)^a$	0.35	1.1			0.8	m/year	kW/m	Medium	Schwimmer (2001)
$E_a = K_w(P_w - P_c)^a$	0.036	1			0.89	m²/year	kW/m	Medium	Marani et al. (2011)
	0.098				0.75	m²/year	kW/m	Seasonal	Bendoni et al. (2016)
	0.117				0.73	m²/year	kW/m	Seasonal	
	0.413				0.77	m²/year	kW/m	Seasonal	
	0.33				0.54	m²/year	kW/m	Seasonal	

[a]"Event" timescales denote time intervals of one or several flood events, "seasonal" timescales indicate time intervals of less than one year, "short" timescales indicate time intervals of 1–5 years, "medium" timescales correspond to time intervals of 5–50 years, and "long" timescales denote a time intervals of more than 50 years. Variables are summarized in Symbols.

in Tables 1 and 2. Following Lawler (1993a), in this review timescales are defined thus: "Event" timescales denote time intervals of one or several flood events, "seasonal" timescales indicate time intervals of less than one year, "short" timescales indicate time intervals of 1–5 years, "medium" timescales correspond to time intervals of 5–50 years, and "long" timescales denote a time intervals of more than 50 years.

4.1. Hydraulic-Based Empirical Relations

There are numerous empirical relations that express the bank retreat rate as a function of some hydraulic parameters. These relations are developed to account for the average bank retreat (including both erosion and collapse) over the measured period. The seepage-induced bank retreat rate E, for both laboratory- and field-scale settings, is commonly estimated in the dimensional form by an excess discharge ($E = K_s(Q_s - Q_c)^a$) or gradient ($E = K_s(i - i_c)^a$) formulation. Here, K_s is seepage erodibility coefficient, Q_s is seepage discharge, Q_c is critical seepage discharge for bank erosion, i is hydraulic gradient driving seepage flow, and i_c is critical hydraulic gradient for seepage erosion. Note that for non-cohesive soils, the excess discharge relation is reduced to a power law correlation ($E = bQ_s^a$, see Table 1) (Akay et al., 2018; Chu-Agor et al., 2009; Fox et al., 2007; Howard & McLane, 1988; Midgley et al., 2013). Given that the direct measurement of E is sometimes complex and time-consuming, especially in the field, other variables, such as seepage sediment concentration and seepage-induced cavity volume, have been used to indirectly evaluate the retreat rate in excess discharge formulas (Masoodi et al., 2017; Wilson et al., 2007). In particular, Masoodi et al. (2017) suggested a linear correlation between seepage-induced cavity volume and soil chemical properties. This suggestion has implications for estuarine contexts, where seepage erosion might be more complicated as a result of the elusive dynamics of salinity (Hua et al., 2019).

Contrary to excess discharge formulas (see Fox et al. (2006) in Table 1), gradient-type relations directly link the retreat rate to boundary conditions (hydraulic head) and bank geometry without requiring additional input data (e.g., seepage velocity). This facilitates data analysis and inter-comparison between experiments, and provides more robust predictions. Since the regression parameters in the above dimensional-form relations are highly affected by hydraulic settings and soil properties, a more generic dimensionless formula ($q_s^* = K_s(\tau_s^* - \tau_{cs}^*)$) was proposed by Fox et al. (2007), where q_s^* and τ_s^* are the dimensionless sediment flux and shear stress, respectively, induced by seepage flow (see Section 2.1 for more details). The proposed dimensionless formula is not restricted to specific sites, and instead can be used for a range of contexts.

For retreat driven by surface flow, power law correlations are usually assumed. The associated controlling factors are distinct for near-bank channel flow and overbank flow conditions (Table 2). For near-bank channel flow, previous studies mainly focused on the effects of peak and annual mean flow discharges (Rutherfurd, 2000; Yao et al., 2011), near-bank flow velocity (J. E. Pizzuto & Meckelnburg, 1989), frost (Lawler, 1986), bend curvature (Lagasse et al., 2004; Nanson & Hickin, 1983), and freeze-thaw cycles (J. Pizzuto, 2009). For overbank flow more attention has been paid to the consequences of precipitation (Capra et al., 2009; Dong, Wu, et al., 2019; Rieke-Zapp & Nichols, 2011), channel slope gradient (Samani et al., 2010), and vegetation cover (Z. Li et al., 2015). A more general controlling factor, the drainage area considered as a surrogate of the flow discharge, is also used for both near-bank channel flow and overbank flow (Figure 10). Contrary to overbank flow, bank retreat induced by near-bank channel flow is more sensitive to temporal scale, as indicated by an evident gap in the observed retreat rate between short- and long-term time scales (e.g., river linear retreat rate, indicated by red dots and yellow squares in Figure 10). Therefore, the drainage area can be taken as a rough index for hydrodynamic intensity discriminating between different spatial and temporal scales (Burkard & Kostaschuk, 1997; Hooke, 1980; Seginer, 1966; Vandekerckhove, Poesen, et al., 2001; Vandekerckhove et al., 2000, 2003). More recently, machine learning algorithms based on large datasets, have been applied to develop predictors of gully erosion induced by overbank flow (Amiri et al., 2019; Arabameri et al., 2019; Rahmati et al., 2017). Since the factors dominating overbank flow are relatively easily collected (e.g., precipitation, drainage area, and soil characteristics), machine learning is likely to improve our predictive skill of gully erosion rates.

Employing laboratory-scale data, Wells et al. (2013) proposed an exponential function to describe changes in channel width over time, with the exponent determined by channel slope and flow discharge (Qin et al., 2018). Clearly, this relation is strictly related to bank retreat and, therefore, can be used to derive a bank retreat predictor. Note that, since the cross-section widening rate was found to decrease gradually with time (due to the increasing channel width), the associated bank retreat relation is deemed to provide more realistic predictions than when assuming a constant bank retreat rate over time.

As for tidal systems, the retreat rate of salt-marsh cliffs has usually been evaluated using a power law of the type $E = K_w(P_w - P_c)^a$, where P_w represents the mean wave power calculated over a representative period, P_c is a threshold value for wave-induced retreat, K_w is the erodibility coefficient for wave erosion, and a is an empirical exponent (here a nonlinear correlation is considered to obtain a more general form) (Bendoni et al., 2016;
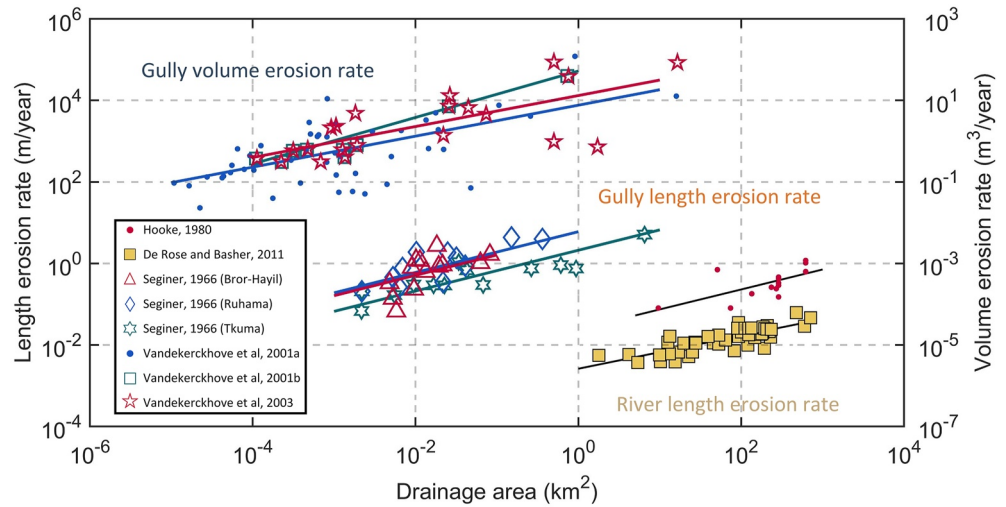
Figure 10. Correlation between drainage area and the linear and volumetric retreat rates, showing the variability of different predictors for bank retreat rate. Dots represent observations collected over short time scales (1–5 years). Open and filled symbols refer to data collected over medium (5–50 years) or long (>50 years) time scales, respectively. Colors are used to distinguish different references.

Marani et al., 2011; Mariotti & Fagherazzi, 2010; Schwimmer, 2001). When accounting for their results in the context of previous studies, Bendoni et al. (2016) found that at short temporal scales (months), the marsh cliff retreat rate is much higher than the one obtained over much larger time intervals (decades), a result consistent with the tendency observed in fluvial systems (Hooke, 1980). This finding can be partly explained by a dynamic equilibrium theory (Zhou et al., 2017) whereby bank dynamic is not only associated with a monotonic retreat, but is possibly characterized by a periodic cycle of erosion and accretion (e.g., the catch-up behavior reported in meander migration (Mason & Mohrig, 2019; Nanson & Hickin, 1983; Zhao et al., 2021)). In other words, when considering the bank retreat rate over relatively long-time periods, other dynamics such as subaerial processes prior to bank erosion/collapse (e.g., freeze-thaw and drying-wetting cycles) (Chassiot et al., 2020), decomposition of collapsed bank soil (C. Hackney et al., 2015; Fagherazzi et al., 2004; K. Zhang et al., 2021), and bank accretion (Asahi et al., 2013) can all lead to a lower than expected bank retreat rate. The issue associated with the choice of a suitable temporal scale thus turns out to be crucial, since it determines the robustness and accuracy of the developed empirical relations given the period of time to be considered for predicting the bank dynamic (Hooke, 1980; J. Pizzuto et al., 2010).

In general, the performance of hydraulic-based empirical relations depends on the choice of the representative discharge (e.g., mean or peak discharge). In the case of banks composed of sand and silt, which constantly undergo erosion, the annual mean discharge is the best choice. It in fact summarizes the overall information concerning the relevant hydrologic processes. In contrast, the peak discharge is more suitable for estimating the retreat rate of cohesive and bedrock banks, for which bank erosion is only active during high flows. In these cases, using the mean discharge likely leads to an overestimation of the overall bank retreat. Anyhow, when using a constant formative discharge, an intermittency factor is needed to account for the effect of temporal variations in hydrological forcings. This factor is defined as the fraction of time the channel is actually experiencing effective erosive conditions (Paola et al., 1992; Parker et al., 1998). However, very few of the empirical relations discussed above have been developed accounting explicitly for the intermittency of the formative discharge. This limitation is possibly one of the factors leading to the large scatter characterizing the various empirical coefficients reported in Table 2. More efforts are needed to provide appropriate criteria for the application of the hydraulic-based empirical relations developed so far for estimating bank retreat.

4.2. Empirical Relations Accounting Directly for Bank Collapse

Hydraulic-based empirical relations commonly fail when including mass failure events at short temporal scales (Bendoni et al., 2016). Indeed, contrary to flow-induced bank erosion, which is mainly related to flow velocity

and soil properties (e.g., critical shear stress for bank erosion), the scale and frequency of bank collapse depends on different factors such as bank geometry, soil properties, near-bank hydrodynamics and biological disturbances (C. Chen, Hsieh, & Yang, 2017; Fox et al., 2006; Nardi et al., 2012; Samadi et al., 2013; Sanders et al., 2021). Numerous empirical relations have thus been developed to predict bank retreat rate accounting explicitly for bank collapse.

The effect of bank geometry on bank collapse and the consequent bank retreat rate is commonly estimated in the form of an excess bank height or bank slope (Jang & Shimizu, 2005; Mosselman, 1995). For field-scale applications (e.g., the Yellow River investigated by Z. Zhang et al. (2019) and Liu et al. (2021)), the relation is reduced to a simple linear correlation, without any threshold. In fact, bank collapse occurs when the driving force overcomes the resisting forces regardless of bank height. Bank height seems only to affect the scale and frequency of bank collapse (see Figure 4 in Section 3.2). Soil properties and near-bank hydrodynamics also affect bank stability, and therefore alter bank retreat rates. Although exhibiting a relative weak correlation, Xia, Zong, Zhang, et al. (2014) suggested that a decrease in clay content or an increase in drawdown rate generally favors bank collapse and, hence, accelerates bank retreat rate. The effect of the former factor can be partly explained by an increased thickness of the cohesive layer in the upper bank implying the formation of heavier overhanging soil blocks, while the effect of the latter is attributed to the fact that a rapid drawdown of water level generates excess pore-water pressure combined with a loss of hydrostatic pressure, both of which favor bank instability. As for biological disturbances, Sanders et al. (2021) found that burrow metrics (e.g., burrow density) have a strong positive linear correlation with bank retreat rate and the area of collapsed bank. Given that salt-marsh channels are generally covered by halophytic vegetation with a strong root matrix, biological disturbances turn out to be crucial to bank stability and, hence, bank collapse (Harvey et al. (2019) and see Section 3.5). Other factors, such as the critical length of overhanging soil blocks and time to collapse, have also been used to indirectly evaluate collapse-induced retreat rates. For event-scale cohesive overhang failures, J. Pizzuto (2009) proposed a critical value of the overhang length depending linearly from overhang height. In the case of seepage-induced bank collapse, several studies suggested a correlation between time to collapse and the seepage gradient (Karmaker & Dutta, 2013; Masoodi et al., 2018). Although providing some useful information, the above correlations only account for the individual effects of hydraulic and geotechnical conditions, without an integrated representation of hydraulic and geotechnical control factors.

The seminal in situ work by Hickin and Nanson (1984) suggests that, in fluvial contexts, the linear migration rate of channel banks, E_l, can be evaluated by a combination of stream power, ω, bank height, H_b, channel width, w_c, and bank soil resistance, γ_b, proposing the linear relation $E_l = a\omega/\gamma_b w_c/H_b$. Subsequently, several studies have used the ratio between bank height and near-bank water depth, H_b/H_w, as a proxy for bank stability when seeking empirical laws for bank/cliff retreat rate. Dapporto et al. (2003) suggested that the critical value of H_b/H_w triggering bank collapse can be estimated based on the peak river stage. This value is taken to surrogate the complex coupling between stress-strain and seepage processes. For tidal settings, Marani et al. (2011) attempted to build a correlation between volumetric retreat rate of salt marsh borders, E_v, mean wave power, P_w, and the ratio H_b/H_w, proposing a linear relation of the type $E_v = P_w \cdot H_b/H_w$. However, the heterogeneity of marshes (Houttuijn Bloemendaal et al., 2021) and the relatively large time intervals over which the data were averaged (decades), smooth out the effects that geotechnical factors exert on cliff retreat rates. As a result, Marani et al. (2011) do not find a clear correlation between E_v/P_w and the ratio H_b/H_w. To separate the effects of bank collapse on bank retreat rate, Zhao et al. (2020) defined a dimensionless linear retreat rate, r_l, quantifying the erosion controlled by near-bank channel flow. It reads

$$r_l = \frac{E_l}{U_c} \cdot \frac{w_t}{w_c} \tag{6}$$

where E_l is the linear retreat rate (m/s), U_c is the near-bank flow velocity (m/s), w_c is the channel width (m), and w_t is the width of the overhanging bank material (m). The ratio w_t/w_c accounts for the protective effect of collapsed bank soil (slump blocks) on the bank retreat rate. Figure 11a shows the normalized retreat rate defined by Equation 6 as a function of the ratio H_b/H_w and the best fit line obtained from the laboratory data available in literature (Braudrick et al., 2009; Patsinghasanee et al., 2017; Qin et al., 2018; Shu et al., 2019; van Dijk et al., 2012; Vargas Luna et al., 2019; Wells et al., 2013; Zhao et al., 2020) (further details on the variables used in Figure 11
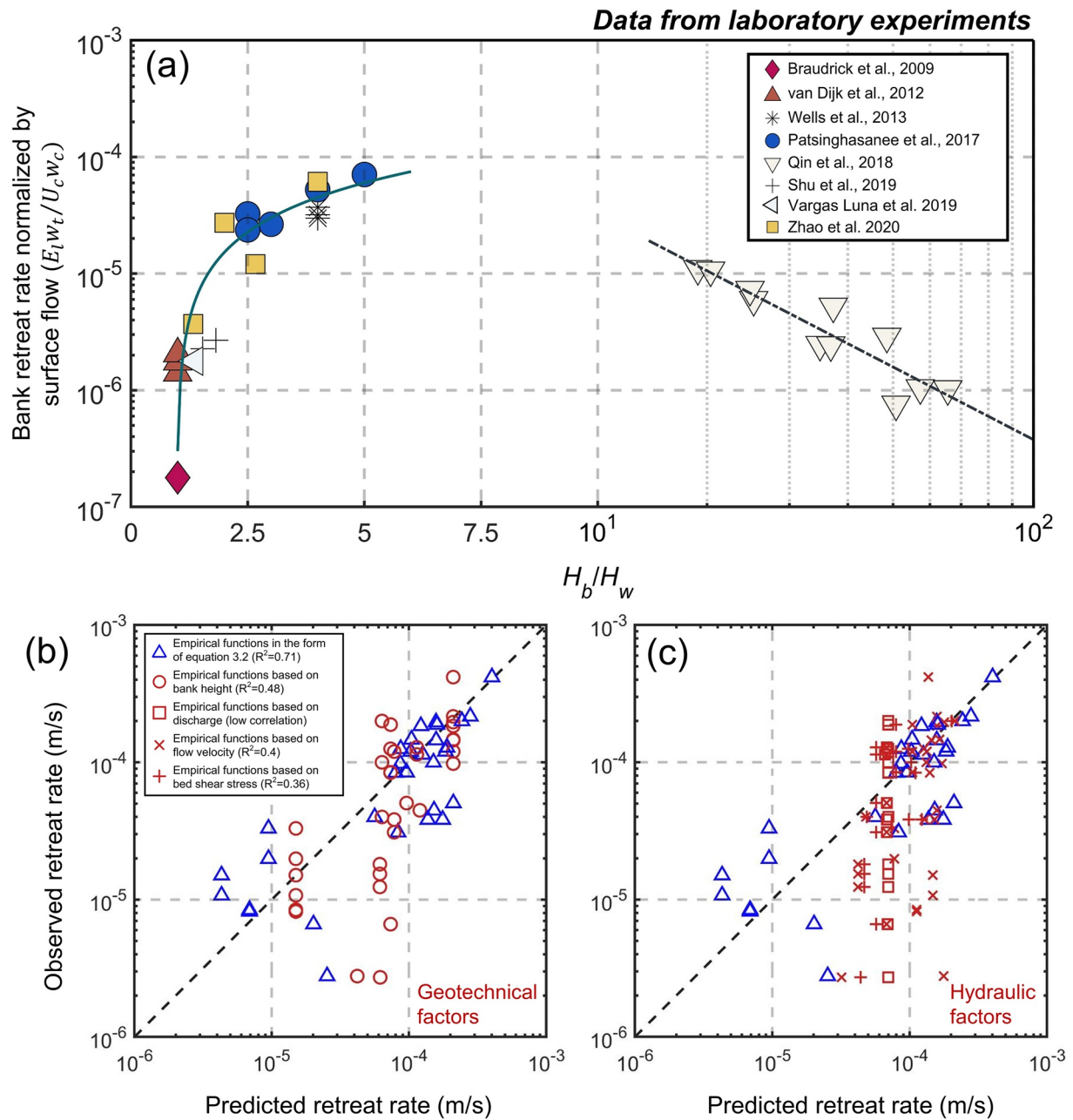
Figure 11. (a) Correlation between the normalized linear bank retreat rate, r_l, and the ratio H_b/H_w. The various quantities have been determined from laboratory experiments available in literature and are defined as follows: U_c, near-bank flow velocity; w_c, channel width; w_t, the width of the overhanging bank material; H_b, bank height; and H_w, near-bank water depth. (b and c) Comparison of linear bank retreat rates predicted by empirical relations (Equations 7a and 7b) (blue triangles) and those formulated by Z. Zhang et al. (2019) (red circles), Rutherfurd (2000) and Yao et al. (2011) (red squares), J. E. Pizzuto and Meckelnburg (1989) (red crosses), and the excess shear stress Equation 1 (red plus). Previous empirical relations are based on (a) geotechnical factors and (b) hydraulic factors. Subplot (a) is adapted from Zhao et al. (2020).

are provided in Data Availability Statement). The normalized retreat rate r_l exhibits two distinct behaviors for small (<7.5) and large (>10) values of the ratio H_b/H_w, namely:

$$r_l = 0.00003\,(H_b/H_w - 1) \quad 1 < H_b/H_w < 7.5 \quad \left(R^2 = 0.83\right) \tag{7a}$$

$$r_l = 0.0097(H_b/H_w)^{-2.05} \quad H_b/H_w > 10 \quad \left(R^2 = 0.94\right) \tag{7b}$$

In the former case (Equation 7a) r_l increases linearly with H_b/H_w. Conversely, in the latter case r_l decreases following a power law. These two trends can be explained by noting that the ratio H_b/H_w can be taken as a measure of the degree of bank stability (Zhao et al., 2020). In general, an increase in H_b/H_w leads to a decreased bank stability enhancing bank collapse and, hence, bank retreat rate. However, for large values of H_b/H_w, the near-bank flow velocity and water depth are small. The bank erosion processes thus weaken leading to a reduction of the frequency of bank collapse and, hence, to the progressively decreasing bank retreat rate shown in Figure 11a.

Figures 11b and 11c report the comparison between the empirical relations (Equations 7a and 7b) and a number of predictors previously proposed in literature accounting separately for hydraulic and geotechnical control factors in terms of bank height (Z. Zhang et al., 2019), discharge (Rutherfurd, 2000; Yao et al., 2011), flow velocity (J. E. Pizzuto & Meckelnburg, 1989) and bed shear stress (see Equation 1 and Table 2 for the considered formulas). Various observations emerge from this comparison. First, it is evident that both hydraulic (flow velocity and discharge) and geotechnical factors (bank height) must be accounted for to obtain robust predictions of bank retreat, at least at laboratory-scale. In particular, geotechnical factors (controlling bank collapse) exert a relative stronger influence on bank retreat rate at the laboratory scale, when compared to hydraulic factors. Second, a discrepancy between the importance of geotechnical factor in the field and laboratory contexts is apparent when noting that an increased bank height decelerates bank retreat rate in the field while accelerates it in the laboratory (Hickin & Nanson, 1984; Zhao et al., 2020). This implies that the inclusion of bank collapse may be far more complex than previously thought, since collapsed bank soil affects the interplay between hydraulic and geotechnical factors, as conjectured by the concept of basal endpoint control (Carson & Kirkby, 1972; Thorne & Tovey, 1981) and discussed by C. Hackney et al. (2015). Third, even though the variables required for empirical relations (e.g., those in Table 2) are commonly available, we highlight that empirical approaches have been usually pursued without a clear physical basis (except for Marani et al. (2011) who adopted dimensional analysis to derive their relations). Most of these empirical relations were instead obtained by direct fitting of a relatively limited amount of data and they also lack systematic validation. Hence, the coefficients appearing in the various relations are strictly valid only for those specific sites where the measurements were originally collected. For instance, the bank erodibility coefficients in Equation 1 can vary by several orders of magnitude (Gong et al., 2018; Parker et al., 2011), and should be regarded as calibration parameters (Crosato, 2007; Rinaldi & Darby, 2007). Overall, the empirical relations are useful for contexts where monitoring of hydrodynamics is impossible (e.g., ephemeral gully) or situations where the key mechanisms are still elusive. Empirical relations are also meaningful when modeling long-term morphodynamic evolution. They in fact provide an acceptable time averaged description of the effects of some complicated processes such as secondary flow and sequences of bank collapse events (see Section 5.2). Although some parameterized relations have been proposed to account for subaerial processes (J. Pizzuto, 2009; Wynn et al., 2008), additional advances are still needed to obtain a more realistic representation of the role which these important processes play on bank erosion and collapse. Finally, we notice that very few empirical bank retreat relations have been developed to include multiple erosion mechanisms in estuaries and tidal channels (e.g., coupled effects of seepage and near-bank channel flow during ebb tides). Efforts are strongly needed to improve our understanding and, hence, the predictive capability of the complex feedbacks acting in estuarine and coastal systems.

5. A Hierarchy of Models for Bank Retreat

Studies carried out to model bank retreat have followed two distinct paths: a *hydraulic approach* and a *geotechnical approach* (Rinaldi & Darby, 2007). The hydraulic approach, based on strong simplifications of bank collapse, relies on some empirical parameterization for bank retreat processes, usually by means of surrogates of the shear stress that the near-bank flow exerts on the bank. This approach has been used to describe the evolution of rivers, estuaries and tidal channels over a range of time scales (Bogoni et al., 2017; Duan & Julien, 2005; Ikeda et al., 1981; Jang & Shimizu, 2005; J. E. Pizzuto, 1990; Jia et al., 2010; Lanzoni & Seminara, 2006; Lopez Dubon & Lanzoni, 2019; Nagata et al., 2000; Parker et al., 2011; van der Wegen et al., 2008; van Dijk et al., 2019). In contrast, the geotechnical approach focuses on the transient process of bank collapse that controls the intermittent evolution of channel cross-sections or salt marsh borders (Bendoni et al., 2014; Gong et al., 2018; Istanbulluoglu et al., 2005; Kleinhans et al., 2009; Langendoen & Simon, 2008; Osman & Thorne, 1988; Samadi et al., 2013; Thorne & Tovey, 1981; Van Eerdt, 1985). The contribution to bank collapse has been investigated numerically by focusing on different factors such as bank height (Zhao et al., 2019), soil properties (Simon
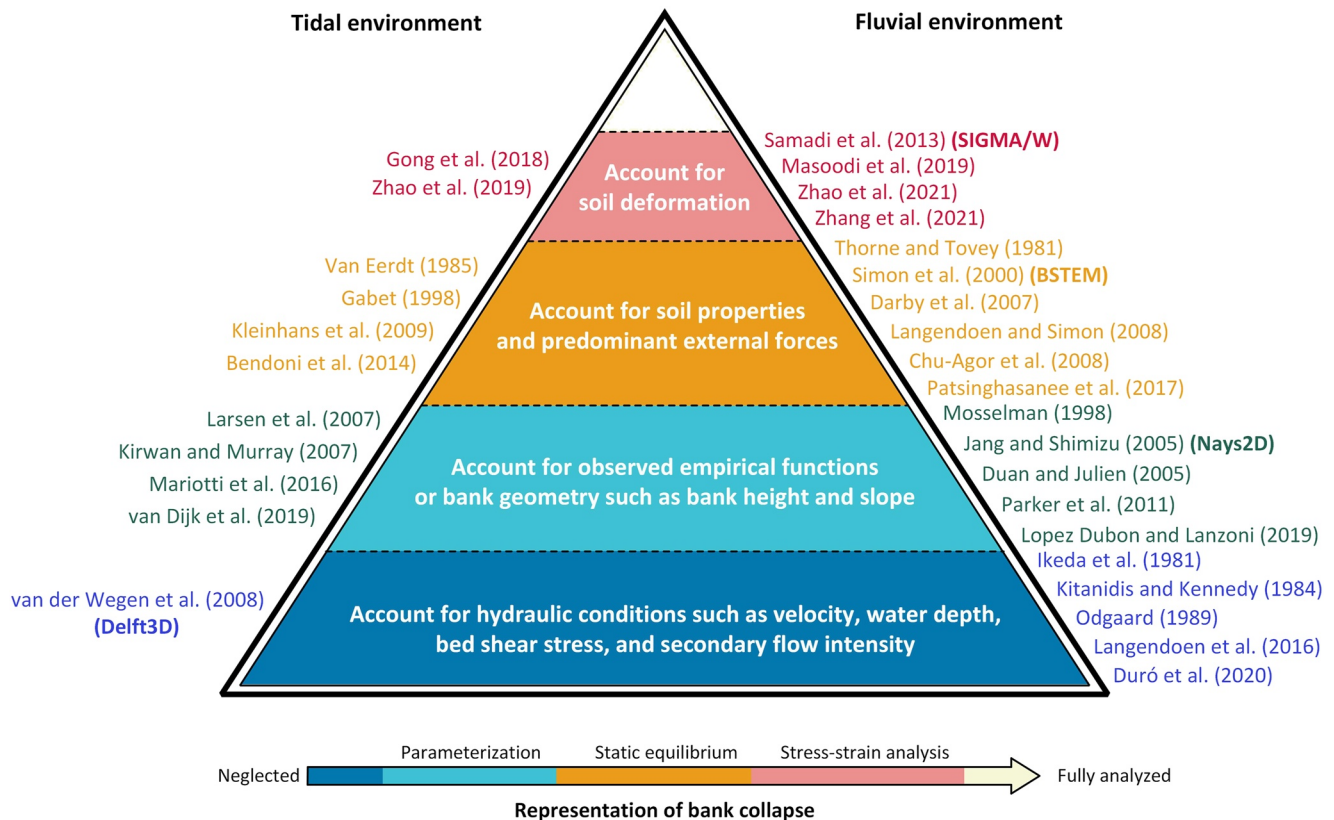
Figure 12. Diagram showing the hierarchy of models used to simulate bank retreat. The color bar represents the degree of simplification used to treat bank collapse. Note that the literature listed in this figure aims to provide some typical examples and is not meant to be comprehensive.

et al., 2000), pore-water pressure (Darby et al., 2007; Darby & Thorne, 1996a), and vegetation roots (Krzeminska et al., 2019; Pollen Bankhead & Simon, 2009; T. H. Wu et al., 1979). Although the classification into a *hydraulic approach* and a *geotechnical approach* proposed by Rinaldi and Darby (2007) is helpful to distinguish between models, it fails to indicate whether a model describes the interplay between flow-driven bank erosion and bank collapse or treats only one of the two mechanisms. We thus propose to categorize the existing models of bank retreat into a hierarchy of models: purely hydraulic models, not accounting explicitly for bank collapse; models based on empirical relations that parameterize bank collapse; models considering the static equilibrium of bank soil through the limit equilibrium method (LEM); and models based on bank soil stress-strain deformations. A summary of these four typical modeling approaches is presented in Figure 12 and Table 3.

5.1. Hydraulic Models

This type of models describes bank retreat from a hydraulic perspective, without any representation of bank collapse. Hence, hydraulic models should not be applied to contexts where bank collapse controls bank retreat, such as in the case of steep and cohesive riverbanks or when assessing the effects of the recession of flood hydrographs and the short-term evolution of tidal creeks on muddy flats.

Many hydraulic models have been developed to simulate bank retreat associated with the long-term evolution of meandering channels using surrogates (i.e., excess velocity, water depth) of the shear stress exerted by the channel flow on the bank (Ikeda et al., 1981; Kitanidis & Kennedy, 1984; Langendoen et al., 2016; Odgaard, 1989). The most common model was introduced by Hasegawa (1977) and Ikeda et al. (1981). In this approach (hereafter denoted as HIPS) the bank retreat rate is taken to be proportional to the curvature-induced difference between the near-bank and the cross-sectionally averaged velocity. Since the thickness of the near-bank boundary layer is commonly uncertain (Parker et al., 2011), the definition of the near-bank velocity in the HIPS equation is sometimes arbitrary. The HIPS equation provides a simple and direct way to simulate channel migration, and it has

Table 3
Summary of Typical Modeling Approaches Used for Computing Bank Retreat

Model	Mechanism of bank retreat		Highlights	References
	Flow-driven bank erosion	Bank collapse		
Hydraulic model/Author				
HIPS	Excess velocity equation	No	Easy to couple with morphodynamic models of long-term evolution of meandering channels	Hasegawa (1977); Ikeda et al. (1981)
Delft3D	Near-bank sediment flux	No	Lateral bank retreat is replaced with a vertical decrease in bank height, which is easy to couple with other processes, for example, tides, waves, and sediment dynamics	van der Wegen et al. (2008)
Duró et al.	Wave-induced shear stress	No	Account for the shear stress distribution induced by ship waves	Duró et al. (2020)
Parameterized bank collapse model/Author				
Hasegawa and Mosselman	No	Critical bank height	Bank collapse promotes bank retreat by collapse events, or alternatively, prevents bank retreat by collapsed bank soil	Hasegawa (1989); Mosselman (1998)
Duan and Julien	Excess shear stress equation	Parameterized	A vertical bank profile is maintained since the upper bank retreat rate due to collapse is assumed to keep up with the basal erosion rate	Duan and Julien (2005)
Nays2D	Integration of the sediment continuity equation	Critical repose angle	Outer bank erosion and inner bank deposition processes are separated and the effects of slump blocks are taken into account	Jang and Shimizu (2005); Parker et al. (2011)
			Bank collapse occurs when the local bank slope exceeds the angle of repose for bank material	Nagata et al. (2000)
Mariotti et al.	No	Critical bank slope	A linear relation linking soil creep with bed slope and soil diffusivity rate	Mariotti et al. (2016)
van Dijk et al.	No	Local slope	Bank collapse is parameterized on the basis of field data, relating collapse frequency to the local slope angle and bed elevation	van Dijk et al. (2019)
Limit equilibrium method/Author (slide failure)				
BSTEM	Excess shear stress equation	Planar failure	Matric suction, positive pore-water pressure, hydrostatic pressure, and vegetation roots are coupled for layered cohesive banks	Simon et al. (2000); Simon and Collison (2002)
			New algorithms are derived to account for the effect of tension cracks on planar failure	Langendoen and Simon (2008)
			The near-bank groundwater table is assumed to change instantly or gradually in response to water level change in the channel	Midgley et al. (2012)
			Coupled with a process-based morphodynamic model accounting for meander migration and planform evolution	Motta et al. (2014); Lai et al. (2015)
Rinaldi and Darby	Excess shear stress equation	Sliding failure	Fluvial erosion, finite element seepage analysis and bank stability analysis are fully coupled	Rinaldi et al. (2004); Darby et al. (2007)
			Near-bank bed deformation is coupled	Deng et al. (2018)

Table 3
Continued

Model	Mechanism of bank retreat		Highlights	References
	Flow-driven bank erosion	Bank collapse		
Chu-Agor et al.	No	Pop-out failure	New algorithms are derived for pop-out failure along a failure plane parallel and perpendicular respectively to the bank face	Chu-Agor et al. (2008)
Thorne and Tovey	No	Cantilever failure	First method specific for cantilever failure	Thorne and Tovey (1981)
Van Eerdt	No	Toppling failure	A triangular distribution of both tensile and compressive stresses is derived along the failure plane	Van Eerdt (1985)
Xia et al.	No	Toppling failure	The effect of tension cracks on the bank top is included and a constant ratio between tensile strength to compressive stress is applied	Xia, Zong, Deng, et al. (2014)
Bendoni et al.	No	Toppling failure	A dynamic wave-induced load is accounted for	Bendoni et al. (2014)
Patsinghasanee et al.	Excess shear stress equation	Cantilever failure	Cantilever stability analysis is coupled with fluvial erosion and bedload sediment transport	Patsinghasanee et al. (2017)
Stress-strain analysis/Author				
Samadi et al.	No	Stress-strain analysis	An elastic-plastic stress-strain model is applied to investigate toppling failure due to undermining	Samadi et al. (2013)
Gong and Zhao	Excess shear stress equation	Stress-strain analysis	Stress-strain analysis is coupled with lateral flow erosion, sediment dynamics, and river meandering	Gong et al. (2018); Zhao et al. (2019, 2021)

been used in numerous studies (see e.g., among many others, Camporeale et al., 2007; Frascati & Lanzoni, 2009; Lanzoni & Seminara, 2006; Parker et al., 2011).

Another common approach pursued for alluvial rivers and estuarine environments is the so called dry-cell erosion (DCE) method, incorporated in models solving the full set of shallow water equations (e.g., Delft3D, Lesser et al. (2004)). It allows the redistribution of an erosion flux from a wet cell to the adjacent dry cells. As a result, the lateral bank retreat is replaced with a vertical decrease in bank height (van der Wegen et al., 2008; Zhao et al., 2019). Because of its convenience, especially for complicated bank alignments, the DCE has been extensively applied to the simulation of large-scale contexts such as estuaries and tidal networks (Guo et al., 2021; Xu et al., 2017).

For bedrock rivers evolving over millennial timescales, the inclusion of a lateral erosion law into long-term landscape evolution models (e.g., cellular models) is a challenge (Lague, 2014). Several models have been proposed at either river-scale (Hancock & Anderson, 2002; Inoue et al., 2021; Malatesta et al., 2017; Murray & Paola, 1994), or catchment-scale (Coulthard et al., 2013). On the basis of empirical data, Howard and Knutson (1984) related bank retreat rate to the local and upstream-integrated curvature. This relation was subsequently adopted in cellular models to drive lateral erosion and consequent meandering (Coulthard & Wiel, 2006), and to investigate how meander migration is affected by bedrock lithology (Limaye & Lamb, 2014). Nevertheless, a physics-based parametrization of bank retreat accounting for the combined action of vertical and lateral incisions in mixed bedrock-alluvial meandering channels is still missing. On the other hand, studies have also been carried out to deal with the broader catchment topography where bedrock rivers are embedded (Carretier et al., 2016; Langston & Tucker, 2018). In these studies, bank retreat is simply related to local erosion flux, or elevation difference between nodes representing bank and channel, respectively. This highly simplified approach is a first step toward a fully understanding of bedrock valleys evolution over long time periods and large space scales.

5.2. Parameterized Bank Collapse Models

This type of models represents the processes of bank collapse using bank geometry (e.g., bank height and slope) or other empirical parameterizations (see Section 4). On the basis of an excess bank height formula, Mosselman (1998) suggested that bank retreat rate is proportional to bank height on the short- or medium-term timescales typical of meandering river dynamics. Alternatively, Hasegawa (1989) assumed that bank retreat is inversely proportional to bank height. This assumption is based on the concept of basal endpoint control, set out by Carson and Kirkby (1972) and Thorne (1982), whereby bank retreat rate is determined by the balance between the supply of slump blocks by bank collapse and their removal by fluvial (grain-by-grain) erosion.

Using bank slope, two alternative approaches have been proposed, depending on the potential failure mechanism. For planar bank failure and non-cohesive bank material, J. E. Pizzuto (1990) and Nagata et al. (2000) derived a model in which failure of the upper bank occurs as the bank slope exceeds the angle of repose, as a result of lower basal erosion (Figure 13a). This approach was improved by Parker et al. (2011), who introduced the sediment continuity equation for the near-bank region (Figure 13b). It was applied by Jang and Shimizu (2005) and Dulal et al. (2010) to simulate flume experiments of meander dynamics through the Nays2D software. This model solves numerically the two-dimensional shallow water equations coupled with the Exner sediment balance equation and relates bank retreat rate directly to the near-bank sediment flux (Shimizu et al., 2019). The characteristic timescale of bank processes is thus of the same order of magnitude as for bed processes. This modeling approach performs well in terms of meander planform and width variations, when compared to channel evolution in both experimental and natural contexts (Asahi et al., 2013; E. C. Eke et al., 2014). In the case of vertical banks composed of cohesive sediment, Duan and Julien (2005) assumed that the upper bank retreat due to bank collapse keeps up with basal erosion, maintaining a vertical bank profile during the retreat. However, this assumption is arbitrary, since recent laboratory experiments have shown that the location of tension cracks on the bank top is always beyond the endpoint of the cantilever (i.e., closer to the landward boundary). To obtain a more realistic representation of bank collapse in meandering rivers, Zhao et al. (2021) suggested that the flow-induced bank erosion rate can be amplified by the contribution of bank collapse to bank retreat, C_{bc}. This contribution, evaluated on the basis of experimental observations, was found to depend on the ratio of bank height to near-bank water depth, H_b/H_w. The contribution of bank collapse to bank retreat is thus taken as continuous, and its average effect is linked to flow-driven bank erosion.

To evaluate the performance of existing approaches to bank retreat, Stecca et al. (2017) set up a framework in which three modeling steps are introduced: bank identification, bank retreat simulation, and bank updating. A set of bank retreat models were then constructed by choosing different options for each step. This approach quantified how the cross-sectional evolution of rivers can be affected by each of the steps, and therefore can guide the practical application of existing bank retreat models. A similar strategy was adopted by J. Pizzuto (2009) who simulated the evolution of bank profiles by assembling several regression equations including lower hydraulic erosion, upper subaerial erosion, and the volume of the failed overhanging block. This research can be regarded as a first attempt to develop a detailed numerical model using empirical methods. More efforts are needed to extend this framework to the entire river reach and to decadal timescales.

More recently, several empirical parameterizations, validated by field data, have been introduced to describe bank retreat in tidal environments. For instance, a shoal margin collapse predictor was introduced by van Dijk et al. (2019), relating collapse frequency to the local maximum bank slope angle. Several authors have assumed a linear relation linking soil creep with slope and soil diffusivity of salt marsh borders (Kirwan & Murray, 2007; Larsen et al., 2007; Mariotti et al., 2016). This approach has been used to study sediment exchanges between tidal flats and creeks. Nevertheless, soil creep is a complicated process related to temperature, soil water content, and vegetation roots, and more research is needed to further validate the simple linear relationship so far employed.

Overall, parameterized bank collapse models can be used to account for collapse-induced retreat rate in long-term and large-scale simulations. However, because of the strong simplifications employed in their derivation, they should be used in contexts where bank stability is mainly related to bank geometry (i.e., homogeneous bank soils without other external forces), or where detailed information of bank materials and external forces are unavailable. Moreover, since models of this type fail to account for the intermittency of bank collapse, they should only be applied to short-term contexts with extreme caution.
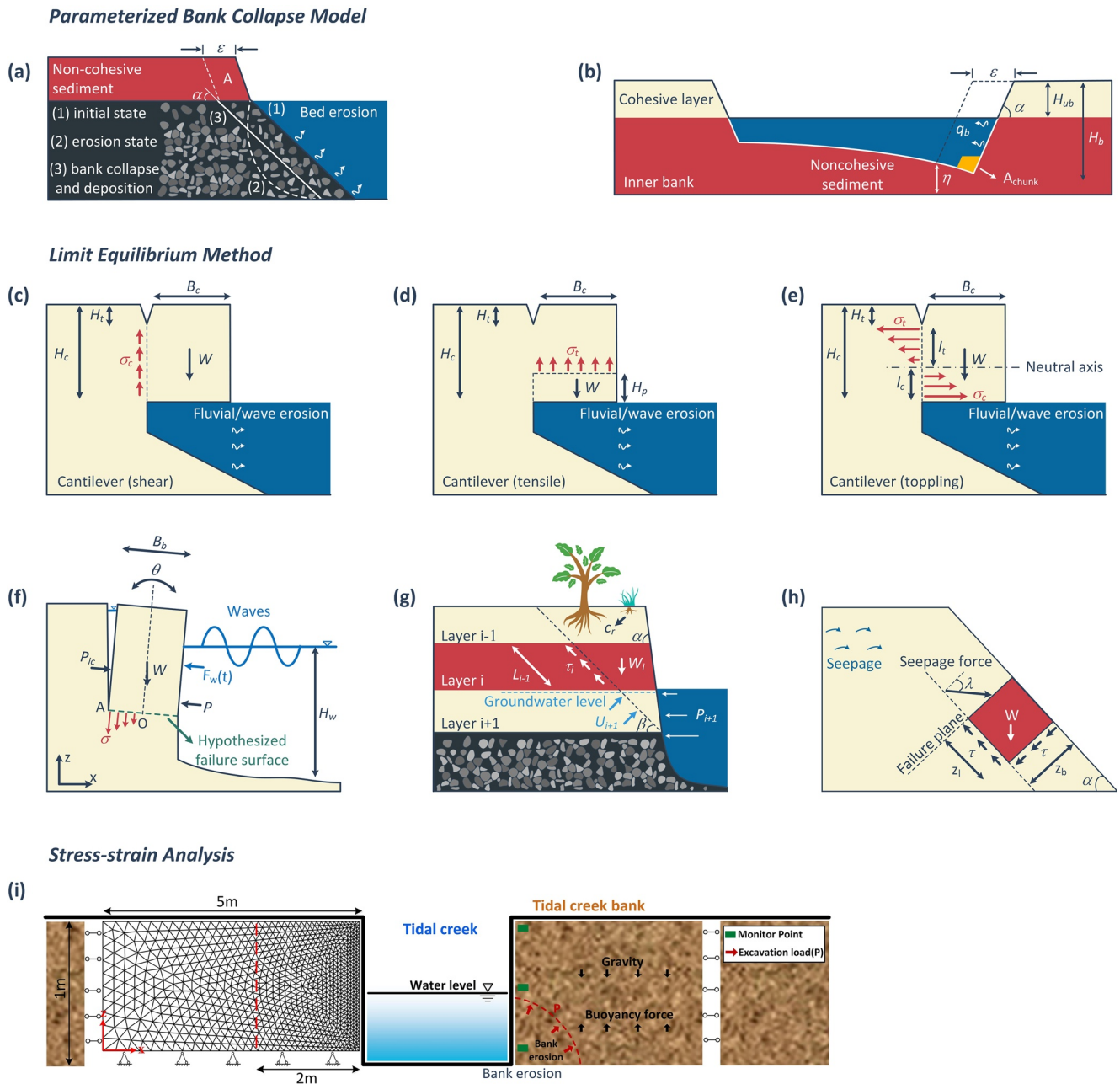
Figure 13. Schematization of the various bank erosion/collapse models proposed in literature: (a) bank collapse of non-cohesive sediment (Nagata et al., 2000); (b) fluvial erosion based on sediment conservation (Parker et al., 2011); (c and d) shear and tensile failure (Thorne & Tovey, 1981); (e) toppling failure (Van Eerdt, 1985); (f) toppling failure under the action of waves (Bendoni et al., 2014); (g) Bank Stability and Toe Erosion Model (Simon et al., 2000); (h) pop-out failure (Chu-Agor et al., 2008); and (i) stress-strain analysis of a tidal channel bank (adapted from Gong et al. (2018)). We refer the reader to the list of Symbols for the description of the parameters appearing in the various sketches.

5.3. Limit Equilibrium Methods

From a geotechnical perspective, bank collapse occurs when the driving forces (or moments), F_D, acting on a potential failure surface overcome the resisting forces (or moments), F_R. As a result, a factor of safety, $F_s = F_R/F_D$, is commonly applied to estimate bank stability. To calculate F_s, a potential failure surface is assumed and one or more equations of static equilibrium (equilibrium of forces or moments) are used to calculate the forces along the incipient failure surface (Duncan et al., 2014). This procedure is termed the *LEM*. It accounts not only for bank geometry, but also for soil properties and some relevant external forces, such as hydrostatic pressure head,

soil pore-water pressure, and reinforcement provided by vegetation roots. Although a number of failure mechanisms have been identified by Thorne (1982), applications of the LEM have concentrated mostly on cantilever and sliding failures. Given the large body of literature concerning LEM (see e.g., the reviews by Rinaldi and Darby (2007) and Klavon et al. (2017)), below we only summarize some recent advances.

For cantilever failures (Figures 13c–13e), recent research has focused on the influence of heterogeneous bank material and tension cracks, as well as on developing a more realistic distribution of stress along the failure surface. On one hand, the potential cantilever block has been divided into horizontal slices, in order to account for the effect of heterogeneous bank material and upper cracks (Langendoen & Simon, 2008). On the other hand, the uniform stress assumption put forward by Thorne and Tovey (1981) has been gradually replaced with a triangular distribution of both tensile and compressive stresses along the failure plane (Figure 13e). This approach, first proposed by Van Eerdt (1985) for tidal environments, was later on widely employed to investigate the relation between the cantilever lengths under tensile (l_t) and compressive stress (l_c) (Arai et al., 2018; Micheli & Kirchner, 2002; Patsinghasanee et al., 2017; Xia, Zong, Deng, et al., 2014). With reference to salt marsh borders, Bendoni et al. (2014) developed a theoretical model to evaluate the effects of dynamic loads on cantilever stability (Figure 13f). Bank failure was assumed to occur when the tensile strength of the bank material is exceeded at least on one point of the failure surface, rather than using an average value for the whole failure surface.

For sliding failures, one of the most advanced and commonly used tools is the Bank Stability and Toe Erosion Model (BSTEM; Figure 13g) first proposed by Simon et al. (2000). This modeling approach accounts for the effects of positive pore water pressure and hydrostatic pressure (Darby & Thorne, 1996a), matric suction in unsaturated soils (Casagli et al., 1999), layered bank materials (Simon et al., 2000), vegetation roots (Simon & Collison, 2002), and upper tension cracks (Langendoen & Simon, 2008). In particular, the procedure introduced by Langendoen and Simon (2008) discretizes the bank soil above the potential failure surface into several vertical slices to deal with complicated bank geometry, upper tension cracks and external actions such as those due to vegetation roots. BSTEM is, however, limited to gentle failure plane angles as a result of computational issues (Lai et al., 2015). BSTEM has also been used in tidal environments to investigate the stability of tidal channel headcuts (Kleinhans et al., 2009). Despite of its comprehensiveness, the main limitation of the BSTEM approach is that the near-bank groundwater table is assumed to be horizontal and constant (except for Midgley et al. (2012)). Hence, soil pore-water pressure variations and seepage forces are completely neglected and the model fails to predict failures due to seepage erosion unless the near-bank groundwater flow is separately considered (Lindow et al., 2009; Wilson et al., 2007).

The transient character of pore-water pressure has been accounted for through a finite element seepage analysis of the saturated and unsaturated flow that establishes inside a bank during a single flood (Rinaldi et al., 2004). The distribution of pore-water pressure can then be used as input data for bank stability analysis by LEM. This approach has been further extended by Darby et al. (2007) and Deng et al. (2018) to account for fluvial erosion and near-bank bed deformation. With respect to seepage force effects, Chu-Agor et al. (2008) computed the safety factor F_s of cohesive slopes subject to pop-out failures (Figure 13h). They derived new equations for F_s along failure planes parallel and perpendicular to the bank face. We refer the reader to Fox and Wilson (2010) and Rinaldi and Nardi (2013) for more details on modeling the interactions between seepage flow and bank collapse.

The LEM evaluates bank stability considering the effects of both soil properties and external forces and, most importantly, provides a simple and direct stability index (F_s). This method is appropriate for engineering projects of bank protection structures such as revetments, breakwaters and seawalls. It is anyhow of great importance to integrate LEMs and hydraulic models to better describe bank retreat processes in the presence of floodplain heterogeneity (e.g., composite riverbanks) or external forces such as pore-water pressure, seepage forces and waves. We therefore suggest using LEMs in conjunction with hydraulic models for short- or medium-term predictions when the effects of floodplain heterogeneity (Bogoni et al., 2017) and external forces are non-negligible.

Finally, it is worthwhile to note that, although the LEM provides a good agreement with field observations in terms of bank retreat rate and bank line evolution (Daly et al., 2015; Lai et al., 2015; Midgley et al., 2012; Patsinghasanee et al., 2017), it also has some limitations (Duncan et al., 2014; Gong et al., 2018; Rinaldi & Darby, 2007). The fundamental one is that bank materials delimited by the potential failure surface are assumed not to be subject to deformation. Besides, additional assumptions are commonly required for toppling failure. For

instance, a relation between the compressive (l_c) and tensile (l_t) lengths along the failure plane is required (Arai et al., 2018; Patsinghasanee et al., 2017; Xia, Zong, Deng, et al., 2014).

5.4. Stress-Strain Analysis

Stress-strain analysis has been developed to account for any deformation of bank material during bank collapse and has been applied to both fluvial and tidal contexts (Gong et al., 2018; K. Zhang et al., 2021; Masoodi et al., 2019; Samadi et al., 2013; Zhao et al., 2019, 2021). In the case of fluvial environments Samadi et al. (2013) employed an elastic-plastic constitutive model (using the SIGMA/W software, see https://www.geoslope.com) to investigate the development of stress and strain under the action of undermining. They found that the location of the maximum tensile stress on the bank top, where tension cracks occur, was always beyond the endpoint of the cantilever (i.e., closer to the landward boundary, see Figure 4a). This finding challenges the commonly adopted assumption that toppling failure occurs along the endpoint of the cantilever (Figure 13e) (Micheli & Kirchner, 2002; Van Eerdt, 1985). It also agrees with laboratory results indicating that failures are in general characterized by a greater retreat distance in the upper portion of the bank as compared to the lower undermining part (K. Zhang et al., 2021; Samadi et al., 2011). For tidal environments, Gong et al. (2018) proposed a process-based bank retreat model coupling the stress-deformation analysis with tide-induced bank erosion (Figure 13i). The Mohr-Coulomb failure criterion was applied to evaluate the state of soil elements after tide-driven bank erosion and, hence, to account for possible bank collapse. According to the state of soil elements (stable or subject to tensile and shear failure), three stages of the failure process are identified, namely, shear failure at the bank toe (Stage I), tensile failure on the bank top (Stage II), and sectional cracking from the bank top to the toe (Stage III). Note that both shear and tensile failures refer to soil element failure, rather than to overall failure of the cantilever block described in Section 2.2. This type of analysis was later extended by Zhao et al. (2019), who considered the effects of suspended sediment transport. Their results highlighted a negative effect of bank height on bank stability, in good agreement with experimental observations (Zhao et al., 2020).

In summary, the stress-strain analysis should be applied when bank deformation and the consequent stress concentrations due to the removal of bank soil (e.g., by near-bank channel flow, seepage flow and waves) are non-negligible, such as the evaluation of overhanging stability. Since this approach captures many details in terms of stress-strain behavior, it can be used for calibration of parameterized bank collapse models or to provide robust assumptions for LEMs. For example, the modeling of soil creep can take advantage of stress-strain analysis. The information provided by stress-strain analysis can in fact be employed to express soil diffusion as a function of effective shear stresses and thus of pore-water pressure. Overall, stress-strain analyses should be used for short- or medium-term predictions in the presence of complex external forces and therefore of soil deformation/stress states that cannot be easily treated through simplified approaches. It could also be used for long-term predictions in order to provide calibration and assumptions for more simplified models.

6. Feedbacks Between Bank Retreat and Morphodynamics

6.1. Effects of Bank Retreat on Morphodynamics

Bank retreat plays a key role on the morphodynamic evolution of natural rivers over a wide range of scales (Figure 1). In general, bank retreat controls the equilibrium river width by eventually reducing the shear stress on the banks to a critical threshold value (Francalanci et al., 2020; K. B. J. Dunne & Jerolmack, 2020). From the perspective of cross-sectional evolution, bank retreat is responsible for the instantaneous adjustment of the bank line (C. Hackney et al., 2015; Darby et al., 2007), which modulates near-bank hydrodynamics and, together with the transverse transport of sediment driven by secondary flow circulations which establish in meandering bends (Bolla Pittaluga & Seminara, 2011), gradually shift the thalweg from one bank to the other (Fryirs & Brierley, 2012; Parker et al., 2011; Stecca et al., 2017; Yuan et al., 2021). In various settings, bank-derived materials have been reported as the dominant factor of sediment budgets (Kronvang et al., 2013; Trimble, 2009). The collapsed sediments not only significantly affect the local morphodynamics but also feed the river reach downstream of the collapsed bank. For rivers in the loess area more than 80% of the total suspended sediment can be ascribed to bank erosion and collapse (Simon et al., 2000). In addition, the transit of bank-derived sediment from a given catchment to the ocean contributes to the global carbon cycle (Galy et al., 2015; Golombek et al., 2021; Repasch et al., 2022). For instance, lateral erosion of rivers cutting through floodplains releases

additional organic carbon fluxes to downstream depositional sinks (e.g., tidal flats and deltas). Hence, rivers with high channel mobility can enhance CO_2 drawdown (Repasch et al., 2021).

At the medium-term timescale (decades), bank retreat contributes significantly to river morphodynamics (Simon et al., 2000; Thorne et al., 1998a). In meandering rivers, the interaction between outer bank retreat and inner bank accretion determines channel widening or narrowing (Asahi et al., 2013; Parker et al., 2011; Zhao et al., 2021; Zolezzi et al., 2012). For instance, high-resolution field observations have documented the continuous interplay between bank-pull and bar-push mechanisms, whereby river bends widen and narrow in discrete steps while maintaining a statistically constant mean channel width (Lopez Dubon & Lanzoni, 2019; Mason & Mohrig, 2019). In the context of braided rivers, divergent flow due to braid bars facilitates channel widening, while the stabilizing action of vegetation counteracts bank erosion and reduces bar and channel dynamics (Bristow & Best, 1993; Schuurman et al., 2013). Laboratory experiments showed that bank strength provided by vegetation to a cohesionless material is the necessary ingredient to narrow and deepen channels favoring, the transition from braiding to meandering pattern (Braudrick et al., 2009; Tal & Paola, 2007; Van Dijk et al., 2013). In other words, an increase in bank stability and, hence, a reduction of bank retreat rate controls the transition between braiding and meandering rivers (Fredsøe, 1978; Gibling & Davies, 2012; Howard, 2009; Ielpi et al., 2022).

Over timescales of hundreds to thousands of years, bank retreat plays a fundamental role in determining floodplain heterogeneity, potentially forming strath terraces, and controlling the overall landscape evolution. Scroll bars and oxbow lakes consequent to river bend cutoffs are responsible for spatial heterogeneity in floodplain erodibility which, in turn, affects the long-term planform evolution of meandering rivers (Bogoni et al., 2017; Güneralp & Rhoads, 2011). The interaction between lateral bank retreat and vertical bed incision controls valley morphology. Remarkable examples are the spectacular lithological structures created by highly sinuous meanders in deep slot canyons and the stepped strath terraces forming within broader mountain valleys (Hancock & Anderson, 2002; Limaye & Lamb, 2014; Venditti et al., 2014). Generally, erosion-resistant rocks and high vertical incision rates favor the formation of narrow canyons, while wide strath terraces tend to develop in relatively weak sedimentary rocks with high bank retreat rates (Brocard & Van der Beek, 2006; Limaye & Lamb, 2014). Field observations indicate a strong lithologic influence on strath terrace formation. Indeed, the asymmetry in erodibility between submerged and emerged rocks promotes lateral widening rather than vertical incision of bedrock rivers (Montgomery, 2004). In contrast, the intermittent collapse of the valley margins due to lateral undercutting can facilitate vertical incision over lateral widening. The formation of talus piles from slump blocks, in fact, shields the valley slopes and potentially prevents terrace formation (Malatesta et al., 2017).

The evolution of open coasts, tidal inlet and estuary systems is also related to bank retreat processes (Anthony et al., 2010; Francalanci et al., 2013; Guo et al., 2021; Hughes, 2012; Zhang et al., 2015). Tidal meanders are one of the most active geomorphic units of unvegetated intertidal mudflats. They migrate frequently owing to outer bank retreat and, hence, can cause damage to coastal infrastructure such as seawalls (Figure 14) and offshore wind structures. The planimetric shape of tidal channels is generally funneled in order to accommodate a seaward increasing tidal prism (Gong et al., 2018; Lanzoni & D'Alpaos, 2015; Marani et al., 2002; van der Wegen et al., 2008), while the bank profile is typically characterized by convex or concave shapes depending on the mechanism dominating bank retreat (Zhao et al., 2019). For small tidal channels composed of highly cohesive sediment, meander dynamics are very slow. The high thresholds for erosion typical of muddy sediment and the limited size of the tidal prism leads to a situation whereby bank retreat typically occurs only in very sharp bends (Kleinhans et al., 2009). Erosion of cohesive sediment in tidal settings is also affected by the possible presence of cohesive extracellular polymeric substances (EPS) generated by microorganisms abundant on intertidal flats (Figure 14c). Although EPS are widely regarded as bed "stabilizers," enhancing sediment strength (Flemming & Wuertz, 2019), recent flume experiments show that under wave actions, the inclusion of EPS may induce higher mobility of the sediment, liquefying an otherwise stable bed (X. Chen et al., 2021). As a result, how EPS affects bank stability and, consequently, tidal channel dynamics remains unclear.

Halophytic vegetation has a stabilizing effect on channel banks (Y. Chen et al., 2019). This effect, coupled with the competing feedbacks produced by vegetation encroachment on salt marsh surfaces (Sgarabotto et al., 2021), leads to small width-to-depth ratios. Moreover, the lateral migration rate can be reduced by several orders of magnitude as compared to unvegetated mudflats (Finotello et al., 2018; Gabet, 1998). Salt marsh channels are thus often thought of as being relatively stable landscape features (D'Alpaos et al., 2007; Kearney & Fagherazzi, 2016). However, when normalized by local channel width, the observed migration rates of tidal and fluvial meanders
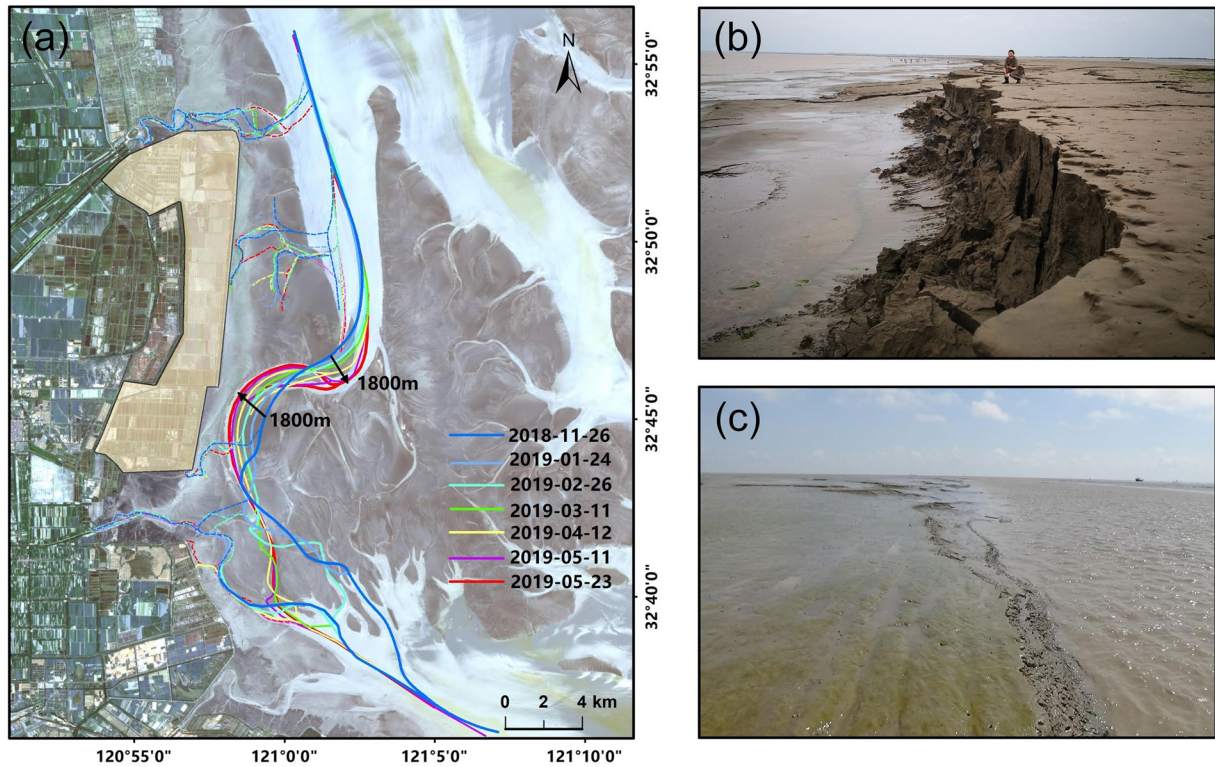
Figure 14. (a) Short-term evolution of tidal meanders showing a fast migration of their centerlines toward seawalls (the centerlines are obtained using the waterline method (Kang et al., 2017)). (b) Bank collapse of tidal channels on unvegetated intertidal mudflats (radial sand ridges in the southern Yellow Sea, China; image taken on May 2019). (c) Evidence of abundant microorganisms on tidal channel banks (Jiangsu coast, China; image taken by K. Zhao on July 2021).

are shown to be quite similar (Finotello et al., 2018). Hence, in the long-term, the role of bank retreat in salt marsh channels is non-negligible. It is also worthwhile to note that existing numerical models fail to reproduce the formation of the highly curved branches that are typically observed in salt marsh channels, partly due to the oversimplification or even exclusion of bank retreat process (Fagherazzi et al., 2012; Geng et al., 2021; Kirwan & Murray, 2007; Temmerman et al., 2007). Over large spatial scales, salt marsh stability or deterioration is controlled by the mutual interaction between vertical sea level rise and sediment supply, as well as the lateral cliff retreat and vegetation colonization (Bendoni et al., 2016; Feagin et al., 2009; Francalanci et al., 2013). Although the adaption to sea level rise can make salt marshes reach equilibrium in the vertical direction (Kirwan et al., 2010), they may be inherently unstable in the horizontal direction (Fagherazzi et al., 2013), leaving unanswered the question of whether a salt marsh can really survive to future rates of sea level rises.

6.2. Integration Between Morphodynamic Models and Bank Retreat Processes

At the beginning of the 1990s, critical issues concerning the integration between morphodynamic and bank retreat models were discussed by the ASCE Task Committee (Thorne et al., 1998b). This discussion included the importance of: (a) the accurate prediction of the boundary shear stress distribution in the near-bank region, (b) the simulation of the corresponding sediment fluxes over the entire channel width, (c) the calculation of the rate of flow-induced bank erosion, and resultant bank profile deformation, (d) the evaluation of bank stability and consequent adjustment of bank line, and (e) the exchanges of sediment (e.g., slump blocks) between the banks and the bed material. Over the last 30 years, researchers have addressed the above issues with particular emphasis on the deformation of the bank profile and its feedbacks on near-bank morphodynamics (Klavon et al., 2017; Rinaldi & Darby, 2007; Rinaldi & Nardi, 2013).

The bank profile caused by erosion of bank material and/or consequent bank collapse has in general been computed using near-bank bed shear stresses, provided by depth-averaged hydrodynamic models, either linearized (E. Eke et al., 2014; Motta et al., 2014; Zhao et al., 2021) or fully numerical (Darby & Thorne, 1996b;
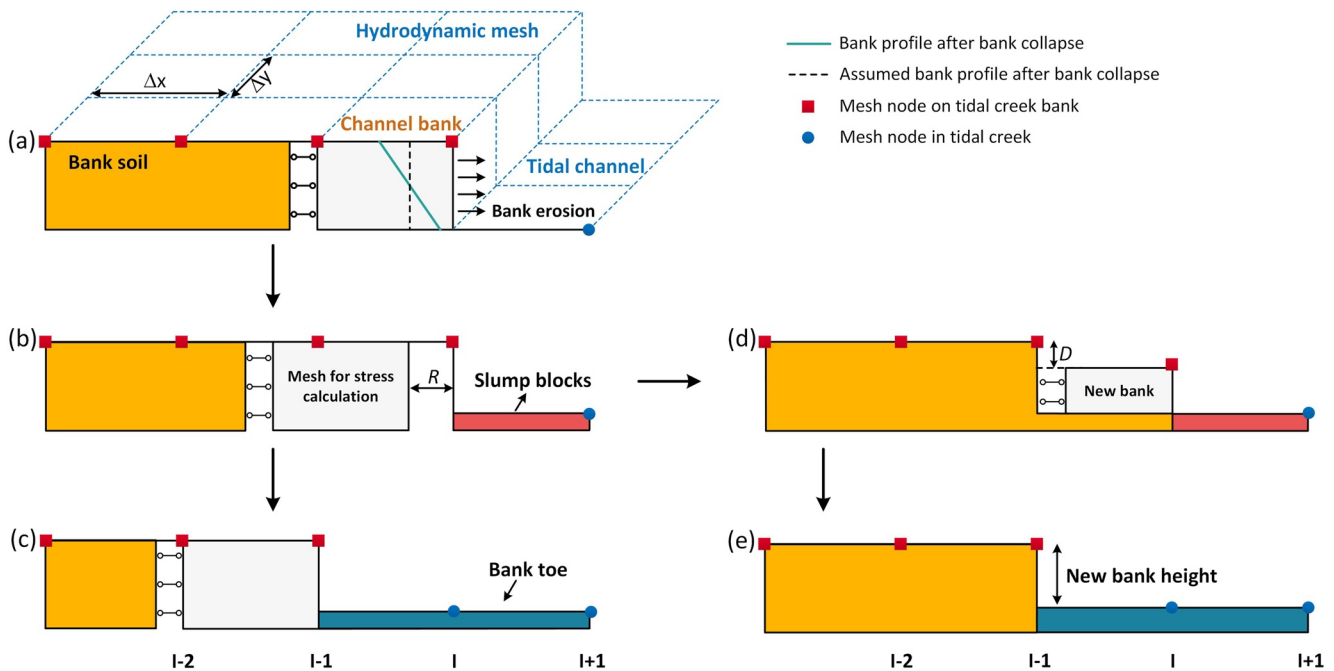
Figure 15. Illustration of the different approaches adopted for coupling hydrodynamic and bank retreat models (adapted from Zhao et al. (2019)). Panels (a–c) show the procedure of the first method discussed in the text, while (a, b, d, e) display the procedure of the second method.

Langendoen et al., 2016; Rinaldi et al., 2008). However, vertical variations in shear stress are neglected by these models and, hence, the submerged part of the bank is inevitably taken to have a rectangular shape. As a result, this modeling approach is suitable only for steep banks controlled by cantilever failure (e.g., tidal creek banks on muddy flats (Gong et al., 2018)). For inclined riverbanks composed of multiple stratigraphic layers, additional procedures are needed to simulate the distribution of shear stresses along the wetted bank (Langendoen, 2000; Motta et al., 2014). For example, the shear stress acting on each layer of the bank can be calculated by scaling the shear stress at the bank toe by the hydraulic radius of the layer (see Figure 2 in Lai et al. (2015)). When part of the bank is eroded by the flow, the computational domain (described through either structured or unstructured grids) must be adjusted to adapt to the new bank geometry (Darby et al., 2007; Gong et al., 2018; Patsinghasanee et al., 2017; Zhao et al., 2019).

Three main approaches have been put forward to couple together hydrodynamic and bank retreat models (Figure 15). The first method records the accumulated retreat distance (Figures 15a–15c), and the hydrodynamic mesh is updated when the cumulative retreat distance exceeds the transverse grid size (Darby et al., 2002; Deng et al., 2019; Gong et al., 2018; Jia et al., 2010). The channel width thus varies intermittently, and instantaneous feedbacks on the flow field are not accounted for. A possible solution to this shortcoming is the use of the so-called immersed boundary method, whereby the bank line is followed with a cut-cell approach (Canestrelli et al., 2016; Mittal & Iaccarino, 2005). The second method replaces bank retreat with a decrease in bank height (Abderrezzak et al., 2016; Rousseau et al., 2017; Stecca et al., 2017; van der Wegen et al., 2008; Zhao et al., 2019). Once the bank height decreases to a threshold value, mesh nodes representing the bank top are transformed to mesh nodes representing the channel bed (e.g., point I in Figure 15d and 15e). Although bank retreat is not simulated by a horizontal widening, this method accounts for a progressive reduction in near-bank flow velocity. Contrary to the above fixed-mesh approaches, the third method re-generates boundary-fitted curvilinear or unstructured grids, based on the simulated bank retreat distance (Asahi et al., 2013; Langendoen et al., 2016). The mesh nodes on the bank top are shifted, and an additional criterion is applied to smooth the bank line. Since the grid lines do not always align with the bank top, this method performs better in terms of river width adjustment (Lai et al., 2015).

Despite the remarkable advances performed in coupling bank retreat process with hydraulic modeling, some challenges deserve further attention. First, the distribution of near-bank shear stresses under complex bank/channel bed topography remains unclear. This complexity is partly the result of bank undermining, which forms a concave
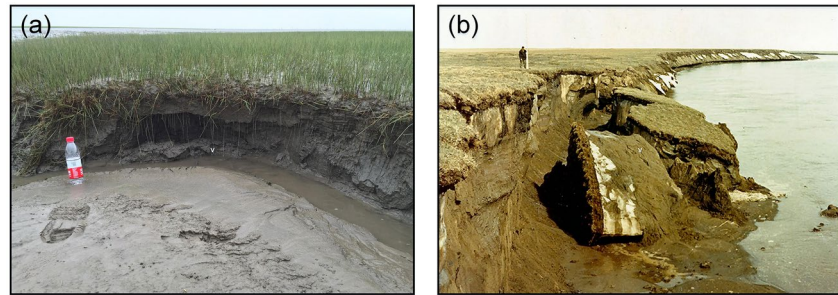
Figure 16. (a) Deformation of bank profile as a result of undermining (Chongming Dongtan wetland, China; image taken by K. Zhao on June 2016). (b) Illustration of dramatic riverbank retreat and resultant slump blocks on the Colville River delta in northern Alaska (adapted from Walker (2013)).

cavity (Figure 16a). Also, the initiation of gullies, streams, and tidal creeks is affected by the configuration of the bank profile and the related shear stress distribution. Second, for medium- and long-term simulations little attention has been paid to the representation of bank retreat as an intermittent process. Since the estimation of bank stability is complex and computationally costly, suitable parametrizations able to account for intermittent bank collapse events are needed. The third issue concerns the interactions between groundwater fluctuations and bank retreat. Notwithstanding much progress achieved in recent years (see Sections 5.3 and 5.4), the need for a continuous adaptation of the computational mesh limits the application of LEMs and stress-strain analyses to a broader context. The last issue is associated with the fate of slump blocks (Figure 16b), as discussed below (Section 7.3).

7. Open Questions and Future Research Needs

The studies reviewed in the previous sections have produced remarkable advances in our understanding of bank retreat in terms of failure mechanisms, development of empirical predictive relations, and numerical modeling. However, many essential questions remain wholly or partially unanswered. In this section, we discuss three challenges that deserve attention in order to improve our fundamental understanding of bank retreat processes. The first challenge is to unravel the complex mechanism of multifactor-driven bank erosion in both fluvial and tidal environments, with particular attention to the interactions between hydrodynamics, soil properties, and biological processes. The second challenge is to clarify whether the assessment of bank retreat in fluvial and tidal environments needs somewhat ad hoc approaches, given the different temporal and spatial scales operating in these different settings. The third issue is to assess the role that collapsed bank soil has on channel morphodynamics, eventually affecting bank retreat, hydrodynamics, and sediment dynamics.

7.1. Multifactor-Driven Bank Retreat

There is ample experimental evidence (at both the field and laboratory scales) that bank retreat is driven by the interactions between hydrodynamics and geotechnical factors, biological processes, and sediment dynamics (Figure 17). However, much of the reviewed literature, with some notable exceptions, focuses on the effects of a single factor and deals with fluvial environments, with their distinctive boundary conditions. Studies that account for two or more factors, especially in the context of tidal environments, are therefore needed to improve our understanding of bank retreat across a broad range of real-world systems.

The consequences of temporal variations in soil pore-water pressure on the physical properties of bank soil surely merit attention. Changes in soil pore-water pressure are commonly associated with floods, periodic tides, overtopping waves, seepage erosion, and drying-wetting cycles. Although quantitative observations have been conducted for soil pore-water pressures (Midgley et al., 2013; Nardi et al., 2012), we still do not fully understand how changes in pore-water pressures may influence bank stability through bank soil properties. Samadi et al. (2013) replaced fluvial erosion processes with artificial undermining, thus separating the effects of soil properties. The results of these controlled laboratory experiments underlined the importance of bank soil properties on bank collapse mode, and indicated that tensile failure is absent when soil cohesion is low. The role of soil pore-water

Multifactor-driven bank retreat

Figure 17. Sketch of the multiple influences that drive bank retreat.

pressure has been long neglected in numerical modeling. Only a few studies have been conducted to explore the interactions with other factors (Darby et al., 2007; Deng et al., 2018; K. Zhang et al., 2021). For instance, Darby et al. (2007) considered the transient variation in pore-water pressure in response to flood events. They found that the deformation of the bank profile due to fluvial erosion can itself alter the hydraulic head driving infiltration into the bank, and hence the distribution of pore-water pressure. These studies are as yet limited to fluvial erosion. Other erosion processes typical of tidal environment, such as recursive water level oscillations, subsurface flow and wind waves, have been shown to affect soil pore-water pressure (Cao et al., 2012; Fox et al., 2006; Francalanci et al., 2013; Xin et al., 2022) and therefore call for their implementation in numerical models.

Surprisingly, the role of vegetation on bank stability has received relatively little attention (Camporeale et al., 2013). While qualitative comparisons have been performed through laboratory experiments carried out with and without vegetation (Cancienne & Fox, 2008; Francalanci et al., 2013), a quantitative and systematic analysis is still lacking. Moreover, previous laboratory experiments have been designed to maintain both geometrical (e.g., bank

height) and material (e.g., soil cohesion) scaling, following the suggestions of D. M. Wood (2014). Neglecting the reinforcement ensured by vegetation roots might explain the field-laboratory discrepancy whereby the dominant failure mechanism in downscaled laboratory experiments is toppling failure (Patsinghasanee et al., 2017; Samadi et al., 2013; Zhao et al., 2020), while shear-type failures are most commonly observed in natural rivers (Langendoen & Simon, 2008; Simon et al., 2000). Vegetation roots counteract the development of tension cracks (Francalanci et al., 2013) typical of toppling failures (Patsinghasanee et al., 2015; Samadi et al., 2013; Zhao et al., 2020). Clearly, maintaining geometrical, material and vegetation (e.g., roots density per unit width and diameter) scaling in laboratory experiments is not a trivial task. More efforts are thus needed to unravel what role vegetation roots play in bank stability, and how vegetation interacts with hydrodynamic forces, finding a reasonable balance between the requirements for geometrical, material, and vegetation scaling.

In numerical models, the role of vegetation is commonly parameterized in terms of root cohesion (i.e., mechanical effects). Hydrological effects (e.g., rainfall interception and soil moisture extraction) have received little attention, as pointed out by Simon and Collison (2002). The mechanical effects so far treated are limited to the root enhancement of shear strength. Little attention has been paid to tensile strength which, as noted above, was proven to be important for toppling failure (Van Eerdt, 1985; Xia, Zong, Deng, et al., 2014). The cyclic fluctuations of pore-water pressure, as a result of tides and waves, are also strongly influenced by vegetation cover, and hence may affect the stability of salt marshes borders. The model developed by Xin et al. (2013), coupling subsurface flow and plant growth, led to the identification of three characteristic zones for plant growth along salt marsh creeks. These zones are determined by the combined influence of spring-neap tides and evapotranspiration. This review thus supports the need to improve the understanding of bank stability with respect to vegetation, particularly for environments such as salt marshes where the toppling mechanism dominates, and where tides and wind waves control subsurface flow and, hence, pore-water pressure variations.

Further evidence for the role of multiple stressors (surface and seepage flow, ship waves) on bank retreat has been provided by field measurements. For instance, Rengers and Tucker (2014) observed the following cycle for multifactor-driven bank retreat. A pop-out failure driven by seepage flow left an overhanging block, followed by toppling failure. The collapsed soil was then eroded by near-bank channel flow. Based on detailed monitoring of upper-bank erosion, Duró et al. (2019) stated that floods were not necessary for the basal clean-out of failed material, since ship waves during the dry season acted to disaggregate and remove the collapsed bank soil. More research is however needed to improve the accuracy of the prediction of multifactor-driven bank retreat. For long-term timescales empirical relations should be developed which integrate factors like water and sediment discharges, wave power, and rainfall. An attempt in this sense has been pursued to predict the vertical incision rate of bedrock rivers under various processes (Lague, 2014). Other factors such as soil chemical properties (e.g., soil dispersion), biological perturbators (e.g., biofilms and crabs) are also likely to play a major role in multifactor-driven bank retreat.

7.2. Similarities and Differences Between Fluvial and Tidal Environments

As reviewed in Section 3, there are some similarities between fluvial and tidal environments, such as the dominant driving forces and failure modes associated with bank stability. Notwithstanding these similarities, that for example, reflect in comparable migration rates of tidal and fluvial meanders when normalized to the channel width (Finotello et al., 2018), the external forces imposed on river banks exhibit somewhat distinct characteristics, arising from the differences in the drivers of flow motion. While hydrodynamic of rivers is governed by topographic gradients, in the case of tidal landscapes water surface gradients drive the flow (Coco et al., 2013). Here, we discuss various aspects that are clearly distinct between fluvial and tidal environments, thus requiring specific attention to improve our understanding of bank retreat process.

Basically, the time-scale typical of water level variations within tidal systems (hours) is much faster than its fluvial counterpart (months). The hydrograph of the pore-water pressure variation is also quite different when dealing with tides and waves (Xin et al., 2011, 2016). In the case of waves (generated either by winds or by boats), the frequency at which bank soil is subject to saturation and unsaturation cycles grows to a large extent as compared to tidal forcing. On the other hand, Xin et al. (2011) found that the simulated groundwater dynamics exhibited significant flow asymmetry over tidal cycles, and the timescale of pore-water circulation decreased landward by orders of magnitude. Their work underlines the hydrological complexity of intertidal marshes, and shows the importance of subsurface flow dynamics over a range of spatial scales. Since bank retreat rate is related

to the ratio H_b/H_w (Figure 11a in Section 4.2), for tidal systems the periodical variation in water level results in an elusive curve of bank retreat rate. Also, tidal channel banks potentially experience two periodical erosion mechanisms over one tidal cycle: coupled erosion by seepage and near-bank channel flow during ebb tides or alternatively, by overbank flow at flood or ebb peak. As a result, previous models or empirical relations developed for riverine morphodynamics (e.g., BSTEM) might be unsuitable for tidal environments, due to their strong simplifications or disregard of some key processes.

Another important distinction is that tidal channel banks experience periodical changes in flow direction. According to bend instability theory, meander bends migrate either upstream or downstream, depending on the phase lag between the bend apex and the peak flow location (Lanzoni & Seminara, 2006). In tidal environments, the flow field and consequently the location characterized by the maximum bank erosion rate differ between flood and ebb tides (Solari et al., 2002). The key factor controlling the phase of the point bar pattern relative to channel curvature is thus the flood- or ebb-dominant character of the basic flow (Tambroni et al., 2017). On the other hand, bidirectional flows result in bank soil heterogeneity mainly in the cross-shore direction (due to sediment sorting (Zhou et al., 2015, 2016)), rather than in the vertical direction as commonly observed in riverbanks (e.g., composite bank (Samadi et al., 2013; Xia, Zong, Deng, et al., 2014)). These processes, for example, can explain why tidal meanders are in general less morphologically complex and display more spatially homogeneous characteristics when compared to fluvial meanders (Finotello et al., 2020). Other processes, such as salinity dynamics, affect bank stability through soil dispersion (Masoodi et al., 2019). More efforts are therefore needed to investigate bank retreat resulting from the above processes, and ultimately to unravel the intrinsic differences between fluvial and tidal systems.

7.3. Collapsed Bank Soil

Collapsed bank soil (also referred to as slump blocks) is the product of bank collapse. When such material deposits at the base of the bank, it modulates bank erosion, affects the flow field, and alters the channel topography. Part of the collapsed bank soil is likely to protect the bank from direct erosion (A. L. Wood et al., 2001). Fagherazzi et al. (2004) observed that collapsed bank soil in salt-marsh creeks was able to persist for several years, and was responsible for the channel erosion paradox (Gabet, 1998), whereby marsh creeks are likely to migrate laterally at a quite slow rate despite the widespread occurrence of bank collapse. Midgley et al. (2013) reported that seepage erosion became temporarily restricted after bank collapse, since the collapsed bank soil blocked flow pathways and limited particle mobilization. From a morphodynamic perspective, collapsed bank soil abruptly alters the local topography and the flow resistance of the near-bank channel bed (K. Zhang et al., 2021), possibly generating complex turbulence at the bank toe and affecting the cross-sectional evolution of channels. Based on three-dimensional flow field observations, C. Hackney et al. (2015) stated that collapsed bank soil may also deflect flow onto the bank, thus enhancing bank erosion rate. In addition, collapsed bank soil is a source of sediment that may alter downstream channel morphology. Large failures are likely to cause the temporary constriction of the cross-sectional area of the flow, especially for small rivers covered by trees. This narrowing induces velocity gradients along the adjacent cross sections, and might be a reason for the inception of bar-pool patterns along channels (Duró et al., 2016). Another distinct phenomenon is detected in cold environments, where collapsed bank soil is often surrounded by ice blocks, and therefore can be transported more downstream by means of drifting ice (Black et al., 2018). Collapsed bank soil has also been proven to act as a bridge between near-bank hydrodynamics and morphodynamics (e.g., through the concept of basal endpoint control mentioned in Section 4.2), and therefore plays an important role in the bank retreat cycle (Figure 17). More research is needed to understand how collapsed bank soil, bank erosion/collapse, hydrodynamics, and sediment dynamics interact to form the overall architecture and morphology of fluvial and tidal settings, depending also on the size of the considered channel and the intensity of the flow therein.

Recently, the fate of collapsed bank soil has been investigated through numerical modeling (Asahi et al., 2013; Darby et al., 2002; Deng et al., 2019; E. Eke et al., 2014; Lai et al., 2015; Langendoen, 2000; Parker et al., 2011; Zhao et al., 2019). Parker et al. (2011) proposed an armoring coefficient, as a multiplier of sediment flux, to account for the armoring effect of collapsed bank soil. While accounting for the protection effects, this method neglects the consequences on local topography and hydrodynamics. The role of apparent cohesion in the removal of collapsed bank soil was also underlined by A. L. Wood et al. (2001), who suggested that not only block size, but also the vertical distribution of apparent cohesion should be accounted for to enable improved estimation of

the entrainment of the collapsed bank soil. An attempt to account globally for all these effects in a probabilistic approach has been recently put forward by Lopez Dubon and Lanzoni (2019). More research is clearly needed to better describe the feedbacks between bank erosion/collapse and the collapsed soil.

8. Summary and Conclusions

We have presented a comprehensive review of bank retreat dynamics with respect to mechanisms, observations, and modeling, covering both rivers and tidal channels. Our review includes the commonly observed failure mechanisms and other factors that can cause bank retreat, synthesizes laboratory and in situ observations of bank retreat rate, and discusses the numerical methods used to simulate bank retreat.

On the basis of observational data, we have reviewed mechanisms of bank collapse with respect to subaerial processes, surface flow (including near-bank channel flow and overbank flow), seepage flow, fluctuations in soil pore-water pressure and waves. Specific attention has been paid to the role of vegetation, biological disturbances, and hydrostatic pressure head. We have provided evidence demonstrating that the various types of external forces, despite their distinct characteristics, may have similar effects on bank stability, leading to the same failure mode: typical erosion and tensile failure in the middle and lower part of the bank, followed by toppling failure.

Existing empirical relations for predicting bank retreat exhibit a large scatter over spatial and temporal scales, a consequence of the inherent complexity of the interactions and feedbacks between the mechanisms controlling bank retreat. When compared with the hydraulic-based or geotechnical-based empirical predictors, the relations that integrate hydraulic and geotechnical impacts are more accurate, thus highlighting the necessity to account for both hydraulic and geotechnical parameters.

Based on the way in which bank collapse is accounted for, we categorize existing modeling approaches into a hierarchy: purely hydraulic (in which only sediment erosion is accounted for), parameterized bank collapse, static equilibrium, and stress-strain analysis. We also discuss the advantages and challenges of these methods, and provide some model recommendations in terms of real-world applications.

Overall, this review recognizes the role of bank retreat on the overall architecture and morphology of rivers and tidal channels. We also propose three research directions (multifactor-driven bank retreat, discrepancy between fluvial and tidal environments, and the role of collapsed bank soil) that we believe are critical to advance the future understanding and prediction of morphodynamics in these systems.

Symbols

a, b, c, d	Empirical regression coefficient
A_{chunk}	Volume of the collapsed bank soil per unit length
A_d	Drainage area (km^2)
$\Phi_{60}A_i$	Effective drainage area (m^2)
B_c	Width of cantilever (m)
B_b	Width of marsh cliff block (m)
c'	Effective soil cohesion (kPa)
C_2''	Empirical parameter depending on sediment packing
c_r	Cohesion provided by vegetation roots (kPa)
CEI	Cavity Erosion Index
C_s	Concentration of sediment mobilized by seepage sediment (g/L)
D	Grain size of bank material (mm)
D_f	Days with air frost (day)
E_m	Mass erosion rate for bank materials (kg/s)
E_l	Linear erosion rate for bank materials (m/year)
E_v	Volumetric erosion rate for bank materials (m^3/year)
E_a	Areal erosion rate for bank materials (m^2/year)
F_s	Safety factor
F_R	Resisting forces used to calculate safety factor
F_D	Destabilizing forces used to calculate safety factor

F_w	Hydrodynamic thrust due to water waves
g	Acceleration due to gravity (m/s^2)
H_b	Bank height (m)
H_c	Height of the cantilever (m)
H_p	Thickness of the cantilever subject to tensile failure (m)
H_t	Depth of tension crack on the bank top (m)
H_{ub}	Upper bank height (m)
H_w	Near-bank water depth (m)
i	Hydraulic gradient driving seepage flow
i_c	Critical hydraulic gradient for seepage erosion
K_l	Volumetric erodibility coefficient for surface flow erosion (m^3/N/s)
K_w	Erodibility coefficient for wave erosion
K_s	Seepage erodibility coefficient
K_{sat}	Saturated hydraulic conductivity (m/s)
l_t	Length of cantilever under tensile stress (m)
l_c	Length of cantilever under compressive stress (m)
P	Hydrostatic pressure per unit width (kN/m)
P_c	Threshold value for wave-induced retreat
P_{ic}	Hydrostatic pressure inside the crack (kN/m)
P_w	Mean wave power calculated over a representative period (W/m)
P_s	Precipitation intensity (mm)
Q_s	Seepage discharge (L/s)
Q_l	Channel flow discharge (L/s)
Q_c	Critical seepage discharge for bank erosion (L/s)
q_s^*	Dimensionless seepage-induced sediment flux
q_b	Volumetric sediment transport rate per unit width in the transverse direction (m^2/s)
r_l	Dimensionless normalized bank retreat rate in response to surface flow
S	Slope gradient
t	Time (s)
t_b	Elapsed time of first collapse (min)
U	Hydrostatic-uplift force per unit width (kN/m)
U_c	Near-bank flow velocity (m/s)
U_d	Darcy velocity (m/s)
u_w	Pore water pressure (kPa)
u_a	Pore air pressure (kPa)
V_s	Seepage-induced cavity volume (cm^3)
V_g	Eroded bank gully volume (m^3)
W	Soil weight per unit width (kN/m)
w_t	Overhanging block width (m)
w_c	Channel width (m)
z_b, z_l	Dimensions of the failure soil block (m)
α	Bank angle (°)
β	Failure-plane angle (°)
η	Near-bank bed elevation (m)
θ	Oscillation angle around an equilibrium configuration (°)
ε	Bank retreat or accretion rate (m/s)
Δ	Ratio of bank soil density to water density
σ	Total normal stress (kPa)
σ_c	Compressive stress along the failure plane (kPa)
σ_t	Tensile strength along the failure plane (kPa)
τ	Shear strength of bank materials (kPa)
τ_s^*	Dimensionless shear stress induced by seepage
τ_b	Boundary shear stress applied by the near-bank flow (Pa)
τ_c	Critical shear stress for bank erosion (Pa)

τ_{cs}^*	Dimensionless critical shear stress for seepage erosion
λ	Direction of the seepage vector (°)
λ_b	Porosity of the bank material
φ'	Effective internal friction angle (°)
φ^b	Angle expressing the rate of increase in strength relative to the matric suction (°)
ω	Stream power per unit bed area
γ_b	Bank soil resistance

Glossary

Apparent cohesion	the cohesion of grains caused by surface tension in the surrounding pore water.
Angle of repose	the steepest angle of descent or dip relative to the horizontal plane without slumping.
Bank stratification	bank composed of heterogeneous layers.
Cohesive	a collection of sediment particles that cohere, or stick together, largely due to electrochemical forces.
Drainage area	the land area where precipitation falls off into river basins and gullies, usually identified by the line along the highest topographic elevation (in fluvial settings) or the zero flux divide (in tidal settings) and connecting its ends to the outer section of the basin/gullies.
Dry granular flow	a kind of bank collapse consisting of an avalanche of granular, loose sediment, creating a fan-shaped debris accumulation close to the angle of repose.
Effective internal friction angle	internal friction angle in the context of saturated soils.
Effective soil cohesion	soil cohesion in the context of saturated soils.
Elastic-plastic model	a description of the relation between stress and strain.
Elastic potential energy	the energy stored as a result of applying a force to deform an elastic object.
Evapotranspiration	sum of evaporation and plant transpiration.
Evaporation	the process by which water changes from liquid to a gas or vapor.
Fluidization	a process similar to liquefaction whereby a granular material is converted from a static solid-like state to a dynamic fluid-like state.
Gully erosion	the removal of soil along drainage lines by surface water runoff.
Headcuts	an erosional feature characterized by an abrupt vertical drop. Also called "knickpoint."
Hydraulic conductivity	the ability of the material to transmit fluid through pore spaces and fractures in the presence of an applied hydraulic gradient.
Hydraulic head	liquid pressure above a vertical datum.
Infiltration	the process by which water on the ground surface enters the soil.
Inner bank	the bank with the smallest radius of curvature around a bend, commonly characterized by bank accretion.
Internal friction angle	measure of the ability of a unit of a soil to withstand a shear stress, defined by the angle between the applied shear stress and the normal effective stress at which shear failure occurs.
Matric suction	the pressure that a dry soil exerts on the surrounding soils to equalize everywhere the moisture content.
Mechanical fatigue	weakening of bank soils caused by cyclic loading such as waves.
Mohr-Coulomb failure criterion	a mathematical model describing the state of soil units.
Normal stress	the stress perpendicular to a specific plane.
Outer bank	the bank with the largest radius of curvature around a bend, commonly characterized by bank erosion.
Perched water table	an aquifer that occurs above the regional water table, in the vadose zone.

Plunge pool erosion	bed erosion immediately downstream of headcuts.
Root cohesion	soil cohesion provided by vegetation roots.
Shear strength	the resistance of a material to breaking under shear.
Shear stress	the component of stress coplanar with a material cross section.
Soil cohesion	soil shear strength that is independent of interparticle friction.
Soil desiccation	soil free from all moisture.
Soil diffusivity	a coefficient to describe soil creep.
Soil dispersion	soils become vulnerable as a result of hydration of sodium ions between clays.
Soil permeability	the property of soils to transmit water and air.
Static liquefaction	the sudden loss of strength when loose soil, typically granular materials such as sand or silt, is loaded and cannot drain.
Stemflow	the flow of intercepted water down the trunk or stem of a plant.
Subaerial process	weathering and mass movement process.
Tensile strength	the resistance of a material to breaking under tension.
Tensile stress	the stress caused by pulling the material.
Tension crack	cracks induced by tensile force.
Undercutting	bank erosion occurring at the lower part of the bank.
Weathering	the process that changes solid rock into sediments.

Data Availability Statement

All data shown in the figures of this review is available on GitHub website (https://github.com/zk1357/Review-on-bank-retreat), and is extracted from the following references: Seginer (1966), Hooke (1980), Vandekerckhove, Muys, et al. (2001), Vandekerckhove, Poesen, et al. (2001), Vandekerckhove et al. (2003), Braudrick et al. (2009), De Rose and Basher (2011), van Dijk et al. (2012), Wells et al. (2013), Patsinghasanee et al. (2017), Qin et al. (2018), Vargas Luna et al. (2019), Shu et al. (2019), and Zhao et al. (2020).

References

Abate, M., Nyssen, J., Steenhuis, T. S., Moges, M. M., Tilahun, S. A., Enku, T., & Adgo, E. (2015). Morphological changes of Gumara River channel over 50 years, upper Blue Nile basin, Ethiopia. *Journal of Hydrology*, *525*, 152–164. https://doi.org/10.1016/j.jhydrol.2015.03.044

Abderrezzak, K. E. K., Moran, A. D., Tassi, P., Ata, R., & Hervouet, J. (2016). Modelling river bank erosion using a 2D depth-averaged numerical model of flow and non-cohesive, non-uniform sediment transport. *Advances in Water Resources*, *93*, 75–88. https://doi.org/10.1016/j.advwatres.2015.11.004

Abernethy, B., & Rutherfurd, I. D. (1998). Where along a river's length will vegetation most effectively stabilise stream banks? *Geomorphology*, *23*(1), 55–75. https://doi.org/10.1016/S0169-555X(97)00089-5

Akay, O., Özer, A. T., Fox, G. A., & Wilson, G. V. (2018). Application of fibrous streambank protection against groundwater seepage erosion. *Journal of Hydrology*, *565*, 27–38. https://doi.org/10.1016/j.jhydrol.2018.08.010

Allen, J. (1989). Evolution of salt-marsh cliffs in muddy and sandy systems: A qualitative comparison of British west-coast estuaries. *Earth Surface Processes and Landforms*, *14*(1), 85–92. https://doi.org/10.1002/esp.3290140108

Amiri, M., Pourghasemi, H. R., Ghanbarian, G. A., & Afzali, S. F. (2019). Assessment of the importance of gully erosion effective factors using Boruta algorithm and its spatial modeling and mapping using three machine learning algorithms. *Geoderma*, *340*, 55–69. https://doi.org/10.1016/j.geoderma.2018.12.042

Anthony, E. J., Gardel, A., Gratiot, N., Proisy, C., Allison, M. A., Dolique, F., & Fromard, F. (2010). The Amazon-influenced muddy coast of South America: A review of mud-bank–shoreline interactions. *Earth-Science Reviews*, *103*(3–4), 99–121. https://doi.org/10.1016/j.earscirev.2010.09.008

Arabameri, A., Yamani, M., Pradhan, B., Melesse, A., Shirani, K., & Bui, D. T. (2019). Novel ensembles of COPRAS multi-criteria decision-making with logistic regression, boosted regression tree, and random forest for spatial prediction of gully erosion susceptibility. *The Science of the Total Environment*, *688*, 903–916. https://doi.org/10.1016/j.scitotenv.2019.06.205

Arai, R., Ota, K., Sato, T., & Toyoda, Y. (2018). Experimental investigation on cohesionless sandy bank failure resulting from water level rising. *International Journal of Sediment Research*, *33*(1), 47–56. https://doi.org/10.1016/j.ijsrc.2017.08.002

Asahi, K., Shimizu, Y., Nelson, J., & Parker, G. (2013). Numerical simulation of river meandering with self-evolving banks. *Journal of Geophysical Research: Earth Surface*, *118*(4), 2208–2229. https://doi.org/10.1002/jgrf.20150

Bassis, J. N., Berg, B., Crawford, A. J., & Benn, D. I. (2021). Transition to marine ice cliff instability controlled by ice thickness gradients and velocity. *Science*, *372*(6548), 1342–1344. https://doi.org/10.1126/science.abf6271

Baynes, E. R., Lague, D., Steer, P., Bonnet, S., & Illien, L. (2020). Sediment flux-driven channel geometry adjustment of bedrock and mixed gravel-bedrock rivers. *Earth Surface Processes and Landforms*, *45*(14), 3714–3731. https://doi.org/10.1002/esp.4996

Beechie, T. J., Liermann, M., Pollock, M. M., Baker, S., & Davies, J. (2006). Channel pattern and river-floodplain dynamics in forested mountain river systems. *Geomorphology*, *78*(1–2), 124–141. https://doi.org/10.1016/j.geomorph.2006.01.030

Bendoni, M., Francalanci, S., Cappietti, L., & Solari, L. (2014). On salt marshes retreat: Experiments and modeling toppling failures induced by wind waves. *Journal of Geophysical Research: Earth Surface*, *119*(3), 603–620. https://doi.org/10.1002/2013JF002967

Bendoni, M., Mel, R., Solari, L., Lanzoni, S., Francalanci, S., & Oumeraci, H. (2016). Insights into lateral marsh retreat mechanism through localized field measurements. *Water Resources Research*, *52*(2), 1446–1464. https://doi.org/10.1002/2015WR017966

Bennett, S. J. (1999). Effect of slope on the growth and migration of headcuts in rills. *Geomorphology*, *30*(3), 273–290. https://doi.org/10.1016/S0169-555X(99)00035-5

Bennett, S. J., Alonso, C. V., Prasad, S. N., & Römkens, M. J. (2000). Experiments on headcut growth and migration in concentrated flows typical of upland areas. *Water Resources Research*, *36*(7), 1911–1922. https://doi.org/10.1029/2000WR900067

Ben Slimane, A., Raclot, D., Evrard, O., Sanaa, M., Lefevre, I., & Le Bissonnais, Y. (2016). Relative contribution of rill/interrill and gully/channel erosion to small reservoir siltation in Mediterranean environments. *Land Degradation & Development*, *27*(3), 785–797. https://doi.org/10.1002/ldr.2387

Bernatchez, P., & Dubois, J. M. M. (2008). Seasonal quantification of coastal processes and cliff erosion on fine sediment shorelines in a cold temperate climate, north shore of the St. Lawrence maritime estuary, Québec. *Journal of Coastal Research*, *24*(10024), 169–180. https://doi.org/10.2112/04-0419.1

Bernatek-Jakiel, A., & Poesen, J. (2018). Subsurface erosion by soil piping: Significance and research needs. *Earth-Science Reviews*, *185*, 1107–1128. https://doi.org/10.1016/j.earscirev.2018.08.006

Best, J. (2019). Anthropogenic stresses on the world's big rivers. *Nature Geoscience*, *12*(1), 7–21. https://doi.org/10.1038/s41561-018-0262-x

Black, C., Hill, P. S., & DeGelleke, L. (2018). Formation, collapse and composition of ice banks in a macrotidal channel of the Bay of Fundy. *Cold Regions Science and Technology*, *155*, 29–36. https://doi.org/10.1016/j.coldregions.2018.06.012

Blondeaux, P., & Seminara, G. (1985). A unified bar–bend theory of river meanders. *Journal of Fluid Mechanics*, *157*, 449–470. https://doi.org/10.1017/S0022112085002440

Bogoni, M., Putti, M., & Lanzoni, S. (2017). Modeling meander morphodynamics over self-formed heterogeneous floodplains. *Water Resources Research*, *53*(6), 5137–5157. https://doi.org/10.1002/2017WR020726

Bolla Pittaluga, M., & Seminara, G. (2011). Nonlinearity and unsteadiness in river meandering: A review of progress in theory and modelling. *Earth Surface Processes and Landforms*, *36*(1), 20–38. https://doi.org/10.1002/esp.2089

Bortolus, A., & Iribarne, O. (1999). Effects of the SW Atlantic burrowing crab Chasmagnathus granulata on a Spartina salt marsh. *Marine Ecology Progress Series*, *178*, 79–88. https://doi.org/10.3354/meps178079

Braudrick, C. A., Dietrich, W. E., Leverich, G. T., & Sklar, L. S. (2009). Experimental evidence for the conditions necessary to sustain meandering in coarse-bedded rivers. *Proceedings of the National Academy of Sciences*, *106*(40), 16936–16941. https://doi.org/10.1073/pnas.0909417106

Bristow, C. S., & Best, J. L. (1993). Braided rivers: Perspectives and problems. *Geological society, London, special publications*, *75*(1), 1–11. https://doi.org/10.1144/gsl.sp.1993.075.01.01

Brocard, G. Y., & Van der Beek, P. A. (2006). Influence of incision rate, rock strength, and bedload supply on bedrock river gradients and valley-flat widths: Field-based evidence and calibrations from western Alpine rivers (southeast France), S. D. Willett et al. *Special Papers – Geological Society of America*, *398*, 101–126.

Bufe, A., Paola, C., & Burbank, D. W. (2016). Fluvial bevelling of topography controlled by lateral channel mobility and uplift rate. *Nature Geoscience*, *9*(9), 706–710. https://doi.org/10.1038/ngeo2773

Bufe, A., Turowski, J. M., Burbank, D. W., Paola, C., Wickert, A. D., & Tofelde, S. (2019). Controls on the lateral channel-migration rate of braided channel systems in coarse non-cohesive sediment. *Earth Surface Processes and Landforms*, *44*(14), 2823–2836. https://doi.org/10.1002/esp.4710

Burkard, M. B., & Kostaschuk, R. A. (1997). Patterns and controls of gully growth along the shoreline of Lake Huron, Earth Surface Processes and landforms. *The Journal of the British Geomorphological Group*, *22*(10), 901–911. https://doi.org/10.1002/(SICI)1096-9837(199710)22:10<901::AIDESP743>3.0.CO;2-O

Camporeale, C., Perona, P., Porporato, A., & Ridolfi, L. (2007). Hierarchy of models for meandering rivers and related morphodynamic processes. *Reviews of Geophysics*, *45*(1), RG1001. https://doi.org/10.1029/2005RG000185

Camporeale, C., Perucca, E., Ridolfi, L., & Gurnell, A. M. (2013). Modeling the interactions between river morphodynamics and riparian vegetation. *Reviews of Geophysics*, *51*(3), 379–414. https://doi.org/10.1002/rog.20014

Cancienne, R. M., & Fox, G. A. (2008). *Laboratory experiments on three-dimensional seepage erosion undercutting of vegetated banks*. American Society of Agricultural and Biological Engineers. https://doi.org/10.13031/2013.25035

Canestrelli, A., Spruyt, A., Jagers, B., Slingerland, R., & Borsboom, M. (2016). A mass-conservative staggered immersed boundary model for solving the shallow water equations on complex geometries. *International Journal for Numerical Methods in Fluids*, *81*(3), 151–177. https://doi.org/10.1002/fld.4180

Cantelli, A., Paola, C., & Parker, G. (2004). Experiments on upstream-migrating erosional narrowing and widening of an incisional channel caused by dam removal. *Water Resources Research*, *40*(3), W03304. https://doi.org/10.1029/2003WR002940

Cao, M., Xin, P., Jin, G., & Li, L. (2012). A field study on groundwater dynamics in a salt marsh-Chongming Dongtan wetland. *Ecological Engineering*, *40*, 61–69. https://doi.org/10.1016/j.ecoleng.2011.12.018

Capra, A., Porto, P., & Scicolone, B. (2009). Relationships between rainfall characteristics and ephemeral gully erosion in a cultivated catchment in Sicily (Italy). *Soil and Tillage Research*, *105*(1), 77–87. https://doi.org/10.1016/j.still.2009.05.009

Carretier, S., Martinod, P., Reich, M., & Godderis, Y. (2016). Modelling sediment clasts transport during landscape evolution. *Earth Surface Dynamics*, *4*(1), 237–251. https://doi.org/10.5194/esurf-4-237-2016

Carson, M. A., & Kirkby, M. J. (1972). *Hillslope form and process*. Cambridge University Press.

Carter, C. L., & Anderson, R. S. (2006). Fluvial erosion of physically modeled abrasion-dominated slot canyons. *Geomorphology*, *81*(1–2), 89–113. https://doi.org/10.1016/j.geomorph.2006.04.006

Casagli, N., Rinaldi, M., Gargini, A., Curini, A., Thorne, C. R., Billi, P., & Rinaldi, M. (1999). Pore water pressure and streambank stability: Results from a monitoring site on the Sieve River, Italy. *Earth Surface Processes and Landforms*, *24*(12), 1095–1114. https://doi.org/10.1002/(SICI)1096-9837(199911)24:12<1095::AIDESP37>3.0.CO;2-F

Castillo, C., & Gómez, J. A. (2016). A century of gully erosion research: Urgency, complexity and study approaches. *Earth-Science Reviews*, *160*, 300–319. https://doi.org/10.1016/j.earscirev.2016.07.009

Castro-Bolinaga, C. F., & Fox, G. A. (2018). Streambank erosion: Advances in monitoring, modeling and management. *Water*, *10*(10), 1346. https://doi.org/10.3390/w10101346

Chassiot, L., Lajeunesse, P., & Bernier, J. F. (2020). Riverbank erosion in cold environments: Review and outlook. *Earth-Science Reviews*, *207*, 103231. https://doi.org/10.1016/j.earscirev.2020.103231

Chen, A., Zhang, D., Peng, H., Fan, J., Xiong, D., & Liu, G. (2013). Experimental study on the development of collapse of overhanging layers of gully in Yuanmou Valley, China. *Catena*, *109*, 177–185. https://doi.org/10.1016/j.catena.2013.04.002

Chen, A., Zhang, D., Yan, B., Lei, B., & Liu, G. (2015). Main types of soil mass failure and characteristics of their impact factors in the Yuanmou Valley, China. *Catena*, *125*, 82–90. https://doi.org/10.1016/j.catena.2014.10.011

Chen, C., Hsieh, T., & Yang, J. (2017). Investigating effect of water level variation and surface tension crack on riverbank stability. *Journal of Hydro-Environment Research*, *15*, 41–53. https://doi.org/10.1016/j.jher.2017.02.002

Chen, X., Zhang, C., Townend, I. H., Paterson, D. M., Gong, Z., Jiang, Q., et al. (2021). Biological cohesion as the architect of bed movement under wave action. *Geophysical Research Letters*, *48*(5), e2020G–e92137G. https://doi.org/10.1029/2020gl092137

Chen, X. D., Zhang, C. K., Paterson, D. M., Thompson, C., Townend, I. H., Gong, Z., et al. (2017). Hindered erosion: The biological mediation of noncohesive sediment behavior. *Water Resources Research*, *53*(6), 4787–4801. https://doi.org/10.1002/2016WR020105

Chen, Y., & Collins, M. B. (2007). *The influence of root systems on the geomorphology of a tidal creek: Exbury Marsh*. Southern England.

Chen, Y., Collins, M. B., & Thompson, C. E. (2011). Creek enlargement in a low-energy degrading saltmarsh in southern England. *Earth Surface Processes and Landforms*, *36*(6), 767–778. https://doi.org/10.1002/esp.2104

Chen, Y., Thompson, C., & Collins, M. (2019). Controls on creek margin stability by the root systems of saltmarsh vegetation. *Beaulieu Estuary, Southern England, Anthropocene Coasts*, *2*(1), 21–38. https://doi.org/10.1139/anc-2018-0005

Chu-Agor, M. L., Fox, G. A., Cancienne, R. M., & Wilson, G. V. (2008). Seepage caused tension failures and erosion undercutting of hillslopes. *Journal of Hydrology*, *359*(3), 247–259. https://doi.org/10.1016/j.jhydrol.2008.07.005

Chu-Agor, M. L., Fox, G. A., & Wilson, G. V. (2009). Empirical sediment transport function predicting seepage erosion undercutting for cohesive bank failure prediction. *Journal of Hydrology*, *377*(1), 155–164. https://doi.org/10.1016/j.jhydrol.2009.08.020

Coco, G., Zhou, Z., van Maanen, B., Olabarrieta, M., Tinoco, R., & Townend, I. (2013). Morphodynamics of tidal networks: Advances and challenges. *Marine Geology*, *346*, 1–16. https://doi.org/10.1016/j.margeo.2013.08.005

Constantine, J. A., Dunne, T., Ahmed, J., Legleiter, C., & Lazarus, E. D. (2014). Sediment supply as a driver of river meandering and floodplain evolution in the Amazon Basin. *Nature Geoscience*, *7*(12), 899–903. https://doi.org/10.1038/ngeo2282

Coops, H., Geilen, N., Verheij, H. J., Boeters, R., & van der Velde, G. (1996). Interactions between waves, bank erosion and emergent vegetation: An experimental study in a wave tank. *Aquatic Botany*, *53*(3–4), 187–198. https://doi.org/10.1016/0304-3770(96)01027-3

Coulthard, T. J., Neal, J. C., Bates, P. D., Ramirez, J., de Almeida, G. A., & Hancock, G. R. (2013). Integrating the LISFLOOD-FP 2D hydrodynamic model with the CAESAR model: Implications for modelling landscape evolution. *Earth Surface Processes and Landforms*, *38*(15), 1897–1906. https://doi.org/10.1002/esp.3478

Coulthard, T. J., & Wiel, M. J. V. D. (2006). A cellular model of river meandering. *Earth Surface Processes and Landforms*, *31*(1), 123–132. https://doi.org/10.1002/esp.1315

Couper, P. (2003). Effects of silt–clay content on the susceptibility of river banks to subaerial erosion. *Geomorphology*, *56*(1–2), 95–108. https://doi.org/10.1016/s0169-555x(03)00048-5

Couper, P. R. (2004). Space and time in river bank erosion research: A review. *Area*, *36*(4), 387–403. https://doi.org/10.1111/j.0004-0894.2004.00239.x

Couper, P. R., & Maddock, I. P. (2001). Subaerial river bank erosion processes and their interaction with other bank erosion mechanisms on the River Arrow, Warwickshire, UK. *Earth Surface Processes and Landforms*, *26*(6), 631–646. https://doi.org/10.1002/esp.212

Crosato, A. (2007). Effects of smoothing and regridding in numerical meander migration models. *Water Resources Research*, *43*(1), W01401. https://doi.org/10.1029/2006wr005087

Dacey, J. W., & Howes, B. L. (1984). Water uptake by roots controls water table movement and sediment oxidation in short *Spartina* marsh. *Science*, *224*(4648), 487–489. https://doi.org/10.1126/science.224.4648.487

D'Alpaos, A., Lanzoni, S., Marani, M., & Rinaldo, A. (2007). Landscape evolution in tidal embayments: Modeling the interplay of erosion, sedimentation, and vegetation dynamics. *Journal of Geophysical Research*, *112*(F1), F01008. https://doi.org/10.1029/2006jf000537

Daly, E. R., Miller, R. B., & Fox, G. A. (2015). Modeling streambank erosion and failure along protected and unprotected composite streambanks. *Advances in Water Resources*, *81*, 114–127. https://doi.org/10.1016/j.advwatres.2015.01.004

Dapporto, S., Rinaldi, M., Casagli, N., & Vannocci, P. (2003). Mechanisms of riverbank failure along the Arno River, Central Italy, Earth Surface Processes and landforms. *The Journal of the British Geomorphological Research Group*, *28*(12), 1303–1323. https://doi.org/10.1002/esp.550

Darby, S. E., Alabyan, A. M., & Van de Wiel, M. J. (2002). Numerical simulation of bank erosion and channel migration in meandering rivers. *Water Resources Research*, *38*(9), 1–2. https://doi.org/10.1029/2001wr000602

Darby, S. E., Rinaldi, M., & Dapporto, S. (2007). Coupled simulations of fluvial erosion and mass wasting for cohesive river banks. *Journal of Geophysical Research*, *112*(F3), F03022. https://doi.org/10.1029/2006JF000722

Darby, S. E., & Thorne, C. R. (1996a). Development and testing of riverbank-stability analysis. *Journal of Hydraulic Engineering*, *122*(8), 443–454. https://doi.org/10.1061/(ASCE)0733-9429(1996)122:8(443)

Darby, S. E., & Thorne, C. R. (1996b). Numerical simulation of widening and bed deformation of straight sand-bed rivers. I: Model development. *Journal of Hydraulic Engineering*, *122*(4), 184–193. https://doi.org/10.1061/(asce)0733-9429(1996)122:4(184)

Das, V. K., Roy, S., Barman, K., Debnath, K., Chaudhuri, S., & Mazumder, B. S. (2019). Investigations on undercutting processes of cohesive river bank. *Engineering Geology*, *252*, 110–124. https://doi.org/10.1016/j.enggeo.2019.03.004

DeConto, R. M., & Pollard, D. (2016). Contribution of Antarctica to past and future sea-level rise. *Nature*, *531*(7596), 591–597. https://doi.org/10.1038/nature17145

Deegan, L. A., Johnson, D. S., Warren, R. S., Peterson, B. J., Fleeger, J. W., Fagherazzi, S., & Wollheim, W. M. (2012). Coastal eutrophication as a driver of salt marsh loss. *Nature*, *490*(7420), 388–392. https://doi.org/10.1038/nature11533

Deng, S., Xia, J., & Zhou, M. (2019). Coupled two-dimensional modeling of bed evolution and bank erosion in the Upper JingJiang Reach of middle Yangtze River. *Geomorphology*, *344*, 10–24. https://doi.org/10.1016/j.geomorph.2019.07.010

Deng, S., Xia, J., Zhou, M., Li, J., & Zhu, Y. (2018). Coupled modeling of bank retreat processes in the Upper Jingjiang Reach, China. *Earth Surface Processes and Landforms*, *43*(14), 2863–2875. https://doi.org/10.1002/esp.4439

Derksen Hooijberg, M., Angelini, C., Hoogveld, J. R., Lamers, L. P., Borst, A., Smolders, A., et al. (2019). Repetitive desiccation events weaken a salt marsh mutualism. *Journal of Ecology*, *107*(5), 2415–2426. https://doi.org/10.1111/1365-2745.13178

De Rose, R. C., & Basher, L. R. (2011). Measurement of river bank and cliff erosion from sequential LIDAR and historical aerial photography. *Geomorphology*, *126*(1–2), 132–147. https://doi.org/10.1016/j.geomorph.2010.10.037

Dong, T. Y., Nittrouer, J. A., Czapiga, M. J., Ma, H., McElroy, B., Il'Icheva, E., et al. (2019). Roles of bank material in setting bankfull hydraulic geometry as informed by the Selenga River delta, Russia. *Water Resources Research*, *55*(1), 827–846. https://doi.org/10.1029/2017WR021985

Dong, Y., Wu, Y., Qin, W., Guo, Q., Yin, Z., & Duan, X. (2019). The gully erosion rates in the black soil region of northeastern China: Induced by different processes and indicated by different indexes. *Catena*, *182*, 104146. https://doi.org/10.1016/j.catena.2019.104146

Dong, Y., Xiong, D., Su, Z., Duan, X., Lu, X., Zhang, S., & Yuan, Y. (2019). The influences of mass failure on the erosion and hydraulic processes of gully headcuts based on an in situ scouring experiment in dry-hot valley of China. *Catena*, *176*, 14–25. https://doi.org/10.1016/j.catena.2019.01.004

Donovan, M., Belmont, P., & Sylvester, Z. (2021). Evaluating the relationship between meander-bend curvature, sediment supply, and migration rates. *Journal of Geophysical Research: Earth Surface*, *126*(3), e2020J–e6058J. https://doi.org/10.1029/2020jf006058

Duan, J. G., & Julien, P. Y. (2005). Numerical simulation of the inception of channel meandering. *Earth Surface Processes and Landforms: The Journal of the British Geomorphological Research Group*, *30*(9), 1093–1110. https://doi.org/10.1002/esp.1264

Dulal, K. P., Kobayashi, K., Shimizu, Y., & Parker, G. (2010). Numerical computation of free meandering channels with the application of slump blocks on the outer bends. *Journal of Hydro-Environment Research*, *3*(4), 239–246. https://doi.org/10.1016/j.jher.2009.10.012

Duncan, J. M., Wright, S. G., & Brandon, T. L. (2014). *Soil strength and slope stability*. John Wiley & Sons.

Dunne, K. B. J., & Jerolmack, D. J. (2020). What sets river width? *Science Advances*, *6*(41), eabc1505. https://doi.org/10.1126/sciadv.abc1505

Dunne, T. (1990). Hydrology, mechanics, and geomorphic implications of erosion by subsurface flow. In C. G. Higgins & D. R. Coates (Eds.), *Groundwater geomorphology: The role of subsurface water in Earth-surface processes and landforms* (pp. 1–28). Geological Society of America Special Paper. 252.

Duró, G., Crosato, A., Kleinhans, M. G., Roelvink, D., & Uijttewaal, W. (2020). Bank erosion processes in regulated navigable rivers. *Journal of Geophysical Research: Earth Surface*, *125*(7), e2019J–e5441J. https://doi.org/10.1029/2019JF005441

Duró, G., Crosato, A., Kleinhans, M. G., Winkels, T. G., Woolderink, H. A., & Uijttewaal, W. S. (2019). Distinct patterns of bank erosion in a navigable regulated river. *Earth Surface Processes and Landforms*, *45*(2), 361–374. https://doi.org/10.1002/esp.4736

Duró, G., Crosato, A., & Tassi, P. (2016). Numerical study on river bar response to spatial variations of channel width. *Advances in Water Resources*, *93*, 21–38. https://doi.org/10.1016/j.advwatres.2015.10.003

Durocher, M. G. (1990). Monitoring spatial variability of forest interception. *Hydrological Processes*, *4*(3), 215–229. https://doi.org/10.1002/hyp.3360040303

Eke, E., Parker, G., & Shimizu, Y. (2014). Numerical modeling of erosional and depositional bank processes in migrating river bends with self-formed width: Morphodynamics of bar push and bank pull. *Journal of Geophysical Research: Earth Surface*, *119*(7), 1455–1483. https://doi.org/10.1002/2013JF003020

Eke, E. C., Czapiga, M. J., Viparelli, E., Shimizu, Y., Imran, J., Sun, T., & Parker, G. (2014). Coevolution of width and sinuosity in meandering rivers. *Journal of Fluid Mechanics*, *760*, 127–174. https://doi.org/10.1017/jfm.2014.556

Fagherazzi, S., Gabet, E. J., & Furbish, D. J. (2004). The effect of bidirectional flow on tidal channel planforms. *Earth Surface Processes and Landforms*, *29*(3), 295–309. https://doi.org/10.1002/esp.1016

Fagherazzi, S., Kirwan, M. L., Mudd, S. M., Guntenspergen, G. R., Temmerman, S., D'Alpaos, A., et al. (2012). Numerical models of salt marsh evolution: Ecological, geomorphic, and climatic factors. *Reviews of Geophysics*, *50*(1), RG1002. https://doi.org/10.1029/2011rg000359

Fagherazzi, S., Mariotti, G., Wiberg, P. L., & McGlathery, K. J. (2013). Marsh collapse does not require sea level rise. *Oceanography*, *26*(3), 70–77. https://doi.org/10.5670/oceanog.2013.47

Faure, Y., Ho, C. C., Chen, R., Le Lay, M., & Blaza, J. (2010). A wave flume experiment for studying erosion mechanism of revetments using geotextiles. *Geotextiles and Geomembranes*, *28*(4), 360–373. https://doi.org/10.1016/j.geotexmem.2009.11.002

Feagin, R. A., Lozada-Bernard, S. M., Ravens, T. M., Möller, I., Yeager, K. M., & Baird, A. H. (2009). Does vegetation prevent wave erosion of salt marsh edges? *Proceedings of the National Academy of Sciences*, *106*(25), 10109–10113. https://doi.org/10.1073/pnas.0901297106

Ferrick, M. G., & Gatto, L. W. (2005). Quantifying the effect of a freeze–thaw cycle on soil erosion: Laboratory experiments, Earth Surface Processes and landforms. *The Journal of the British Geomorphological Research Group*, *30*(10), 1305–1326. https://doi.org/10.1002/esp.1209

Finnegan, N. J., Sklar, L. S., & Fuller, T. K. (2007). Interplay of sediment supply, river incision, and channel morphology revealed by the transient evolution of an experimental bedrock channel. *Journal of Geophysical Research*, *112*(F3), F03S11. https://doi.org/10.1029/2006jf000569

Finotello, A., D'Alpaos, A., Bogoni, M., Ghinassi, M., & Lanzoni, S. (2020). Remotely-sensed planform morphologies reveal fluvial and tidal nature of meandering channels. *Scientific Reports*, *10*, 1–13. https://doi.org/10.1038/s41598-019-56992-w

Finotello, A., Lanzoni, S., Ghinassi, M., Marani, M., Rinaldo, A., & D'Alpaos, A. (2018). Field migration rates of tidal meanders recapitulate fluvial morphodynamics. *Proceedings of the National Academy of Sciences*, *115*(7), 1463–1468. https://doi.org/10.1073/pnas.1711330115

Flemming, H., & Wuertz, S. (2019). Bacteria and archaea on Earth and their abundance in biofilms. *Nature Reviews Microbiology*, *17*(4), 247–260. https://doi.org/10.1038/s41579-019-0158-9

Florsheim, J. L., Mount, J. F., & Chin, A. (2008). Bank erosion as a desirable attribute of rivers. *BioScience*, *58*(6), 519–529. https://doi.org/10.1641/B580608

Fox, G. A., Chu-Agor, M. L. M., & Wilson, G. V. (2007). Erosion of noncohesive sediment by ground water seepage: Lysimeter experiments and stability modeling. *Soil Science Society of America Journal*, *71*(6), 1822–1830. https://doi.org/10.2136/sssaj2007.0090

Fox, G. A., & Felice, R. G. (2014). Bank undercutting and tension failure by groundwater seepage: Predicting failure mechanisms. *Earth Surface Processes and Landforms*, *39*(6), 758–765. https://doi.org/10.1002/esp.3481

Fox, G. A., & Wilson, G. V. (2010). The role of subsurface flow in hillslope and stream bank erosion: A review. *Soil Science Society of America Journal*, *74*(3), 717–733. https://doi.org/10.2136/sssaj2009.0319

Fox, G. A., Wilson, G. V., Periketi, R. K., & Cullum, R. F. (2006). Sediment transport model for seepage erosion of streambank sediment. *Journal of Hydrologic Engineering*, *11*(6), 603–611. https://doi.org/10.1061/(ASCE)1084-0699(2006)11:6(603)

Francalanci, S., Bendoni, M., Rinaldi, M., & Solari, L. (2013). Ecomorphodynamic evolution of salt marshes: Experimental observations of bank retreat processes. *Geomorphology*, *195*(Supplement C), 53–65. https://doi.org/10.1016/j.geomorph.2013.04.026

Francalanci, S., Lanzoni, S., Solari, L., & Papanicolaou, A. N. (2020). Equilibrium cross section of river channels with cohesive erodible banks. *Journal of Geophysical Research: Earth Surface*, *125*(1), 1–20. https://doi.org/10.1029/2019JF005286

Frascati, A., & Lanzoni, S. (2009). Morphodynamic regime and long-term evolution of meandering rivers. *Journal of Geophysical Research*, *114*(2), F02002. https://doi.org/10.1029/2008JF001101

Fredlund, D. G., & Rahardjo, H. (1993). *Soil mechanics for unsaturated soils*. John Wiley & Sons.

Fredsøe, J. (1978). Meandering and braiding of rivers. *Journal of Fluid Mechanics*, *84*(4), 609–624. https://doi.org/10.1017/s0022112078000373

Fryirs, K. A., & Brierley, G. J. (2012). *Geomorphic analysis of river systems: An approach to reading the landscape*. John Wiley & Sons.

Fuller, T. K., Gran, K. B., Sklar, L. S., & Paola, C. (2016). Lateral erosion in an experimental bedrock channel: The influence of bed roughness on erosion by bed load impacts. *Journal of Geophysical Research: Earth Surface*, *121*(5), 1084–1105. https://doi.org/10.1002/2015jf003728

Gabel, F., Lorenz, S., & Stoll, S. (2017). Effects of ship-induced waves on aquatic ecosystems. *The Science of the Total Environment*, *601*, 926–939. https://doi.org/10.1016/j.scitotenv.2017.05.206

Gabet, E. J. (1998). Lateral migration and bank erosion in a saltmarsh tidal channel in San Francisco Bay, California. *Estuaries and Coasts*, *21*(4), 745–753. https://doi.org/10.2307/1353278

Galy, V., Peucker-Ehrenbrink, B., & Eglinton, T. (2015). Global carbon export from the terrestrial biosphere controlled by erosion. *Nature*, *521*(7551), 204–207. https://doi.org/10.1038/nature14400

Gaskin, S. J., Pieterse, J., Shafie, A. A., & Lepage, S. (2003). Erosion of undisturbed clay samples from the banks of the St. Lawrence River. *Canadian Journal of Civil Engineering*, *30*(3), 585–595. https://doi.org/10.1139/l03-008

Geng, L., D'Alpaos, A., Sgarabotto, A., Gong, Z., & Lanzoni, S. (2021). Intertwined eco-morphodynamic evolution of Salt marshes and emerging tidal channel networks. *Water Resources Research*, *57*(11), e2021W–e30840W. https://doi.org/10.1029/2021wr030840

Geng, L., Gong, Z., Zhou, Z., Lanzoni, S., & D'Alpaos, A. (2019). Assessing the relative contributions of the flood tide and the ebb tide to tidal channel network dynamics. *Earth Surface Processes and Landforms*, *45*(1), 237–250. https://doi.org/10.1002/esp.4727

Gibling, M. R., & Davies, N. S. (2012). Palaeozoic landscapes shaped by plant evolution. *Nature Geoscience*, *5*(2), 99–105. https://doi.org/10.1038/ngeo1376

Ginsberg, S. S., & Perillo, G. M. E. (1990). Channel bank recession in the Bahía Blanca estuary, Argentina. *Journal of Coastal Research*, *6*(4), 999–1009.

Golombek, N. Y., Scheingross, J. S., Repasch, M. N., Hovius, N., Menges, J., Sachse, D., et al. (2021). Fluvial organic carbon composition regulated by seasonal variability in lowland river migration and water discharge. *Geophysical Research Letters*, *48*(24), e2021G–e93416G. https://doi.org/10.1029/2021gl093416

Gong, Z., Zhao, K., Zhang, C., Dai, W., Coco, G., & Zhou, Z. (2018). The role of bank collapse on tidal creek ontogeny: A novel process-based model for bank retreat. *Geomorphology*, *311*, 13–26. https://doi.org/10.1016/j.geomorph.2018.03.016

Griffiths, G. A. (1979). Recent sedimentation history of the Waimakariri River, New Zealand. *Journal of Hydrology*, *18*(1), 6–28.

Güneralp, İ, & Rhoads, B. L. (2011). Influence of floodplain erosional heterogeneity on planform complexity of meandering rivers. *Geophysical Research Letters*, *38*(14), L14401. https://doi.org/10.1029/2011gl048134

Guo, L., Xu, F., Van Der Wegen, M., Townend, I., Wang, Z. B., & He, Q. (2021). Morphodynamic adaptation of a tidal basin to centennial sea-level rise: The importance of lateral expansion. *Continental Shelf Research*, *226*, 104494. https://doi.org/10.1016/j.csr.2021.104494

Hackney, C., Best, J., Leyland, J., Darby, S. E., Parsons, D., Aalto, R., & Nicholas, A. (2015). Modulation of outer bank erosion by slump blocks: Disentangling the protective and destructive role of failed material on the three-dimensional flow structure. *Geophysical Research Letters*, *42*(24), 10–663. https://doi.org/10.1002/2015GL066481

Hackney, C. R., Darby, S. E., Parsons, D. R., Leyland, J., Best, J. L., Aalto, R., et al. (2020). River bank instability from unsustainable sand mining in the lower Mekong River. *Nature Sustainability*, *3*(3), 1–9. https://doi.org/10.1038/s41893-019-0455-3

Han, M., & Brierley, G. (2020). Channel geomorphology and riparian vegetation interactions along four anabranching reaches of the Upper Yellow River. *Progress in Physical Geography: Earth and Environment*, *44*(6), 898–922. https://doi.org/10.1177/0309133320938768

Hancock, G. S., & Anderson, R. S. (2002). Numerical modeling of fluvial strath-terrace formation in response to oscillating climate. *The Geological Society of America Bulletin*, *114*(9), 1131–1142. https://doi.org/10.1130/0016-7606(2002)114<1131:nmofst>2.0.co;2

Hanson, G. J., & Simon, A. (2001). Erodibility of cohesive streambeds in the loess area of the midwestern USA. *Hydrological Processes*, *15*(1), 23–38. https://doi.org/10.1002/hyp.149

Hartshorn, K., Hovius, N., Dade, W. B., & Slingerland, R. L. (2002). Climate-driven bedrock incision in an active mountain belt. *Science*, *297*(5589), 2036–2038. https://doi.org/10.1126/science.1075078

Harvey, G. L., Henshaw, A. J., Brasington, J., & England, J. (2019). Burrowing invasive species: An unquantified erosion risk at the aquatic-terrestrial Interface. *Reviews of Geophysics*, *57*(3), 1018–1036. https://doi.org/10.1029/2018RG000635

Hasegawa, K. (1977). Computer simulation of the gradual migration of meandering channels. *Proceedings of the Hokkaido Branch, Japan Society of Civil Engineering* (pp. 197–202).

Hasegawa, K. (1989). Universal bank erosion coefficient for meandering rivers. *Journal of Hydraulic Engineering*, *115*(6), 744–765. https://doi.org/10.1061/(ASCE)0733-9429(1989)115:6(744)

Henshaw, A. J., Thorne, C. R., & Clifford, N. J. (2013). Identifying causes and controls of river bank erosion in a British upland catchment. *Catena*, *100*, 107–119. https://doi.org/10.1016/j.catena.2012.07.015

Hickin, E. J., & Nanson, G. C. (1984). Lateral migration rates of river bends. *Journal of Hydraulic Engineering*, *110*(11), 1557–1567. https://doi.org/10.1061/(ASCE)0733-9429(1984)110:11(1557)

Hooke, J. M. (1979). An analysis of the processes of river bank erosion. *Journal of Hydrology*, *42*(1), 39–62. https://doi.org/10.1016/0022-1694(79)90005-2

Hooke, J. M. (1980). Magnitude and distribution of rates of river bank erosion. *Earth Surface Processes*, *5*(2), 143–157. https://doi.org/10.1002/esp.3760050205

Houser, C. (2010). Relative importance of vessel-generated and wind waves to salt marsh erosion in a restricted fetch environment. *Journal of Coastal Research*, *262*, 230–240. https://doi.org/10.2112/08-1084.1

Houttuijn Bloemendaal, L. J., FitzGerald, D. M., Hughes, Z. J., Novak, A. B., & Phippen, P. (2021). What controls marsh edge erosion? *Geomorphology*, *386*, 107745. https://doi.org/10.1016/j.geomorph.2021.107745

Howard, A. D. (2009). How to make a meandering river. *Proceedings of the National Academy of Sciences*, *106*(41), 17245–17246. https://doi.org/10.1073/pnas.0910005106

Howard, A. D., & Knutson, T. R. (1984). Sufficient conditions for river meandering: A simulation approach. *Water Resources Research*, *20*(11), 1659–1667. https://doi.org/10.1029/wr020i011p01659

Howard, A. D., & McLane, C. F., III. (1988). Erosion of cohesionless sediment by groundwater seepage. *Water Resources Research*, *24*(10), 1659–1674. https://doi.org/10.1029/WR024i010p01659

Hua, X., Huang, H., Wang, Y., Lan, Y., Zhao, K., & Chen, D. (2019). Abnormal ETM in the North Passage of the Changjiang River estuary: Observations in the wet and dry seasons of 2016, estuarine. *Coastal and Shelf Science*, *227*, 106334. https://doi.org/10.1016/j.ecss.2019.106334

Hughes, Z. J. (2012). Tidal channels on tidal flats and marshes. In *Principles of tidal sedimentology* (pp. 269–300). Springer.

Ielpi, A., Lapôtre, M. G. A., Gibling, M. R., & Boyce, C. K. (2022). The impact of vegetation on meandering rivers. *Nature Reviews Earth & Environment*, *3*(3), 165–178. https://doi.org/10.1038/s43017-021-00249-6

Ikeda, S., Parker, G., & Sawai, K. (1981). Bend theory of river meanders. Part 1. Linear development. *Journal of Fluid Mechanics*, *112*, 363–377. https://doi.org/10.1017/S0022112081000451

Inoue, T., Mishra, J., & Parker, G. (2021). Numerical simulations of meanders migrating laterally as they incise into bedrock. *Journal of Geophysical Research: Earth Surface*, *126*(5), e2020J–e5645J. https://doi.org/10.1029/2020jf005645

Istanbulluoglu, E., Bras, R. L., Flores Cervantes, H., & Tucker, G. E. (2005). Implications of bank failures and fluvial erosion for gully development: Field observations and modeling. *Journal of Geophysical Research*, *110*(F1), F01014. https://doi.org/10.1029/2004JF000145

Jang, C., & Shimizu, Y. (2005). Numerical simulation of relatively wide, shallow channels with erodible banks. *Journal of Hydraulic Engineering*, *131*(7), 565–575. https://doi.org/10.1061/(ASCE)0733-9429(2005)131:7(565)

Ji, F., Liu, C., Shi, Y., Feng, W., & Wang, D. (2019). Characteristics and parameters of bank collapse in coarse-grained-material reservoirs based on back analysis and long sequence monitoring. *Geomorphology*, *333*, 92–104. https://doi.org/10.1016/j.geomorph.2019.02.018

Ji, F., Shi, Y., Zhou, H., Liu, H., & Liao, Y. (2017). Experimental research on the effect of slope morphology on bank collapse in mountain reservoir. *Natural Hazards*, *86*(1), 165–181. https://doi.org/10.1007/s11069-016-2679-0

Jia, D., Shao, X., Wang, H., & Zhou, G. (2010). Three-dimensional modeling of bank erosion and morphological changes in the Shishou bend of the middle Yangtze River. *Advances in Water Resources*, *33*(3), 348–360. https://doi.org/10.1016/j.advwatres.2010.01.002

Kang, Y., Ding, X., Xu, F., Zhang, C., & Ge, X. (2017). Topographic mapping on large-scale tidal flats with an iterative approach on the waterline method, Estuarine. *Coastal and Shelf Science*, *190*, 11–22. https://doi.org/10.1016/j.ecss.2017.03.024

Karmaker, T., & Dutta, S. (2013). Modeling seepage erosion and bank retreat in a composite river bank. *Journal of Hydrology*, *476*, 178–187. https://doi.org/10.1016/j.jhydrol.2012.10.032

Kearney, W. S., & Fagherazzi, S. (2016). Salt marsh vegetation promotes efficient tidal channel networks. *Nature Communications*, *7*(1), 1–7. https://doi.org/10.1038/ncomms12287

Khatun, S., Ghosh, A., & Sen, D. (2019). An experimental investigation on effect of drawdown rate and drawdown ratios on stability of cohesion-less river bank and evaluation of factor of safety by total strength reduction method. *International Journal of River Basin Management*, *17*(3), 289–299. https://doi.org/10.1080/15715124.2018.1498856

Kimiaghalam, N., Goharrokhi, M., Clark, S. P., & Ahmari, H. (2015). A comprehensive fluvial geomorphology study of riverbank erosion on the Red River in Winnipeg, Manitoba, Canada. *Journal of Hydrology*, *529*, 1488–1498. https://doi.org/10.1016/j.jhydrol.2015.08.033

Kirwan, M. L., Guntenspergen, G. R., D'Alpaos, A., Morris, J. T., Mudd, S. M., & Temmerman, S. (2010). Limits on the adaptability of coastal marshes to rising sea level. *Geophysical Research Letters*, *37*(23). https://doi.org/10.1029/2010gl045489

Kirwan, M. L., & Mudd, S. M. (2012). Response of salt-marsh carbon accumulation to climate change. *Nature*, *489*(7417), 550–553. https://doi.org/10.1038/nature11440

Kirwan, M. L., & Murray, A. B. (2007). A coupled geomorphic and ecological model of tidal marsh evolution. *Proceedings of the National Academy of Sciences*, *104*(15), 6118–6122. https://doi.org/10.1073/pnas.0700958104

Kitanidis, P. K., & Kennedy, J. F. (1984). Secondary current and river-meander formation. *Journal of Fluid Mechanics*, *144*, 217–229. https://doi.org/10.1017/S0022112084001580

Klavon, K., Fox, G., Guertault, L., Langendoen, E., Enlow, H., Miller, R., & Khanal, A. (2017). Evaluating a process-based model for use in streambank stabilization: Insights on the Bank Stability and Toe Erosion Model (BSTEM). *Earth Surface Processes and Landforms*, *42*(1), 191–213. https://doi.org/10.1002/esp.4073

Kleinhans, M. G., Schuurman, F., Bakx, W., & Markies, H. (2009). Meandering channel dynamics in highly cohesive sediment on an intertidal mud flat in the Westerschelde estuary, The Netherlands. *Geomorphology*, *105*(3), 261–276. https://doi.org/10.1016/j.geomorph.2008.10.005

Kleinhans, M. G., van der Vegt, M., van Scheltinga, R. T., Baar, A. W., & Markies, H. (2012). Turning the tide: Experimental creation of tidal channel networks and ebb deltas. *Netherlands Journal of Geosciences*, *91*(3), 311–323. https://doi.org/10.1017/S0016774600000469

Kronvang, B., Andersen, H. E., Larsen, S. E., & Audet, J. (2013). Importance of bank erosion for sediment input, storage and export at the catchment scale. *Journal of Soils and Sediments*, *13*(1), 230–241. https://doi.org/10.1007/s11368-012-0597-7

Krzeminska, D., Kerkhof, T., Skaalsveen, K., & Stolte, J. (2019). Effect of riparian vegetation on stream bank stability in small agricultural catchments. *Catena*, *172*, 87–96. https://doi.org/10.1016/j.catena.2018.08.014

Lagasse, P. F., Zevenbergen, L. W., Spitz, W. J., & Thorne, C. R. (2004). Methodology for predicting channel migration. *National Cooperative Highway Research Program, Web-Only Document*, 67, 162.

Lague, D. (2014). The stream power river incision model: Evidence, theory and beyond. *Earth Surface Processes and Landforms*, *39*(1), 38–61. https://doi.org/10.1002/esp.3462

Lai, Y. G., Thomas, R. E., Ozeren, Y., Simon, A., Greimann, B. P., & Wu, K. (2015). Modeling of multilayer cohesive bank erosion with a coupled bank stability and mobile-bed model. *Geomorphology*, *243*, 116–129. https://doi.org/10.1016/j.geomorph.2014.07.017

Langendoen, E. J. (20*00*). *Concepts: Conservational channel evolution and pollutant transport s*ystem. USDA-ARS National Sedimentation Laboratory.

Langendoen, E. J., Mendoza, A., Abad, J. D., Tassi, P., Wang, D., Ata, R., et al. (2016). Improved numerical modeling of morphodynamics of rivers with steep banks. *Advances in Water Resources*, *93*, 4–14. https://doi.org/10.1016/j.advwatres.2015.04.002

Langendoen, E. J., & Simon, A. (2008). Modeling the evolution of incised streams. II: Streambank erosion. *Journal of Hydraulic Engineering*, *134*(7), 905–915. https://doi.org/10.1061/(ASCE)0733-9429(2008)134:7(905)

Langston, A. L., & Tucker, G. E. (2018). Developing and exploring a theory for the lateral erosion of bedrock channels for use in landscape evolution models. *Earth Surface Dynamics*, *6*(1), 1–27. https://doi.org/10.5194/esurf-6-1-2018

Lanzoni, S., & D'Alpaos, A. (2015). On funneling of tidal channels. *Journal of Geophysical Research: Earth Surface*, *120*(3), 433–452. https://doi.org/10.1002/2014jf003203

Lanzoni, S., & Seminara, G. (2006). On the nature of meander instability. *Journal of Geophysical Research*, *111*(F4), F04006. https://doi.org/10.1029/2005JF000416

Larsen, L. G., Harvey, J. W., & Crimaldi, J. P. (2007). A delicate balance: Ecohydrological feedbacks governing landscape morphology in a lotic peatland. *Ecological Monographs*, *77*(4), 591–614. https://doi.org/10.1890/06-1267.1

Lawler, D. M. (1986). *River bank erosion and the influence of frost: A statistical examination* (pp. 227–242). Transactions of the Institute of British Geographers. https://doi.org/10.2307/622008

Lawler, D. M. (1992). Process dominance in bank erosion systems. *Paper presented at Lowland Floodplain Rivers Geomorphological Perspectives*.

Lawler, D. M. (1993a). The measurement of river bank erosion and lateral channel change: A review. *Earth Surface Processes and Landforms*, *18*(9), 777–821. https://doi.org/10.1002/esp.3290180905

Lawler, D. M. (1993b). Needle ice processes and sediment mobilization on river banks: The River Ilston, West Glamorgan, UK. *Journal of Hydrology*, *150*(1), 81–114. https://doi.org/10.1016/0022-1694(93)90157-5

Lawler, D. M., Grove, J. R., Couperthwaite, J. S., & Leeks, G. (1999). Downstream change in river bank erosion rates in the Swale–Ouse system, northern England. *Hydrological Processes*, *13*(7), 977–992. https://doi.org/10.1002/(sici)1099-1085(199905)13:7<977::aid-hyp785>3.0.co;2-5

Lesser, G. R., Roelvink, J. A., van Kester, J. A. T. M., & Stelling, G. S. (2004). Development and validation of a three-dimensional morphological model. *Coastal Engineering*, *51*(8–9), 883–915. https://doi.org/10.1016/j.coastaleng.2004.07.014

Li, C., Holden, J., & Grayson, R. (2018). Effects of needle ice on peat erosion processes during overland flow events. *Journal of Geophysical Research: Earth Surface*, *123*(9), 2107–2122. https://doi.org/10.1029/2017jf004508

Li, T., Fuller, T. K., Sklar, L. S., Gran, K. B., & Venditti, J. G. (2020). A mechanistic model for lateral erosion of bedrock channel banks by bedload particle impacts. *Journal of Geophysical Research: Earth Surface*, *125*(6), e2019J–e5509J. https://doi.org/10.1029/2019jf005509

Li, Z., Zhang, Y., Zhu, Q., He, Y., & Yao, W. (2015). Assessment of bank gully development and vegetation coverage on the Chinese Loess Plateau. *Geomorphology*, *228*, 462–469. https://doi.org/10.1016/j.geomorph.2014.10.005

Limaye, A. B., & Lamb, M. P. (2014). Numerical simulations of bedrock valley evolution by meandering rivers with variable bank material. *Journal of Geophysical Research: Earth Surface*, *119*(4), 927–950. https://doi.org/10.1002/2013jf002997

Lindow, N., Fox, G. A., & Evans, R. O. (2009). Seepage erosion in layered stream bank material. *Earth Surface Processes and Landforms*, *12*(34), 1693–1701. https://doi.org/10.1002/esp.1874

Liu, C., Liu, A., He, Y., & Chen, Y. (2021). Migration rate of river bends estimated by tree ring analysis for a meandering river in the source region of the Yellow River. *International Journal of Sediment Research*, *36*(5), 593–601. https://doi.org/10.1016/j.ijsrc.2021.04.001

Lopez Dubon, S., & Lanzoni, S. (2019). Meandering evolution and width variations: A physics-statistics-based modeling approach. *Water Resources Research*, *55*(1), 76–94. https://doi.org/10.1029/2018WR023639

Malatesta, L. C., Prancevic, J. P., & Avouac, J. P. (2017). Autogenic entrenchment patterns and terraces due to coupling with lateral erosion in incising alluvial channels. *Journal of Geophysical Research: Earth Surface*, *122*(1), 335–355. https://doi.org/10.1002/2015jf003797

Marani, M., D'Alpaos, A., Lanzoni, S., & Santalucia, M. (2011). Understanding and predicting wave erosion of marsh edges. *Geophysical Research Letters*, *38*(21), L21401. https://doi.org/10.1029/2011gl048995

Marani, M., Lanzoni, S., Zandolin, D., Seminara, G., & Rinaldo, A. (2002). Tidal meanders. *Water Resources Research*, *38*(11), 7-1–7-14. https://doi.org/10.1029/2001WR000404

Mariotti, G., & Fagherazzi, S. (2010). A numerical model for the coupled long-term evolution of salt marshes and tidal flats. *Journal of Geophysical Research*, *115*(F1), F01004. https://doi.org/10.1029/2009jf001326

Mariotti, G., Kearney, W. S., & Fagherazzi, S. (2016). Soil creep in salt marshes. *Geology*, *44*(6), 459–462. https://doi.org/10.1130/G37708.1

Mariotti, G., Kearney, W. S., & Fagherazzi, S. (2019). Soil creep in a mesotidal salt marsh channel bank: Fast, seasonal, and water table mediated. *Geomorphology*, *334*, 126–137. https://doi.org/10.1016/j.geomorph.2019.03.001

Marron, D. C. (1992). Floodplain storage of mine tailings in the Belle Fourche river system: A sediment budget approach. *Earth Surface Processes and Landforms*, *17*(7), 675–685. https://doi.org/10.1002/esp.3290170704

Mason, J., & Mohrig, D. (2019). Differential bank migration and the maintenance of channel width in meandering river bends. *Geology*, *47*(12), 1136–1140. https://doi.org/10.1130/G46651.1

Masoodi, A., Majdzadeh Tabatabai, M. R., Noorzad, A., & Samadi, A. (2017). Effects of soil physico-chemical properties on stream bank erosion induced by seepage in northeastern Iran. *Hydrological Sciences Journal*, *62*(16), 2597–2613. https://doi.org/10.1080/02626667.2017.1403030

Masoodi, A., Majdzadeh Tabatabai, M. R., Noorzad, A., & Samadi, A. (2019). Riverbank stability under the influence of soil dispersion phenomenon. *Journal of Hydrologic Engineering*, *24*(3), 5019001. https://doi.org/10.1061/(ASCE)HE.1943-5584.0001756

Masoodi, A., Noorzad, A., Majdzadeh Tabatabai, M. R., & Samadi, A. (2018). Application of short-range photogrammetry for monitoring seepage erosion of riverbank by laboratory experiments. *Journal of Hydrology*, *558*, 380–391. https://doi.org/10.1016/j.jhydrol.2018.01.051

McKew, B. A., Taylor, J. D., McGenity, T. J., & Underwood, G. J. (2011). Resistance and resilience of benthic biofilm communities from a temperate saltmarsh to desiccation and rewetting. *The ISME Journal*, *5*(1), 30–41. https://doi.org/10.1038/ismej.2010.91

Micheli, E. R., & Kirchner, J. W. (2002). Effects of wet meadow riparian vegetation on streambank erosion. 2. Measurements of vegetated bank strength and consequences for failure mechanics. *Earth Surface Processes and Landforms*, *27*(7), 687–697. https://doi.org/10.1002/esp.340

Midgley, T. L., Fox, G. A., & Heeren, D. M. (2012). Evaluation of the Bank Stability and Toe Erosion Model (BSTEM) for predicting lateral retreat on composite streambanks. *Geomorphology*, *145–146*, 107–114. https://doi.org/10.1016/j.geomorph.2011.12.044

Midgley, T. L., Fox, G. A., Wilson, G. V., Heeren, D. M., Langendoen, E. J., & Simon, A. (2013). Seepage-induced streambank erosion and instability: In situ constant-head experiments. *Journal of Hydrologic Engineering*, *18*(10), 1200–1210. https://doi.org/10.1061/(ASCE)HE.1943-5584.0000685

Mishra, J., Inoue, T., Shimizu, Y., Sumner, T., & Nelson, J. M. (2018). Consequences of abrading bed load on vertical and lateral bedrock erosion in a curved experimental channel. *Journal of Geophysical Research: Earth Surface*, *123*(12), 3147–3161. https://doi.org/10.1029/2017jf004387

Mittal, R., & Iaccarino, G. (2005). Immersed boundary methods. *Annual Review of Fluid Mechanics*, *37*(1), 239–261. https://doi.org/10.1146/annurev.fluid.37.061903.175743

Montgomery, D. R. (2004). Observations on the role of lithology in strath terrace formation and bedrock channel width. *American Journal of Science*, *304*(5), 454–476. https://doi.org/10.2475/ajs.304.5.454

Mosselman, E. (1995). A review of mathematical models of river planform changes. *Earth Surface Processes and Landforms*, *20*(7), 661–670. https://doi.org/10.1002/esp.3290200708

Mosselman, E. (1998). Morphological modelling of rivers with erodible banks. *Hydrological Processes*, *12*(8), 1357–1370. https://doi.org/10.1002/(SICI)1099-1085(19980630)12:8<1357::AID-HYP619>3.0.CO;2-7

Motta, D., Langendoen, E. J., Abad, J. D., & García, M. H. (2014). Modification of meander migration by bank failures. *Journal of Geophysical Research: Earth Surface*, *119*(5), 1026–1042. https://doi.org/10.1002/2013JF002952

Murray, A. B., & Paola, C. (1994). A cellular model of braided rivers. *Nature*, *371*(6492), 54–57. https://doi.org/10.1038/371054a0

Nagata, N., Hosoda, T., & Muramoto, Y. (2000). Numerical analysis of river channel processes with bank erosion. *Journal of Hydraulic Engineering*, *126*(4), 243–252. https://doi.org/10.1061/(ASCE)0733-9429(2000)126:4(243)

Nanson, G. C., & Hickin, E. J. (1983). Channel migration and incision on the Beatton River. *Journal of Hydraulic Engineering*, *109*(3), 327–337. https://doi.org/10.1061/(ASCE)0733-9429(1983)109:3(327)

Nanson, G. C., & Hickin, E. J. (1986). A statistical analysis of bank erosion and channel migration in western Canada. *The Geological Society of America Bulletin*, *97*(4), 497–504. https://doi.org/10.1130/0016-7606(1986)97<497:ASAOBE>2.0.CO;2

Nanson, G. C., Von Krusenstierna, A., Bryant, E. A., & Renilson, M. R. (1994). Experimental measurements of river-bank erosion caused by boat-generated waves on the Gordon River, Tasmania. *Regulated Rivers: Research & Management*, *9*(1), 1–14. https://doi.org/10.1002/rrr.3450090102

Nardi, L., Rinaldi, M., & Solari, L. (2012). An experimental investigation on mass failures occurring in a riverbank composed of sandy gravel. *Geomorphology*, *163–164*, 56–69. https://doi.org/10.1016/j.geomorph.2011.08.006

Ni, W., Wang, Y. P., Symonds, A. M., & Collins, M. B. (2014). Intertidal flat development in response to controlled embankment retreat: Freiston Shore, The Wash, UK. *Marine Geology*, *355*, 260–273. https://doi.org/10.1016/j.margeo.2014.06.001

Odgaard, A. J. (1989). River-meander model. I: Development. *Journal of Hydraulic Engineering*, *115*(11), 1433–1450. https://doi.org/10.1061/(ASCE)0733-9429(1989)115:11(1433)

Okura, Y., Kitahara, H., Ochiai, H., Sammori, T., & Kawanami, A. (2002). Landslide fluidization process by flume experiments. *Engineering Geology*, *66*(1–2), 65–78. https://doi.org/10.1016/S0013-7952(02)00032-7

Osman, A. M., & Thorne, C. R. (1988). Riverbank stability analysis. I: Theory. *Journal of Hydraulic Engineering*, *114*(2), 134–150. https://doi.org/10.1061/(ASCE)0733-9429(1988)114:2(134)

Paola, C., Heller, P. L., & Angevine, C. L. (1992). The large-scale dynamics of grain-size variation in alluvial basins, 1: Theory. *Basin Research*, *4*(2), 73–90. https://doi.org/10.1111/j.1365-2117.1992.tb00145.x

Parker, G., Paola, C., Whipple, K. X., & Mohrig, D. (1998). Alluvial fans formed by channelized fluvial and sheet flow. I: Theory. *Journal of Hydraulic Engineering*, *124*(10), 985–995. https://doi.org/10.1061/(asce)0733-9429(1998)124:10(985)

Parker, G., Shimizu, Y., Wilkerson, G. V., Eke, E. C., Abad, J. D., Lauer, J. W., et al. (2011). A new framework for modeling the migration of meandering rivers. *Earth Surface Processes and Landforms*, *36*(1), 70–86. https://doi.org/10.1002/esp.2113

Partheniades, E. (1965). Erosion and deposition of cohesive soils. *Journal of the Hydraulics Division*, *91*(1), 105–139. https://doi.org/10.1061/jyceaj.0001165

Patsinghasanee, S., Kimura, I., Shimizu, Y., & Nabi, M. (2015). Cantilever failure investigations for cohesive riverbanks. *Proceedings of the Institution of Civil Engineers-Water Management* (pp. 93–108). Thomas Telford Ltd. https://doi.org/10.1680/jwama.15.00033

Patsinghasanee, S., Kimura, I., Shimizu, Y., & Nabi, M. (2018). Experiments and modelling of cantilever failures for cohesive riverbanks. *Journal of Hydraulic Research*, *56*(1), 76–95. https://doi.org/10.1080/00221686.2017.1300194

Patsinghasanee, S., Kimura, I., Shimizu, Y., Nabi, M., & Chub-Uppakarn, T. (2017). Coupled studies of fluvial erosion and cantilever failure for cohesive riverbanks: Case studies in the experimental flumes and U-Tapao River. *Journal of Hydro-Environment Research*, *16*(Supplement C), 13–26. https://doi.org/10.1016/j.jher.2017.04.002

Piégay, H., Cuaz, M., Javelle, E., & Mandier, P. (1997). Bank erosion management based on geomorphological, ecological and economic criteria on the Galaure River, France, Regulated Rivers. *Research Management*, *13*(5), 433–448. https://doi.org/10.1002/(SICI)1099-1646(199709/10)13:5<433::AID-RRR467>3.0.CO;2-L

Piégay, H., Darby, S. E., Mosselman, E., & Surian, N. (2005). A review of techniques available for delimiting the erodible river corridor: A sustainable approach to managing bank erosion. *River Research and Applications*, *21*(7), 773–789. https://doi.org/10.1002/rra.881

Pizzuto, J. (2009). An empirical model of event scale cohesive bank profile evolution. *Earth Surface Processes and Landforms*, *34*(9), 1234–1244. https://doi.org/10.1002/esp.1808

Pizzuto, J., O'Neal, M., & Stotts, S. (2010). On the retreat of forested, cohesive riverbanks. *Geomorphology*, *116*(3–4), 341–352. https://doi.org/10.1016/j.geomorph.2009.11.008

Pizzuto, J. E. (1984). Bank erodibility of shallow sandbed streams. *Earth Surface Processes and Landforms*, *9*(2), 113–124. https://doi.org/10.1002/esp.3290090203

Pizzuto, J. E. (1990). Numerical simulation of gravel river widening. *Water Resources Research*, *26*(9), 1971–1980. https://doi.org/10.1029/WR026i009p01971

Pizzuto, J. E., & Meckelnburg, T. S. (1989). Evaluation of a linear bank erosion equation. *Water Resources Research*, *25*(5), 1005–1013. https://doi.org/10.1029/WR025i005p01005

Poesen, J., Nachtergaele, J., Verstraeten, G., & Valentin, C. (2003). Gully erosion and environmental change: Importance and research needs. *Catena*, *50*(2–4), 91–133. https://doi.org/10.1016/S0341-8162(02)00143-1

Poesen, J. W., Vandaele, K., & Van Wesemael, B. (1996). Contribution of gully erosion to sediment production on cultivated lands and range-lands. *IAHS Publications-Series of Proceedings and Reports-Intern Assoc Hydrological Sciences* (Vol. *236*, pp. 251–266).

Pollen Bankhead, N., & Simon, A. (2009). Enhanced application of root-reinforcement algorithms for bank-stability modeling. *Earth Surface Processes and Landforms*, *34*(4), 471–480. https://doi.org/10.1002/esp.1690

Pollen-Bankhead, N., & Simon, A. (2010). Hydrologic and hydraulic effects of riparian root networks on streambank stability: Is mechanical root-reinforcement the whole story? *Geomorphology*, *116*(3–4), 353–362. https://doi.org/10.1016/j.geomorph.2009.11.013

Prosser, I. P., Hughes, A. O., & Rutherfurd, I. D. (2000). Bank erosion of an incised upland channel by subaerial processes: Tasmania, Australia, Earth Surface Processes and Landforms. *The Journal of the British Geomorphological Research Group*, *25*(10), 1085–1101. https://doi.org/10.1002/1096-9837(200009)25:10<1085::aid-esp118>3.0.co;2-k

Qin, C., Zheng, F., Wells, R. R., Xu, X., Wang, B., & Zhong, K. (2018). A laboratory study of channel sidewall expansion in upland concentrated flows. *Soil and Tillage Research*, *178*, 22–31. https://doi.org/10.1016/j.still.2017.12.008

Quaresma, V. D. S., Amos, C. L., & Bastos, A. C. (2007). The influence of articulated and disarticulated cockle shells on the erosion of a cohesive bed. *Journal of Coastal Research*, *236*, 1443–1451. https://doi.org/10.2112/05-0449.1

Rahmati, O., Tahmasebipour, N., Haghizadeh, A., Pourghasemi, H. R., & Feizizadeh, B. (2017). Evaluation of different machine learning models for predicting and mapping the susceptibility of gully erosion. *Geomorphology*, *298*, 118–137. https://doi.org/10.1016/j.geomorph.2017.09.006

Rajaram, G., & Erbach, D. C. (1999). Effect of wetting and drying on soil physical properties. *Journal of Terramechanics*, *36*(1), 39–49. https://doi.org/10.1016/S0022-4898(98)00030-5

Reneau, S. L., Drakos, P. G., Katzman, D., Malmon, D. V., McDonald, E. V., & Ryti, R. T. (2004). Geomorphic controls on contaminant distribution along an ephemeral stream. *Earth Surface Processes and Landforms: The Journal of the British Geomorphological Research Group*, *29*(10), 1209–1223. https://doi.org/10.1002/esp.1085

Rengers, F. K., & Tucker, G. E. (2014). Analysis and modeling of gully headcut dynamics, North American high plains. *Journal of Geophysical Research: Earth Surface*, *119*(5), 983–1003. https://doi.org/10.1002/2013JF002962

Rengers, F. K., & Tucker, G. E. (2015). The evolution of gully headcut morphology: A case study using terrestrial laser scanning and hydrological monitoring. *Earth Surface Processes and Landforms*, *40*(10), 1304–1317. https://doi.org/10.1002/esp.3721

Repasch, M., Scheingross, J. S., Hovius, N., Lupker, M., Wittmann, H., Haghipour, N., et al. (2021). Fluvial organic carbon cycling regulated by sediment transit time and mineral protection. *Nature Geoscience*, *14*(11), 842–848. https://doi.org/10.1038/s41561-021-00845-7

Repasch, M., Scheingross, J. S., Hovius, N., Vieth-Hillebrand, A., Mueller, C. W., Höschen, C., et al. (2022). River organic carbon fluxes modulated by hydrodynamic sorting of particulate organic matter. *Geophysical Research Letters*, *49*(3), e2021G–e96343G. https://doi.org/10.1029/2021gl096343

Rieke-Zapp, D. H., & Nichols, M. H. (2011). Headcut retreat in a semiarid watershed in the southwestern United States since 1935. *Catena*, *87*(1), 1–10. https://doi.org/10.1016/j.catena.2011.04.002

Rinaldi, M., Casagli, N., Dapporto, S., & Gargini, A. (2004). Monitoring and modelling of pore water pressure changes and riverbank stability during flow events. *Earth Surface Processes and Landforms*, *29*(2), 237–254. https://doi.org/10.1002/esp.1042

Rinaldi, M., & Darby, S. E. (2007). 9 Modelling river-bank-erosion processes and mass failure mechanisms: Progress towards fully coupled simulations. *Developments in Earth Surface Processes*, *11*, 213–239. https://doi.org/10.1016/S0928-2025(07)11126-3

Rinaldi, M., Mengoni, B., Luppi, L., Darby, S. E., & Mosselman, E. (2008). Numerical simulation of hydrodynamics and bank erosion in a river bend. *Water Resources Research*, *44*(9), W09428. https://doi.org/10.1029/2008WR007008

Rinaldi, M., & Nardi, L. (2013). Modeling interactions between Riverbank Hydrology and mass failures. *Journal of Hydrologic Engineering*, *10*(18), 1231–1240. https://doi.org/10.1061/(ASCE)HE.1943-5584.0000716

Rousseau, Y. Y., Van de Wiel, M. J., & Biron, P. M. (2017). Simulating bank erosion over an extended natural sinuous river reach using a universal slope stability algorithm coupled with a morphodynamic model. *Geomorphology*, *295*, 690–704. https://doi.org/10.1016/j.geomorph.2017.08.008

Roy, S., Barman, K., Das, V. K., Debnath, K., & Mazumder, B. S. (2019). Experimental investigation of undercut mechanisms of river bank erosion based on 3D turbulence characteristics. *Environmental Processes*, *7*, 1–26. https://doi.org/10.1007/s40710-019-00417-3

Rutherfurd, I. D. (2000). Some human impacts on Australian stream channel morphology. In S. Brizga & B. Finlayson, (Eds.), *River management: The Australasian experience* (pp. 11–49). John Wiley and Sons.

Samadi, A., Amiri-Tokaldany, E., Davoudi, M. H., & Darby, S. E. (2013). Experimental and numerical investigation of the stability of overhanging riverbanks. *Geomorphology*, *184*, 1–19. https://doi.org/10.1016/j.geomorph.2012.03.033

Samadi, A., Davoudi, M. H., & Amiri-Tokaldany, E. (2011). Experimental study of cantilever failure in the upper part of cohesive riverbanks. *Research Journal of Environmental Sciences*, *5*(5), 444–460. https://doi.org/10.3923/rjes.2011.444.460

Samani, A. N., Ahmadi, H., Mohammadi, A., Ghoddousi, J., Salajegheh, A., Boggs, G., & Pishyar, R. (2010). Factors controlling gully advancement and models evaluation (Hableh Rood Basin, Iran). *Water Resources Management*, *24*(8), 1531–1549. https://doi.org/10.1007/s11269-009-9512-4

Sanders, H., Rice, S. P., & Wood, P. J. (2021). Signal crayfish burrowing, bank retreat and sediment supply to rivers: A biophysical sediment budget. *Earth Surface Processes and Landforms*, *46*(4), 837–852. https://doi.org/10.1002/esp.5070

Schuurman, F., Marra, W. A., & Kleinhans, M. G. (2013). Physics-based modeling of large braided sand-bed rivers: Bar pattern formation, dynamics, and sensitivity. *Journal of Geophysical Research: Earth Surface*, *118*(4), 2509–2527. https://doi.org/10.1002/2013jf002896

Schwimmer, R. A. (2001). Rates and processes of marsh shoreline erosion in Rehoboth Bay, Delaware, USA. *Journal of Coastal Research*, 672–683.

Seginer, I. (1966). Gully development and sediment yield. *Journal of Hydrology*, *4*, 236–253. https://doi.org/10.1016/0022-1694(66)90082-5

Seminara, G. (2006). Meanders. *Journal of Fluid Mechanics*, *554*, 271–297. https://doi.org/10.1017/S0022112006008925

Sgarabotto, A., D'Alpaos, A., & Lanzoni, S. (2021). Effects of vegetation, sediment supply and sea level rise on the morphodynamic evolution of tidal channels. *Water Resources Research*, *57*(7), e2020WR028577. https://doi.org/10.1029/2020wr028577

Shimizu, Y., Nelson, J., Arnez Ferrel, K., Asahi, K., Giri, S., Inoue, T., et al. (2019). Advances in computational morphodynamics using the International River Interface Cooperative (iRIC) software. *Earth Surface Processes and Landforms*, *45*(1), 11–37. https://doi.org/10.1002/esp.4653

Shu, A., Duan, G., Rubinato, M., Tian, L., Wang, M., & Wang, S. (2019). An experimental study on mechanisms for sediment transformation due to riverbank collapse. *Water*, *11*(3), 529. https://doi.org/10.3390/w11030529

Simon, A., & Collison, A. J. C. (2002). Quantifying the mechanical and hydrologic effects of riparian vegetation on streambank stability. *Earth Surface Processes and Landforms*, *27*(5), 527–546. https://doi.org/10.1002/esp.325

Simon, A., Curini, A., Darby, S. E., & Langendoen, E. J. (2000). Bank and near-bank processes in an incised channel. *Geomorphology*, *35*(3–4), 193–217. https://doi.org/10.1016/S0169-555X(00)00036-2

Simon, A., & Darby, S. (2002). Effectiveness of grade-control structures in reducing erosion along incised river channels: The case of Hotophia Creek, Mississippi. *Geomorphology*, *42*(3–4), 229–254. https://doi.org/10.1016/S0169-555X(01)00088-5

Simon, A., & Thomas, R. E. (2002). Processes and forms of an unstable alluvial system with resistant, cohesive streambeds. *Earth Surface Processes and Landforms: The Journal of the British Geomorphological Research Group*, *27*(7), 699–718. https://doi.org/10.1002/esp.347

Solari, L., Seminara, G., Lanzoni, S., Marani, M., & Rinaldo, A. (2002). Sand bars in tidal channels Part 2. Tidal meanders. *Journal of Fluid Mechanics*, *451*, 203–238. https://doi.org/10.1017/S0022112001006565

Stecca, G., Measures, R., & Hicks, D. M. (2017). A framework for the analysis of noncohesive bank erosion algorithms in morphodynamic modeling. *Water Resources Research*, *53*(8), 6663–6686. https://doi.org/10.1002/2017WR020756

Stein, O. R., & LaTray, D. A. (2002). Experiments and modeling of head cut migration in stratified soils. *Water Resources Research*, *38*(12), 20–21. https://doi.org/10.1029/2001WR001166

Sunamura, T. (1982). A wave tank experiment on the erosional mechanism at a cliff base. *Earth Surface Processes and Landforms*, *7*(4), 333–343. https://doi.org/10.1002/esp.3290070405

Symonds, A. M., & Collins, M. B. (2007). The establishment and degeneration of a temporary creek system in response to managed coastal realignment: The Wash, UK. *Earth Surface Processes and Landforms: The Journal of the British Geomorphological Research Group*, *32*(12), 1783–1796. https://doi.org/10.1002/esp.1495

Tal, M., & Paola, C. (2007). Dynamic single-thread channels maintained by the interaction of flow and vegetation. *Geology*, *35*(4), 347–350. https://doi.org/10.1130/g23260a.1

Tambroni, N., Luchi, R., & Seminara, G. (2017). Can tide dominance be inferred from the point bar pattern of tidal meandering channels? *Journal of Geophysical Research: Earth Surface*, *122*(2), 492–512. https://doi.org/10.1002/2016JF004139

Temmerman, S., Bouma, T. J., Van de Koppel, J., Van der Wal, D., De Vries, M. B., & Herman, P. (2007). Vegetation causes channel erosion in a tidal landscape. *Geology*, *35*(7), 631–634. https://doi.org/10.1130/g23502a.1

Terzaghi, K. (1951). *Theoretical soil mechanics*. Chapman and Hall, Limited.

Thompson, C., & Amos, C. L. (2002). The impact of mobile disarticulated shells ofCerastoderma edulis on the abrasion of a cohesive substrate. *Estuaries*, *25*(2), 204–214. https://doi.org/10.1007/BF02691308

Thorne, C. R. (1982). Processes and mechanisms for river bank erosion. In R. D. Hey, J. C. Bathurst & C. R. Thorne (Eds.), *Gravel-bed rivers: Fluvial Processes, Engineering, and Management* (pp. 227–259). John Wiley & Sons.

Thorne, C. R., Alonso, C., Borah, D., Darby, S., Diplas, P., Julien, P., et al. (1998a). River width adjustment. I: Processes and mechanisms. *Journal of Hydraulic Engineering*, *124*(9), 881–902. https://doi.org/10.1061/(ASCE)0733-9429(1998)124:9(881)

Thorne, C. R., Alonso, C., Borah, D., Darby, S., Diplas, P., Julien, P., et al. (1998b). River width adjustment. II: Modeling. *Journal of Hydraulic Engineering*, *124*(9), 903–917. https://doi.org/10.1061/(ASCE)0733-9429(1998)124:9(903)

Thorne, C. R., & Tovey, N. K. (1981). Stability of composite river banks. *Earth Surface Processes and Landforms*, *5*(6), 469–484. https://doi.org/10.1002/esp.3290060507

Trimble, S. W. (2009). Fluvial processes, morphology and sediment budgets in the Coon Creek Basin, WI, USA, 1975–1993. *Geomorphology*, *108*(1–2), 8–23. https://doi.org/10.1016/j.geomorph.2006.11.015

Turner, R. E. (1990). Landscape development and coastal wetland losses in the northern Gulf of Mexico. *American Zoologist*, *30*(1), 89–105. https://doi.org/10.1093/icb/30.1.89

Turowski, J. M., Hovius, N., Meng Long, H., Lague, D., & Men Chiang, C. (2008). Distribution of erosion across bedrock channels. *Earth Surface Processes and Landforms: The Journal of the British Geomorphological Research Group*, *33*(3), 353–363. https://doi.org/10.1002/esp.1559

Valentin, C., Poesen, J., & Li, Y. (2005). Gully erosion: Impacts, factors and control. *Catena*, *63*(2–3), 132–153. https://doi.org/10.1016/j.catena.2005.06.001

Vandekerckhove, L., Muys, B., Poesen, J., De Weerdt, B., & Coppé, N. (2001). A method for dendrochronological assessment of medium-term gully erosion rates. *Catena*, *45*(2), 123–161. https://doi.org/10.1016/S0341-8162(01)00142-4

Vandekerckhove, L., Poesen, J., & Govers, G. (2003). Medium-term gully headcut retreat rates in Southeast Spain determined from aerial photographs and ground measurements. *Catena*, *50*(2–4), 329–352. https://doi.org/10.1016/S0341-8162(02)00132-7

Vandekerckhove, L., Poesen, J., Wijdenes, D. O., & Gyssels, G. (2001). Short-term bank gully retreat rates in Mediterranean environments. *Catena*, *44*(2), 133–161. https://doi.org/10.1016/S0341-8162(00)00152-1

Vandekerckhove, L., Poesen, J., Wijdenes, D. O., Gyssels, G., Beuselinck, L., & De Luna, E. (2000). Characteristics and controlling factors of bank gullies in two semi-arid Mediterranean environments. *Geomorphology*, *33*(1–2), 37–58. https://doi.org/10.1016/S0169-555X(99)00109-9

Van De Wiel, M. J. (2003). *Numerical modelling of channel adjustment in alluvial meandering rivers with riparian vegetation*. University of Southampton.

van der Wegen, M., Wang, Z. B., Savenije, H. H. G., & Roelvink, J. A. (2008). Long-term morphodynamic evolution and energy dissipation in a coastal plain, tidal embayment. *Journal of Geophysical Research*, *113*(F3), F03001. https://doi.org/10.1029/2007JF000898

van Dijk, W. M., Hiatt, M. R., van der Werf, J. J., & Kleinhans, M. G. (2019). Effects of shoal margin collapses on the morphodynamics of a sandy estuary. *Journal of Geophysical Research: Earth Surface*, *124*(1), 195–215. https://doi.org/10.1029/2018JF004763

van Dijk, W. M., Lageweg, W. I., & Kleinhans, M. G. (2012). Experimental meandering river with chute *cutoffs. Journal of Geophysical Research*, *117*(F3), F03023. https://doi.org/10.1029/2011JF002314

Van Dijk, W. M., Teske, R., Van de Lageweg, W. I., & Kleinhans, M. G. (2013). Effects of vegetation distribution on experimental river channel dynamics. *Water Resources Research*, *49*(11), 7558–7574. https://doi.org/10.1002/2013wr013574

Van Eerdt, M. M. (1985). Salt marsh cliff stability in the Oosterschelde. *Earth Surface Processes and Landforms*, *10*(2), 95–106. https://doi.org/10.1002/esp.3290100203

Vargas Luna, A., Duró, G., Crosato, A., & Uijttewaal, W. (2019). Morphological adaptation of river channels to vegetation establishment: A laboratory study. *Journal of Geophysical Research: Earth Surface*, *124*(7), 1981–1995. https://doi.org/10.1029/2018JF004878

Veihe, A., Jensen, N. H., Schiøtz, I. G., & Nielsen, S. L. (2011). Magnitude and processes of bank erosion at a small stream in Denmark. *Hydrological Processes*, *25*(10), 1597–1613. https://doi.org/10.1002/hyp.7921

Venditti, J. G., Rennie, C. D., Bomhof, J., Bradley, R. W., Little, M., & Church, M. (2014). Flow in bedrock canyons. *Nature*, *513*(7519), 534–537. https://doi.org/10.1038/nature13779

Walker, H. J. (2013). A picture is Worth 934 words: Riverbank erosion and Block Collapse in an Arctic delta. *Focus on Geography*, *56*(3), 114–115. https://doi.org/10.1111/foge.12019

Watson, A. J., & Basher, L. R. (2006). *Stream bank erosion: A review of processes of bank failure, measurement and assessment techniques, and modelling approaches*. A report prepared for stakeholders of the Motueka Integrated Catchment Management Programme and the Raglan Fine Sediment Study. Landcare Research.

Wells, R. R., Alonso, C. V., & Bennett, S. J. (2009). Morphodynamics of headcut development and soil erosion in upland concentrated flows. *Soil Science Society of America Journal*, *73*(2), 521–530. https://doi.org/10.2136/sssaj2008.0007

Wells, R. R., Momm, H. G., Rigby, J. R., Bennett, S. J., Bingner, R. L., & Dabney, S. M. (2013). An empirical investigation of gully widening rates in upland concentrated flows. *Catena*, *101*, 114–121. https://doi.org/10.1016/j.catena.2012.10.004

Wilson, G. V., Nieber, J. L., Sidle, R. C., & Fox, G. A. (2013). Internal erosion during soil pipeflow: State of the science for experimental and numerical analysis. *Transactions of the ASABE*, *56*(2), 465–478. https://doi.org/10.13031/2013.42667

Wilson, G. V., Periketi, R. K., Fox, G. A., Dabney, S. M., Shields, F. D., & Cullum, R. F. (2007). Soil properties controlling seepage erosion contributions to streambank failure. *Earth Surface Processes and Landforms: The Journal of the British Geomorphological Research Group*, *32*(3), 447–459. https://doi.org/10.1002/esp.1405

Wood, A. L., Simon, A., Downs, P. W., & Thorne, C. R. (2001). Bank-toe processes in incised channels: The role of apparent cohesion in the entrainment of failed bank materials. *Hydrological Processes*, *15*(1), 39–61. https://doi.org/10.1002/hyp.151

Wood, D. M. (2014). *Geotechnical modelling*. CRC press.

Wu, L. Z., Zhou, Y., Sun, P., Shi, J. S., Liu, G. G., & Bai, L. Y. (2017). Laboratory characterization of rainfall-induced loess slope failure. *Catena*, *150*, 1–8. https://doi.org/10.1016/j.catena.2016.11.002

Wu, T. H., McKinnell, W. P., III, & Swanston, D. N. (1979). Strength of tree roots and landslides on prince of Wales Island, Alaska. *Canadian Geotechnical Journal*, *16*(1), 19–33. https://doi.org/10.1139/t79-003

Wynn, T. M., Henderson, M. B., & Vaughan, D. H. (2008). Changes in streambank erodibility and critical shear stress due to subaerial processes along a headwater stream, southwestern Virginia, USA. *Geomorphology*, *97*(3–4), 260–273. https://doi.org/10.1016/j.geomorph.2007.08.010

Wynn, T. M., & Mostaghimi, S. (2006). Effects of riparian vegetation on stream bank subaerial processes in southwestern Virginia, USA. *Earth Surface Processes and Landforms: The Journal of the British Geomorphological Research Group*, *31*(4), 399–413. https://doi.org/10.1002/esp.1252

Xia, J., Deng, S., Lu, J., Xu, Q., Zong, Q., & Tan, G. (2016). Dynamic channel adjustments in the Jingjiang Reach of the middle Yangtze River. *Scientific Reports*, *6*(1), 22802. https://doi.org/10.1038/srep22802

Xia, J., Deng, S., Zhou, M., Lu, J., & Xu, Q. (2017). Geomorphic response of the Jingjiang Reach to the Three Gorges Project operation. *Earth Surface Processes and Landforms*, *42*(6), 866–876. https://doi.org/10.1002/esp.4043

Xia, J., Zong, Q., Deng, S., Xu, Q., & Lu, J. (2014). Seasonal variations in composite riverbank stability in the Lower Jingjiang Reach, China. *Journal of Hydrology*, *519*(Part D), 3664–3673. https://doi.org/10.1016/j.jhydrol.2014.10.061

Xia, J., Zong, Q., Zhang, Y., Xu, Q., & Li, X. (2014). Prediction of recent bank retreat processes at typical sections in the Jingjiang Reach. *Science China Technological Sciences*, *57*(8), 1490–1499. https://doi.org/10.1007/s11431-014-5597-y

Xin, P., Dan, H., Zhou, T., Lu, C., Kong, J., & Li, L. (2016). An analytical solution for predicting the transient seepage from a subsurface drainage system. *Advances in Water Resources*, *91*, 1–10. https://doi.org/10.1016/j.advwatres.2016.03.006

Xin, P., Kong, J., Li, L., & Barry, D. A. (2013). Modelling of groundwater–vegetation interactions in a tidal marsh. *Advances in Water Resources*, *57*, 52–68. https://doi.org/10.1016/j.advwatres.2013.04.005

Xin, P., Wilson, A., Shen, C., Ge, Z., Moffett, K. B., Santos, I. R., et al. (2022). Surface water and groundwater interactions in salt marshes and their impact on plant ecology and coastal biogeochemistry. *Reviews of Geophysics*, *60*(1), e2021R–e2740R. https://doi.org/10.1029/2021rg000740

Xin, P., Yuan, L. R., Li, L., & Barry, D. A. (2011). Tidally driven multiscale pore water flow in a creek-marsh system. *Water Resources Research*, *47*(7), W07534. https://doi.org/10.1029/2010wr010110

Xu, F., Coco, G., Tao, J., Zhou, Z., Zhang, C., Lanzoni, S., & D'Alpaos, A. (2019). On the morphodynamic equilibrium of a short tidal channel. *Journal of Geophysical Research: Earth Surface*, *124*(2), 639–665. https://doi.org/10.1029/2018JF004952

Xu, F., Coco, G., Zhou, Z., Tao, J., & Zhang, C. (2017). A numerical study of equilibrium states in tidal network morphodynamics. *Ocean Dynamics*, *12*(67), 1593–1607. https://doi.org/10.1007/s10236-017-1101-0

Yamamuro, J. A., & Lade, P. V. (1998). Steady-state concepts and static liquefaction of silty sands. *Journal of Geotechnical and Geoenvironmental Engineering*, *124*(9), 868–877. https://doi.org/10.1061/(ASCE)1090-0241(1998)124:9(868)

Yao, Z., Ta, W., Jia, X., & Xiao, J. (2011). Bank erosion and accretion along the Ningxia-Inner Mongolia reaches of the Yellow River from 1958 to 2008. *Geomorphology*, *127*(1–2), 99–106. https://doi.org/10.1016/j.geomorph.2010.12.010

Yu, M., Wei, H., & Wu, S. (2015). Experimental study on the bank erosion and interaction with near-bank bed evolution due to fluvial hydraulic force. *International Journal of Sediment Research*, *30*(1), 81–89. https://doi.org/10.1016/s1001-6279(15)60009-9

Yuan, S., Tang, H., Li, K., Xu, L., Xiao, Y., Gualtieri, C., et al. (2021). Hydrodynamics, sediment transport and morphological features at the confluence between the Yangtze River and the Poyang Lake. *Water Resources Research*, *57*(3), e2020W–e28284W. https://doi.org/10.1029/2020wr028284

Yumoto, M., Ogata, T., Matsuoka, N., & Matsumoto, E. (2006). Riverbank freeze-thaw erosion along a small mountain stream. *Nikko Volcanic Area, Central Japan, Permafrost and Periglacial Processes*, *17*(4), 325–339. https://doi.org/10.1002/ppp.569

Zech, Y., Soares-Frazão, S., Spinewine, B., & Le Grelle, N. (2008). Dam-break induced sediment movement: Experimental approaches and numerical modelling. *Journal of Hydraulic Research*, *46*(2), 176–190. https://doi.org/10.1080/00221686.2008.9521854

Zeng, H., Tang, C., Cheng, Q., Zhu, C., Lin, Z., Yin, L., & Shi, B. (2022). Desiccation-induced curling of mud layers: Field observations and experimental insights. *Engineering Geology*, *296*, 106458. https://doi.org/10.1016/j.enggeo.2021.106458

Zhang, K., Gong, Z., Zhao, K., Wang, K., Pan, S., & Coco, G. (2021). Experimental and numerical modeling of overhanging riverbank stability. *Journal of Geophysical Research: Earth Surface*, *126*(10), e2021J–e6109J. https://doi.org/10.1029/2021JF006109

Zhang, L. L., Zhang, J., Zhang, L. M., & Tang, W. H. (2011). Stability analysis of rainfall-induced slope failure: A review. *Proceedings of the Institution of Civil Engineers-Geotechnical Engineering*, *164*(5), 299–316. https://doi.org/10.1680/geng.2011.164.5.299

Zhang, Z., Shu, A., Zhang, K., Liu, H., Wang, J., & Dai, J. (2019). Quantification of river bank erosion by RTK GPS monitoring: Case studies along the Ningxia-Inner Mongolia reaches of the Yellow River, China. *Environmental Monitoring and Assessment*, *191*(3), 140. https://doi.org/10.1007/s10661-019-7269-7

Zhang, W., Xu, Y., Hoitink, A. J. F., Sassi, M. G., Zheng, J., Chen, X., & Zhang, C. (2015). Morphological change in the Pearl River Delta, *China*. *Marine Geology*, *363*, 202–219. https://doi.org/10.1016/j.margeo.2015.02.012

Zhao, K., Gong, Z., Xu, F., Zhou, Z., Zhang, C. K., Perillo, G., & Coco, G. (2019). The role of collapsed bank soil on tidal channel evolution: A process-based model involving bank collapse and sediment dynamics. *Water Resources Research*, *55*(11), 9051–9071. https://doi.org/10.1029/2019WR025514

Zhao, K., Gong, Z., Zhang, K., Wang, K., Jin, C., Zhou, Z., et al. (2020). Laboratory experiments of bank collapse: The role of bank height and near-bank water depth. *Journal of Geophysical Research: Earth Surface*, *125*(5), e2019JF005281. https://doi.org/10.1029/2019JF005281

Zhao, K., Lanzoni, S., Gong, Z., & Coco, G. (2021). A numerical model of bank collapse and river meandering. *Geophysical Research Letters*, *48*(12), e2021G–e93516G. https://doi.org/10.1029/2021GL093516

Zhou, Z., Coco, G., Townend, I., Olabarrieta, M., Van Der Wegen, M., Gong, Z., et al. (2017). Is "morphodynamic equilibrium" an oxymoron? *Earth-Science Reviews*, *165*, 257–267. https://doi.org/10.1016/j.earscirev.2016.12.002

Zhou, Z., Coco, G., van der Wegen, M., Gong, Z., Zhang, C., & Townend, I. (2015). Modeling sorting dynamics of cohesive and non-cohesive sediments on intertidal flats under the effect of tides and wind waves. *Continental Shelf Research*, *104*, 76–91. https://doi.org/10.1016/j.csr.2015.05.010

Zhou, Z., Ye, Q., & Coco, G. (2016). A one-dimensional biomorphodynamic model of tidal flats: Sediment sorting, marsh distribution, and carbon accumulation under sea level rise. *Advances in Water Resources*, *93*, 288–302. https://doi.org/10.1016/j.advwatres.2015.10.011

Zolezzi, G., Luchi, R., & Tubino, M. (2012). Modeling morphodynamic processes in meandering rivers with spatial width variations. *Reviews of Geophysics*, *50*(4), RG4005. https://doi.org/10.1029/2012rg000392